Advances in Local Stereology

with Emphasis on Surface Area Estimation and Wicksell's Problem

PhD Thesis by **Ólöf Thórisdóttir**

Supervised by **Markus Kiderlen**

September 2013

Department of Mathematics
Aarhus University

Contents

Preface

Stereology concerns the estimation of geometric characteristics of spatial structures from lower dimensional information about the structures. I was introduced to the fascinating and creative world of stereology in my master's studies at Aarhus University, primarily through the writing of my master's thesis. It is in particular the interplay of geometrical and statistical issues in stereology that has a great appeal to me. A more recent and less developed branch of stereology is local stereology. This thesis is a contribution to local stereology and presents the outcome of the research part of my PhD studies. The studies were carried out at the Department of Mathematics, Aarhus University, from October 2010 to September 2013, under the careful supervision of Markus Kiderlen. The PhD studies were partly financed by Center for Stochastic Geometry and Advanced Bioimaging (CSGB), funded by the Villum Foundation.

The thesis consists of three independently written and self-contained papers:

Besides being submitted to international journals, all three papers can be found as CSGB research reports. The technical parts that were omitted in the accepted version of Paper A and only included in the CSGB research report can be found as supplementary material on pages 54–58. The thesis also contains an introductory chapter, where the three papers are connected together, their main results summarized and their importance for the stereological community emphasized.

The work constituting the three papers has been presented at the following conferences and workshops:

- 16th Workshop on Stochastic Geometry, Stereology and Image Analysis. Sandbjerg, Denmark, June 2011,
- 13th International Conference on Stereology, Beijing, China, October 2011,
- 4th Internal CSGB Workshop, Aarhus, Denmark, November 2011,
- GPSRS Workshop, Erlangen, Germany, September 2012
- 6th Internal CSGB Workshop, Skagen, Denmark, May 2013
- 11th European Congress of Stereology and Image Analysis, Kaiserslautern, Germany, July 2013.

Acknowledgement

This thesis would not exist if it were not for my supervisor's, Markus Kiderlen, sincere dedication to our work. I am indebted to him for originally encouraging me to take on the challenge of PhD studies and for continuously stimulating me throughout the studies.

I am grateful to have been a part of Eva B. Vedel Jensen's center CSGB. The interdisciplinary research undertaken at the center has broadened my horizon and added a sense of importance and practical relevance to my work. Furthermore, it has been a privilege to work on ground-breaking research under the guidance of outstanding professors. Paper C is the fruit of a collaboration with the Stereology and EM Research Laboratory, Aarhus University, and I want to thank Ali H. Rafati for nice collaboration. I also want to acknowledge Lars Madsen's generous support concerning the final layout of this thesis.

I would like to thank my dear colleagues in 'statistisk strikkeklub', in particular Camilla Mondrup Andreassen and Ina Trolle Andersen for their invaluable support. Furthermore, I want to thank my family and friends and the never-failing F-myndum.

Ólöf Thórisdóttir
Aarhus, September 2013

Abstract

This thesis presents advances in local stereology. The goal is to make statistical inference about geometric characteristics of a spatial structure. The inference is typically made from flat sections taken through a fixed reference point of the structure. Local stereology has proven to be very useful for applications in biomedicine.

When the aim is to estimate the distribution of the particle shape from random samples, strict shape assumptions on the particles under study have to be imposed. There exists much literature on the classical *Wicksell problem*, which is concerned with the estimation of the radius distribution of balls from the radius distribution of isotropic uniform random (IUR) flat sections through the balls. We treat Wicksell's classical problem in a local setting. Here the balls are (up to rotations) characterized by two random variables: their radius and the position of their reference point inside the ball. We derive several results that are analogue to results for the classical Wicksell problem such as unfolding of the arising integral equations, moment relations and stereology of extremes, but we also emphasize differences between the local and the classical problem.

Without strict shape assumptions on the particles of interest, we have to settle for mean geometric characteristics of the particles, instead of their distribution. These characteristics could for example be intrinsic volumes, like volume or surface area. We derive a new local stereological estimator for surface area which we call the *Morse type surface area estimator*. The estimator is obtained by combining Morse theory, Crofton's formula and the invariator principle, which is a Blaschke-Petkantschin type measure decomposition. The estimator can also be described as a modification of the 'area tangent count method' in stereology. We show that the Morse type estimator is better (in terms of efficiency and precision) than existing local surface area estimators and illustrate its practicability in a biological application.

The above mentioned combination of the classical Crofton formula with the invariator principle is a powerful tool to derive *rotational Crofton formulae*. As rotational Crofton formulae in turn are the basis for local stereological estimators, we discuss these formulae more systematically. Rotational Crofton formulae deal with sections of an object with isotropically randomized flats that pass through the origin. They answer the question which measurement function of the section to choose to obtain an unbiased estimator of a geometric characteristic of the object. We first review known measurement functions that yield intrinsic volumes or, more generally Minkowski tensors. We then show that there are also rotational Crofton formulae

for support measures and curvature measures. Often, the measurement function is not given explicitly but only as an integral geometric expression. We derive several different, more explicit representations of the measurement function. The most important of these representations involves writing the measurement function in terms of so-called critical values of the section profile. This is first achieved for smooth manifolds using Morse theory and then for polyconvex sets using Hadwiger's index. All the different representations play an important role when rotational Crofton formulae are applied in local stereology.

Resumé

Denne afhandling præsenterer fremskridt i lokal stereologi. Formålet er at lave statistisk inferens om geometriske karakteristika af et objekt i rummet. Inferensen laves typisk fra affine snit taget igennem et fast referencepunkt i objektet. Lokal stereologi har vist sig at være meget nyttig for anvendelser i biomedicin.

Når formålet er at estimere fordelingen af formen af partikler fra tilfældige snit, er det nødvendigt at lægge strenge antagelser på formen af partiklerne. Der eksisterer en betydelig mængde litteratur om det klassiske *Wicksell-problem*, som involverer estimationen af radiusfordelingen af kugler fra radiusfordelingen af isotropiske uniforme (IUR) snit gennem kuglerne. Vi betragter Wicksells klassiske problem i et lokalt setting. Her er kuglerne (op til rotationer) karakteriserede ved to stokastiske variable: deres radius og positionen af deres referencepunkt inden i kuglen. Vi udleder adskillige resultater, der svarer til resultater for det klassiske Wicksell-problem som for eksempel inversion af de integral-ligninger der opstår, moment-relationer og stereologi af ekstremer, men vi beskriver også forskelle mellem det lokale og det klassiske problem.

Uden strenge antagelser på formen af partiklerne som vi betragter, må vi nøjes med gennemsnittet af geometriske karakteristika, i stedet for deres fordeling. Disse karakteristika kunne for eksempel være de indre volumina, som volumen eller overfladeareal. Vi udleder en ny lokal stereologisk estimator for overfladeareal som vi kalder „Morse-type estimatoren af overfladeareal “. Estimatoren er baseret på at kombinere Morse-teori, Croftons formel og invariator-princippet, som er en måldekomposition af Blaschke-Petkantschin-type. Estimatoren kan også beskrives ved en modificering af „areal-tangent-optælningsmetoden“ i stereologi. Vi viser, at estimatoren af Morse-type er bedre (hvad angår effektivitet og præcision) end eksisterende estimatorer og illustrerer dens brugbarhed i en biologisk anvendelse.

Den ovennævnte kombination af den klassiske Crofton-formel og invariator-princippet er et nyttigt redskab for at udlede rotations-Crofton-formler. Da rotations-Crofton-formler udgør grundlaget for lokale stereologiske estimatorer, diskuterer vi disse formler mere systematisk. Rotations-Crofton-formler beskæftiger sig med snit af objekter med isotropiske randomiserede planer, der går igennem origo. De giver svar på spørgsmålet om, hvilken målingsfunktion af snittet, der burde betragtes for at få en middelværdiret estimator af geometriske karakteristika af objektet. Vi giver først en oversigt over kendte målingsfunktioner, der giver de indre volumina, eller mere generelt Minkowski-tensorer. Dernæst viser vi, at der også findes

rotations-Crofton-formler for supportmålene og krumningsmålene. Målingsfunktionen er ofte ikke udtrykt eksplicit men kun som et integralgeometrisk udtryk. Vi udleder adskillige forskellige mere eksplicitte repræsentationer af målingsfunktionen. Den mest vigtige af disse repræsentationer udtrykker målingsfunktionen ved hjælp af såkaldte kristiske værdier af snit-profilen. Dette gøres først for glatte mangfoldigheder ved at bruge Morse-teori og så for polykonvekse mængder ved at bruge Hadwigers indeks. Alle de forskellige repræsentationer spiller en vigtig rolle, når rotations-Crofton-formler er anvendt i lokal stereologi.

Introduction

The three papers that constitute this thesis are all facets of local stereology that were missing in the general picture. This introductory chapter serves to bind the papers together, present their main results and emphasize their importance for the stereological community. In order to achieve this we give a few pages of introduction to stereology and important concepts in stochastic and integral geometry.

1 Stereology

The International Society for Stereology (ISS) was founded in 1961 and gathered researchers from as different fields as biology, mathematics, medicine and metallurgy. The common goal of these researchers was to obtain better understanding of three-dimensional objects from microscopy images. Today, the objectives of stereology still remain the same. Recent advances in technology, both in microscopy and measurement techniques, have only increased the need for methods for analyzing advanced microscopy and bioimaging data, that require as little manual workload as possible without making the resulting information insufficient. Although the term *stereology* was first coined only around 50 years ago its roots stretch back much further, of which Buffon's needle problem [Buf77] may be considered as a first example. An extensive list of classic stereology references can be found in [BJ05, pp. 52–54] and [Jen98, pp. 33–34]. We mention in particular the early introduction given in [WE66a] and [WE66b], the theoretical framework for stereology laid down in the important papers [DM77], [MD76], [MD77], [Mil78a] and [Mil78b], and the surveys [CO87] and [Sto90].

Stereology can be considered a subdiscipline of stochastic geometry and spatial statistics. Many stereological results are obtained by applying classical results from stochastic geometry and sampling theory in this new setting, where the emphasis is on practical applications. Exactly this interdisciplinarity, combining well established results from related fields with a creative and innovative use of modern technology, is what makes stereology so fascinating.

In stereology, statistical inference about geometric characteristics of an object of interest, e.g. its volume or the surface area of its boundary, is made by sampling the object. Hence stereology can also be thought of as geometric sampling theory [BJ05]. Opposed to classical survey sampling, where typically units are sampled at random from a discrete target population, e.g. by simple random sampling, affine

flats, windows, lattices (digital stereology) or a combination of these are used to sample a spatial structure in stereology. A structure can be sampled by, for instance, intersecting it with an affine flat or by projecting it onto a flat.

There are two different approaches for making statistical inference in stereology and these are referred to as *model-based stereology* and *design-based stereology*. In model-based stereology the object of interest is assumed to be random and the affine subspace, the *sampling probe*, to be arbitrary (deterministic). To obtain a representative sample, the random object under study is assumed to be homogeneous, an assumption which was first made mathematically rigorous later by using random closed sets; see [SKM95] and references therein. This assumption of homogeneity works well in many applications in material science and geology but is often inappropriate in biological applications where the structure of interest is usually highly organized. Design-based stereology does not require any assumptions on the object under study. The object is considered to be deterministic and a representative sample is obtained by using a random sampling probe. The setting of this thesis is design-based.

This thesis presents advances in an even more recent branch of stereology called *local stereology*. Local stereology has been developed since the beginning of the eighties in close collaboration with users of stereological tools. The mathematical foundations of local stereology can be found in the monograph [Jen98]. In local stereology the goal is the same as in classical stereology, namely to obtain geometric characteristics of spatial structures, but the sampling designs are different. Instead of using affine subspaces, only linear subspaces, taken through a fixed reference point, are considered. This is of interest in many biological applications where the structure of interest has a fixed reference point. The fixed reference point can e.g. be a nucleus or a nucleolus of a biological cell. Local procedures are most conveniently implemented if *optical sectioning* is available. Sections taken through a fixed reference point are often called *central sections*, as reference points are often centrally located. The advantages of central sections as compared to arbitrary sections are that they often carry more information about the object of interest and they diminish the 'overprojection effect' which occurs when cells are sectioned with planes that are almost tangent to the cell. Such sections show a very blurred cell boundary in confocal microscopy and are therefore often useless for stereological measurements.

2 Theoretical background

As previously mentioned the goal of local stereology is to obtain some geometric characteristics of a spatial structure. Throughout this thesis there are different regularity assumptions imposed on the spatial structure, of which convexity is one of the most basic ones. Convexity is convenient as estimators and formulae, when present, often simplify under this assumption. A *convex body* in n-dimensional Euclidean space $\mathbb{R}^n$ is a compact, convex subset of $\mathbb{R}^n$ and it is uniquely determined by its

support function h_X given by

$$h_X(u) = \max_{x \in X} \langle u, x \rangle ,$$

where u is an element of the unit sphere $S^{n-1} = \{x \in \mathbb{R}^n \mid \|x\| = 1\}$. We write $\mathcal{K}^n$ for the family of all convex bodies in $\mathbb{R}^n$. The *radial function* is dual to the support function. If X is nonempty, compact and *star-shaped* at O (i.e. every line through O that hits X does so in a (possibly degenerate) line segment), its radial function ρ_X is defined by

$$\rho_X(x) = \sup\{\alpha \in \mathbb{R} \mid \alpha x \in X\},$$

for $x \in \mathbb{R}^n \setminus \{O\}$. The set X is uniquely determined by its radial function.

2.1 The intrinsic volumes

The desired geometric characteristic is often one of the *intrinsic volumes*. The intrinsic volumes are important functionals in convex geometry and they can for instance be defined via the Steiner formula. We write $X + Y = \{x + y \mid x \in X, y \in Y\}$ for the Minkowski sum of $X, Y \subseteq \mathbb{R}^n$. For $X \in \mathcal{K}^n$ and $\varepsilon > 0$, the set

$$X_\varepsilon = X + \varepsilon B_n = \{x \in \mathbb{R}^n \mid d(x, X) \leq \varepsilon\},$$

is the *parallel body* of X at distance ε. Here $B_n = \{x \in \mathbb{R}^n \mid \|x\| \leq 1\}$ is the unit ball in $\mathbb{R}^n$ and $d(x, X) = \min_{y \in X} \|x - y\|$, where $\|x - y\|$ is the Euclidean distance between x and y. We write κ_n for the volume of B_n. According to the Steiner formula the volume V_n of X_ε is a polynomial in ε of degree at most n

$$V_n(X_\varepsilon) = \sum_{j=0}^{n} \varepsilon^{n-j} \kappa_{n-j} V_j(X).$$

This formula defines the intrinsic volumes $V_0, V_1, \ldots, V_n$ and we extend the definition by $V_j(\emptyset) = 0$. The *volume* V_n, *surface area* $2V_{n-1}$ and the *Euler characteristic* V_0 are of special interest. We also write $\chi(X)$ for the Euler characteristic of X, whenever defined. We note that if $X \subseteq \mathbb{R}^1$ is compact, $\chi(X)$ is the number of connected components of X. We equip $\mathcal{K}^n \setminus \{\emptyset\}$ with the Hausdorff metric δ defined by

$$\delta(X, Y) = \min\{\varepsilon \geq 0 \mid X \subseteq Y_\varepsilon, Y \subseteq X_\varepsilon\}.$$

The intrinsic volumes can be characterized by simple geometric properties. A real function $\phi : \mathcal{K}^n \to \mathbb{R}$ is additive if

$$\phi(X \cup Y) + \phi(X \cap Y) = \phi(X) + \phi(Y),$$

for all $X, Y \in \mathcal{K}^n$ with $X \cup Y \in \mathcal{K}^n$, and $\phi(\emptyset) = 0$. Hadwiger's famous characterization theorem states that any additive, motion invariant and continuous function $\phi : \mathcal{K}^n \setminus \{\emptyset\} \to \mathbb{R}$ is a linear combination of intrinsic volumes. A proof of the characterization theorem in three dimensions was given in [Had51] and in arbitrary

dimension in [Had52]; see also [Had57]. We will frequently work with a generalization of $\mathcal{K}^n$, the so-called class of *polyconvex* sets. If a set can be represented by a finite union of convex bodies in $\mathbb{R}^n$ we say that it is a polyconvex set in $\mathbb{R}^n$. The intrinsic volumes can be additively extended to polyconvex sets (but then continuity is lost) and to even more general set classes.

2.2 Linear and affine subspaces

Most stereological formulae that we will consider later on, will be based on sections with *linear* or *affine* subspaces. We let $\mathcal{L}^n_{j[O]}$ be the family of all j-dimensional linear subspaces of $\mathbb{R}^n$, $j \in \{0, 1, \ldots, n\}$, and $\mathcal{L}^n_j$ be the family of all j-dimensional affine subspaces of $\mathbb{R}^n$. We typically denote their elements by $L^n_{j[O]}$ and L^n_j, respectively. These spaces are equipped with their standard topologies [SW08]. There exists a unique rotation invariant measure on $\mathcal{L}^n_{j[O]}$ and a unique motion invariant measure on $\mathcal{L}^n_j$, up to multiplications with a positive constant. We write $\mathrm{d}L^n_{j[O]}$ and $\mathrm{d}L^n_j$, respectively, when integrating with respect to these invariant measures and refer to [SW08] for their construction. We use the same normalization as in [SW08]:

$$\int_{\mathcal{L}^n_{j[O]}} \mathrm{d}L^n_{j[O]} = 1 \quad \text{and} \quad \int_{\{L^n_j \in \mathcal{L}^n_j \mid L^n_j \cap B_n \neq \emptyset\}} \mathrm{d}L^n_j = \kappa_{n-j}.$$

We call a random linear subspace whose distribution is given by the rotation invariant measure an *isotropic random* (IR) subspace. Similarly we say that a random $L^n_j \in \mathcal{L}^n_j$ is *isotropic uniform random* (IUR) *hitting a compact object* Y if and only if its distribution is given by

$$\mathbb{P}_{L^n_j}(A) = c \int_{\mathcal{L}^n_j} \mathbf{1}_{A \cap \{L^n_j \in \mathcal{L}^n_j \mid L^n_j \cap Y \neq \emptyset\}} \, \mathrm{d}L^n_j,$$

where c is a normalizing constant and A is a Borel-set on $\mathcal{L}^n_j$.

2.3 Blaschke-Petkantschin type measure decompositions

Measure decompositions are of great importance when constructing local stereological estimators. Frequently used decompositions are the ones of Blaschke-Petkantschin type. We adopt the explanation in [SW08] to describe the common feature of these formulae: When a tuple of geometric objects is to be integrated over a product of measure spaces, we can associate a so-called 'pivot' to the tuple (typically span or intersection) and decompose the integration into an inner integration of the tuple restricted to one pivot and an outer integration which is over all possible pivots. The integrations are with respect to the natural measures. This decomposition of the integration often allows for much simpler computation of the initial integral.

In the linear (classical) Blaschke-Petkantschin formula the geometric objects are j points in $\mathbb{R}^n$, $j \in \{1, \ldots, n\}$, the initial integration space is the j-fold product of Lebesgue measure in $\mathbb{R}^n$, the pivot is $L^n_{j[O]} \in \mathcal{L}^n_{j[O]}$ that is (almost surely) spanned

by the j-tuples of points and the outer integration space is $\mathcal{L}^n_{j[O]}$. The linear formula is due to [Bla35] and [Pet35] but as remarked in [Mil79], it was first fully stated in [Mil71]. The linear formula has led to a series of further measure decompositions for which [Mil79] and [San04] are good references. A generalized Blaschke-Petkantschin formula, where Lebesgue measures are replaced by Hausdorff measures, was presented in [Zäh90] and [JK92].

We are in particular interested in a formula of Blaschke-Petkantschin type where there is only one geometric object, which is an affine subspace $L^n_j \in \mathcal{L}^n_j$, $j \in \{0, \ldots, n-1\}$, the initial integration space is $\mathcal{L}^n_j$, the pivot is a linear subspace of dimension $j+1$ containing the affine subspace, the inner integration space is over all affine subspaces in the fixed linear subspace and the outer integration space is $\mathcal{L}^n_{j+1[O]}$. This is a special case of [Pet35, Formula (49)]. For all non-negative measurable functions f on $\mathcal{L}^n_j$ and $j \in \{0, 1, \ldots, n-1\}$ it can be written as

$$\int_{\mathcal{L}^n_j} f(L^n_j) \mathrm{d}L^n_j = c_1^{n-j} \int_{\mathcal{L}^n_{j+1[O]}} \int_{\mathcal{L}^{j+1}_j} f(L^{j+1}_j) d(O, L^{j+1}_j)^{n-j-1} \mathrm{d}L^{j+1}_j \mathrm{d}L^n_{j+1[O]}, \qquad (1)$$

where c_1^{n-j} is a known constant that depends on n and j (see (B.1)). Notice that for $0 \leq j \leq r \leq n$ and a fixed $L^n_{r[O]} \in \mathcal{L}^n_{r[O]}$ we write $\mathcal{L}^r_j$ for the family of all j-dimensional affine subspaces L^r_j within this linear subspace. In stereological terms, (1) states how an affine hyperplane in an IR subspace must be chosen such that it is motion invariant in $\mathbb{R}^n$. For example, with $n = 3$ and $j = 1$ this gives another way of generating a line that is IUR in three-dimensions. As the line is chosen in an IR two-dimensional section plane this eliminates the need for three-dimensional scanning of objects. This construction of an IUR line was rediscovered in local stereology in [CO05] and (1) (with $n = 3$ and $j = 1$) was given the name *invariator principle* in [CO09]. In [GACO09] equation (1) was generalized to Riemannian manifolds with constant sectional curvature.

3 Classical vs. local stereology

Local stereology came later than classical stereology but it is gradually developing and is now considered a very powerful tool in biomedicine, in particular in neuroscience and cancer grading. Examples of recent applications of local stereology are [AGP03], [HSN07] and [HKK$^+$06]. All the results obtained in this thesis are important bricks that complement local stereology, where classical stereology is more developed. To emphasize this we give an overview of typical methods in classical stereology and compare them with their counterparts in local stereology, if present. We divide this brief survey into procedures for obtaining specific geometric summary statistics and procedures for constructing particle distributions.

3.1 Geometric summary statistics

The essence of stereology is to reduce complicated measurements to simpler ones. Hence integral geometric identities of the form

$$\beta(X) = \int \alpha(X \cap T)\mathrm{d}T, \tag{2}$$

are essential. Here X is the object of interest, $\alpha(\cdot)$ and $\beta(\cdot)$ are geometric characteristics, T is the sampling probe and the integration is over all possible positions of the probe with respect to a natural measure (appropriate 'uniform integration'). The functional $\alpha(\cdot)$ to be measured on a section will be called a *measurement function*. In many cases considered in this thesis, the measurement function is itself obtained by sampling the section profile in T. We will discuss efficient ways to calculate this measurement function focusing in particular on simplicity (low workload) and precision (low variance). The *Fundamental Formulae of Stereology* are a collection of results of the form (2), where T runs through all affine subspaces; see for example [BJ05, Chapter 2]. The oldest of these is Delesse's principle which shows that the average fraction of volume of a mineral in a homogeneous rock equals the average fraction of area of the mineral on a plane section of the rock; see [Del47] and [Del48]. More specifically, the observed area fraction in a plane section of a homogenous structure is an unbiased estimator for the true volume fraction in the original structure. This gives a practical method for determining the composition of rocks as volume estimation has been reduced to the more simple area measurement.

All the Fundamental Formulae of Stereology are applications of Crofton's formula, which is a classical result of integral geometry. The classical Crofton formula is of the form (2) where the probe is an affine subspace $L_j^n \in \mathcal{L}_j^n$, $\beta(\cdot)$ and $\alpha(\cdot)$ are the intrinsic volumes and the integration is over $\mathcal{L}_j^n$ with respect to its motion invariant measure. Hence Crofton's formula relates geometric characteristics of a spatial structure to properties on affine sections of the structure. According to Hadwiger's theorem, Crofton's formula cannot be extended to any other geometric characteristics without loosing desirable properties. This does though not imply that Crofton's formula is the only integral geometric identity with practical relevance for stereology. The counterpart of Crofton's formula in local stereology are so called *rotational Crofton formulae*. These are versions of (2) where the probe is a linear subspace $L_{j[O]}^n \in \mathcal{L}_{j[O]}^n$ and the integration is over $\mathcal{L}_{j[O]}^n$ with respect to its rotation invariant measure. In other words, rotational Crofton formulae are versions of Crofton's classical formula that only use linear sections.

Examples of important choices of $\beta(\cdot)$ in (2) are the *area* and the *boundary length* of planar objects and the *volume* and the *surface area* of three-dimensional objects. We describe in the following procedures from classical stereology and local stereology for obtaining unbiased estimators of these important summary statistics. Unbiasedness is a desirable property of an estimator but good precision obtained with 'reasonable' amount of workload is as important. A commonly used procedure to increase the precision of an estimator is to apply systematic sampling. Systematic sampling is a standard variance reduction method in classical sampling theory and

it is typically much more efficient than simple random sampling. Throughout this section we assume that the object of interest X is fixed and arbitrary and we sample it with a random probe, that is we describe estimators in a design-based setting. More details for the classical procedures can be found in [BJ05] and references therein. For the local procedures we recommend [Jen98].

3.1.1 Geometric summary statistics obtained using classical procedures

When X is a compact planar object, its area can be estimated by superimposing a random point grid on the plane. The grid can for example be a rectangular grid with horizontal spacing r and vertical spacing s and with the origin chosen uniformly in a square of area rs. An unbiased estimate of the area of X is obtained by counting the number of grid points that hit X (and multiplying by rs). An explicit analytic expression for the variance of this estimator is not available but there is much literature on this subject; see [BJ05, p. 327] for references. In analogy, a spatial point grid can be used to estimate the volume of a compact three-dimensional object X. A more frequently used estimator for volume is the *Cavalieri estimator* (also called 'estimation of volume by Cavalieri's principle'). The three-dimensional object X is sliced by a systematic equally spaced stack of parallel, two-dimensional affine planes. An unbiased estimator for the volume of X is obtained by measuring the area covered by the object in each slice, summing up these areas for all the sections and multiplying by the spacing between the planes.

These estimators for volume and area do not require a randomized orientation of the probe but this randomization is essential for estimating length and surface area. The key tool here is Crofton's formula. A well-known estimator for the length of a planar rectifiable curve is the *Steinhaus estimator*. The procedure has its roots in Buffon's famous needle problem. An equally spaced IUR grid of parallel test lines is superimposed on the plane and the number of intersections of the line grid with the curve are counted. By summing up over the number of intersections and multiplying by a known constant, an unbiased estimator for the length of the curve is obtained. The length of a curve in space can be obtained from an equally spaced IUR stack of parallel two-dimensional affine planes. This is equivalent to the Cavalieri estimator but now the orientation of the planes needs to be IR (that is the unit normal of the planes is IR). Hence this design is sometimes referred to as the *isotropic Cavalieri* design. An estimate of the length of a rectifiable curve in space is obtained by counting the number of intersections of the curve with the IUR stack of planes (and multiplying by a known constant). An IUR stack of planes can also be used to estimate the surface area of the boundary of a three-dimensional object X. Then counting is replaced by measuring the boundary length of the object in each slice, summing up the contributions from all slices and multiplying by a known constant. Counting the number of intersections with a systematic grid of IUR lines (and multiplying by a known constant) also gives an unbiased estimator for the surface area.

The length of a planar curve can also be estimated by a method known as

the *area tangent count* method. The idea of the method is to sweep a line, at a uniformly chosen direction, through the plane and find all translates of the line that are tangent to the curve. Tangents that represent an increase in the number of connected components (of the sweeping line section with the curve) are called 'positive tangents' and those that represent a decrease in the number of connected components are called 'negative tangents'. All other tangents, for instance tangents through inflection points, are disregarded (these tangents do almost surely not occur). An estimate of the length of the curve is obtained by subtracting the number of negative tangents from the number of positive tangents (and multiplying by a known constant). When the planar curve is the result of taking a random section through a surface in space, this method gives the integral mean curvature of the surface.

3.1.2 Geometric summary statistics obtained using local procedures

Many of the well-established procedures in local stereology can be derived from rotational Crofton formulae. A rotational Crofton formula, in its most general form, can be written as

$$\beta(X) = \int_{\mathcal{L}^n_{j+1[O]}} \alpha(X \cap L^n_{j+1[O]}) \mathrm{d}L^n_{j+1[O]}, \tag{3}$$

$j = 0, 1, \ldots, n-1$, for suitable X and functionals $\alpha(\cdot)$ and $\beta(\cdot)$. In [JR08] the functional $\beta(\cdot)$ was calculated when the measurement function is an intrinsic volume of the section profile. As already implied, the 'opposite' problem, i.e. how to calculate $\alpha(\cdot)$ to obtain a desired geometric characteristic $\beta(X)$ of X, is of more interest in stereology. When the work behind this thesis started there existed well established local procedures for estimating the area of a planar region, the length of a planar curve (the *Horvitz-Thompson* estimator) and the volume of a three-dimensional object (the *nucleator*). There also existed surface area estimators but none which had gained critical acclaim. We describe the typical local procedures for the estimation of these geometric characteristics. For simplicity we assume that the objects contain O in their interior, are star-shaped at O and have smooth boundaries. As mentioned earlier, more details about these procedures can be found in [Jen98].

The area of a compact, planar object and its boundary length can be unbiasedly estimated by sampling the object at a uniformly chosen direction in the section plane. To obtain the area we need to measure the squared radial function (distance to the boundary) at the uniformly chosen direction. In order to obtain the length of the boundary, both the radial function at the sampled direction and an angle in the section plane need to be measured. The angle that needs to be measured is formed by the outer unit normal to the object at the boundary point (for the given direction) and the line connecting this boundary point with O. The variance of both procedures can be decreased by applying angular systematic sampling in the section plane, for example also considering the opposite direction, which corresponds to sampling with an IR line in the plane instead of only a ray, or even using two perpendicular lines passing through O.

The volume and the surface area of a three-dimensional structure can be unbiasedly estimated by using a sampling procedure that consists of two steps. First the object is intersected by an IR two-dimensional plane and then in that section plane a uniform direction is chosen. To estimate the volume, the radial function at the sampled direction needs to be measured (and raised to the power of three). The resulting estimator is the nucleator. Here, variance reduction can also be achieved by using angular systematic sampling and the nucleator with four sampled rays (two perpendicular lines) is much used in practice. The integrated nucleator requires measuring the distance to every boundary point of the section profile and it is therefore only feasible in practice if automatic identification of the boundary of the section profile is possible. The available local stereological estimator for surface area is the *surfactor*. It requires measuring both the radial function at the sampled direction in the section plane and the angle between the unit normal to the section profile at the boundary point and the line connecting this boundary point with O. On the contrary to what was implied in [CO05], the surfactor does neither seem to be much affected by the singularity in its representation nor by inaccuracies in the necessary angle measurements as shown very recently in a simulation study involving ellipsoids [DJ13]. Nonetheless, angle measurements are cumbersome in practice and, to our knowledge, the surfactor has only been used to estimate surface area in [KCO97] and [TGJ97]. As for the other procedures the variance can be decreased by applying angular systematic sampling in the plane.

Quite recently, new local estimators for surface area and volume were derived. These estimators are based on a rotational Crofton formula that is obtained by combining the invariator principle (1), with $n = 3$ and $j = 1$, and the classical Crofton formula and they are referred to as *invariator estimators*; see [CO05]. The invariator estimator for volume does not seem to enjoy any particular advantages over the nucleator but the invariator estimator for surface area presents a very simple and interesting alternative to the surfactor. The invariator estimator for surface area (which we call the invariator estimator from now on) plays a central role in this thesis and is discussed further in Section 4.1. We propose a new surface area estimator, which is based on the invariator estimator. This new estimator does not involve angle measurements and it requires less workload than the invariator estimator to obtain a given precision. One of the main goals of this thesis is to promote this new estimator and show its applicability in biological sciences.

3.2 Particle distributions

We now discuss problems of a different nature, where the goal is not only to estimate some geometric summary statistics of objects but rather the distribution of objects, that is, the distribution of the shape, where the objects are assumed to belong to a certain family of shapes. An introduction to stereological particle analysis can be found in [BJ05, Chapter 11]. In this section we restrict attention to three-dimensional objects.

3.2.1 Particle analysis using classical procedures

In the tissue of many organs, e.g. in the thymus, there are a number of small, regularly shaped particles. These particles can vary considerably in size within the same organ. The number of particles and their size distribution can also vary considerably between different organs and between different individuals. Almost a century ago anatomists were interested in estimating the *size distribution* of these particles from observations in plane sections. Determining size distributions from random samples is intractable without strict shape assumptions. The mathematical statistician S.D. Wicksell showed that under the assumption that the particles are spherical, their size distribution can be uniquely determined from plane sections [Wic25]. Wicksell's arguments were made rigorous in [SKM95] where it was shown that when a stationary particle process of non-overlapping balls, with finite mean radius, is intersected by a plane, the size distribution of the original balls and the size-distribution of the section profiles are essentially connected by an *Abel integral equation* which can be inverted explicitly. It was shown in [Jen84] that the aforementioned integral equation also holds in a design-based setting. There exists much literature on Wicksell's classical problem, as can be seen from the surveys [SKM95, Section 11.4] and [CO83] and references therein. It has for example been shown that the radius of the section profile can be expressed in terms of the size-weighted radius of the intersected ball [BJ05], which also lead to moment relations.

Wicksell was aware of the fact that planes sample balls with probability proportional to their radii and that the radii of section profiles are almost surely smaller than the original radii. These two sampling effects can cancel each other. When the radii of the balls follow a Rayleigh distribution, the profile radii also follow this distribution with the same parameter. It was shown in [DR92] that the Rayleigh distribution is the only *reproducing distribution* in this sense. Despite the fact that the Abel integral equation associated to Wicksell's problem can be solved explicitly, there are both statistical and numerical obstacles in implementing the solution. Several methods have been suggested in order to overcome the moderate *ill-posed* nature of the problem. As remarked in [SKM95] it could even be claimed that the problem serves as a playground for the application of regularization methods in inverse problem theory.

Wicksell [Wic26] extended some of his results to prolate spheroids (ellipsoids with main axes a_1, a_2 and a_3 satisfying $a_1 = a_2 < a_3$) and oblate spheroids ($a_1 = a_2 > a_3$), of variable size but fixed shape. In [CO76] it was shown in full generality that Wicksell's problem can be solved for spheroids of the same type but that the problem is indetermined for general ellipsoids and for populations consisting of both prolate and oblate spheroids

In some practical applications the distribution of the tail of a particle size distribution is of more interest than the whole distribution. This tail behaviour can for example be of interest when damage of materials is studied [MB99]. *Stereology of extremes* is concerned with the study of extremal parameters using lower dimensional sections and it has received increasing interest in the recent years. It has been shown

that in the classical Wicksell problem the size distributions of the balls and their section profiles belong to the same type of extreme value distribution. This has also been studied for the size and shape parameters of spheroidal particles; see [Hlu03a], [Hlu03b], [Hlu06] and [BBH03].

3.2.2 Particle analysis using local procedures

In [Jen91] it was remarked that Wicksell's problem in a local setting is trivial when the reference point coincides with the ball's center. Another main goal of this thesis is to show that Wicksell's problem in a local setting is far from trivial when this restrictive assumption is violated.

Stereology of extremes in a local setting was treated in [Paw12] for spheroids where the isotropic section plane was passing through the spheroid's center. We remark that this assumption on the position of the section plane is quite restrictive. We show in Paper A that this restriction is not necessary when dealing with spherical particles. To the best of our knowledge, [Paw12] has been the only study of stereology of extremes in a local setting before the present thesis.

4 Motivation

As pointed out earlier, the invariator principle was rediscovered in local stereology in [CO05], a paper that was the starting point of the master's thesis [Thó10]. The results obtained in [Thó10] in turn prompted the work presented in this thesis. We introduce the invariator estimator, describe the main results obtained in [Thó10] and give an outline of the papers that constitute this thesis.

4.1 The invariator estimator

One of the ultimate goals of this thesis is to derive a new improved surface area estimator that would become the preferred stereological tool for surface area estimation in local stereology and applicable to a broad class of objects. Surface area estimation is important in many practical applications. For example, cells with larger surface area often have a larger ability of exchanging ions and organic molecules with their environment than cells with small surface area. Surface area is also of interest when studying schizophrenia. In [PMJ$^+$11] it was shown that patients with schizophrenia have regions in the brain with significant localised surface area contraction as compared to healthy individuals (after age and total surface area have been corrected for).

In Section 3.1.1 it was mentioned that in classical stereology the surface area of the boundary of a three-dimensional object can be unbiasedly estimated by sampling the object with an IUR line and counting the number of intersections of the line with the boundary of the object. The invariator principle (1), with $n = 3$ and $j = 1$, presents a local analogue of this estimator, as it shows how a line in a two-dimensional IR plane should be generated such that it is IUR in three-dimensions.

The resulting estimator is the invariator estimator [CO05, first eq. (2.12)]. As the invariator estimator is based on sampling the object of interest with an IUR line, the object should be contained in a reference set (as the motion invariant measure on the family of all affine subspaces is not finite). We take the reference set to be a ball RB_3 of radius $R > 0$, centered at O. Let $X \subseteq RB_3$ be a compact object with smooth boundary. The invariator estimator can be expressed as

$$\hat{S}_{\text{inv}} = 4\pi R^2 \chi(X \cap L^3_{2[O]} \cap (z + z^\perp)), \tag{4}$$

where $L^3_{2[O]} \in \mathcal{L}^3_{2[O]}$ is an IR plane, $z \sim \text{unf}(RB_3 \cap L^3_{2[O]})$ and $z + z^\perp$ is the line in the section plane $L^3_{2[O]}$, that passes through O and is orthogonal to the axis joining z with O. We note that $\hat{S}_{\text{inv}}$ is an unbiased estimator for the surface area of the boundary of X for any given reference set containing X.

4.2 Variance decomposition

The main goal of the master's thesis [Thó10] was to study the variance of the invariator estimator $\hat{S}_{\text{inv}}$. This study gave some interesting results which we briefly describe in the following. In [Thó10] we restricted attention to convex bodies in $\mathbb{R}^3$ as then the estimator $\hat{S}_{\text{inv}}$ is particularly easy to calculate. When $X \in \mathcal{K}^3$, the Euler characteristic in (4) equals one if the line hits the section profile $X \cap L^3_{2[O]}$ and is otherwise zero, that is

$$\chi(X \cap L^3_{2[O]} \cap (z + z^\perp)) = \mathbf{1}_{\{X \cap L^3_{2[O]} \cap (z+z^\perp) \neq \emptyset\}}.$$

The invariator estimator is obtained by choosing three random variables: an IR section plane and each of the two polar coordinates of a uniformly distributed point in the section plane. The variance of $\hat{S}_{\text{inv}}$ can be decomposed into the contribution due to each of these three random variables. For a given IR section plane $L^3_{2[O]}$, let (r, u) be the polar coordinates of $z \sim \text{unf}(RB_3 \cap L^3_{2[O]})$, with $r \in [0, \infty)$ and $u \in S^2 \cap L^3_{2[O]}$. From the conditional version of the law of total variance [BS12], we find that

$$\mathbb{V}\text{ar}(\hat{S}_{\text{inv}}) = V_{\text{dist}} + V_{\text{orient}} + V_{\text{plane}}, \tag{5}$$

where

$$V_{\text{dist}} = \mathbb{E}\,\mathbb{V}\text{ar}(\hat{S}_{\text{inv}} | L^3_{2[O]}, u)$$

is the variance contribution from choosing the distance of the line $ru + u^\perp$ from O,

$$V_{\text{orient}} = \mathbb{E}\,\mathbb{V}\text{ar}(\mathbb{E}[\hat{S}_{\text{inv}} | L^3_{2[O]}, u] | L^3_{2[O]})$$

is the variance contribution from choosing the orientation of the line $ru + u^\perp$ in the section plane and

$$V_{\text{plane}} = \mathbb{V}\text{ar}\,\mathbb{E}[\hat{S}_{\text{inv}} | L^3_{2[O]}]$$

is the variance contribution from choosing the IR section plane $L^3_{2[O]}$. These different variance contributions were given more explicitly in [Thó10, Theorem 22] and were

in particular studied for ellipsoids. It is presumably not possible to obtain explicit analytic expressions for the different variance contributions when X is a three-dimensional ellipsoid and we therefore turned to numerical methods for calculating them. The general conclusion of an extensive simulation study in [Thó10] was that V_{dist}, the variance from choosing the distance of a uniformly distributed point from O, is much larger than the other two variance contributions. This result of [Thó10] was exciting as it is possible to eliminate V_{dist} without too much workload and hence obtain a new improved surface area estimator. The contribution V_{dist} can be eliminated by, instead of generating a line, measuring the support function for a uniformly chosen direction in the section plane. This was already suggested in [CO05] and called one-ray *pivotal estimator* in [CO08]. The draw-back of the pivotal estimator is that it only holds for convex bodies.

In [CO05] another improvement of the invariator estimator for surface area was suggested, which also reduces variance. The estimator is called the *invariator grid estimator* and we denote it by $\hat{S}_{\text{grid}}$. It does not require that the object of interest is a convex body. It obtains its variance reduction from random systematic sampling in the section plane. Instead of only using one test line, a random grid of test lines is used in the section plane. This is expected to decrease V_{orient} and possibly also V_{dist}. We considered an alternative systematic sampling approach in the section plane, which also does not require convexity assumptions. For a given direction in the section plane a random grid of parallel test lines could be used to decrease the variance. The distances of the test lines should though not be uniform, but weighted. This would expectedly decrease V_{dist}. We did not follow this idea through as we found a way to eliminate this variance contribution V_{dist} altogether. More specifically, we succeded in deriving an estimator, which enjoys the variance reduction of the pivotal estimator but does not require that the object under study is convex. This is a major advantage as clinical experts are often skeptic of convexity assumptions. We call this new estimator *Morse-type surface area estimator* and present it in Paper B and Paper C.

4.3 Composition of the papers

In the following sections we summarize the main results obtained in Paper A, Paper B and Paper C.

In Section 3.2.1 we saw that the size-distribution of spherical particles can be uniquely determined from the size-distribution of plane sections. It is of interest to analyse if an analogue result can be obtained in a local setting. This is the goal of Paper A. Without the strong shape assumption of spherical particles, a local shape distribution estimation is out of reach, and expectedly impossible. However, it is possible to estimate certain geometric characteristics as detailed in 3.1. The main geometric characteristic of interest in Paper B and Paper C is the surface area.

Although the invariator principle was only rediscovered in local stereology a few years ago its use and applications have stretched far. Paper B collects and, where possible, generalizes invariator related results. The main new contribution is

a new rotational Crofton formula involving *Morse theory*. The Morse type surface area estimator is based on this new rotational Crofton type formula. Paper B is rather mathematical and Paper C is meant to make the Morse type estimator more easily accessible to the applied stereological community. In Paper C the estimator is illustrated in a study of giant-cell glioblastoma using an expert-assisted procedure. Although stereology is mainly concerned with three-dimensional objects, most of the results in Paper A and Paper B are presented for objects in arbitrary dimension, as this does not pose any essential extra difficulties. In Paper C we restrict attention to $\mathbb{R}^3$ but many of the results can easily be generalized to arbitrary dimension.

5 Wicksell's problem in local stereology

As mentioned in Section 3.2.1 there exists a vast amount of literature on the classical Wicksell problem but it has never been studied in a local setting. Paper A is meant to fill that gap and is therefore a good complement to the existing literature. In the accepted version of the paper, some technical parts have been suppressed and the interested reader is instead referred to the technical report [TK12]. We have included these technical parts as 'Supplementary material' in A.I–A.III.

5.1 Local Wicksell

In a local design-based setting of Wicksell's corpuscle problem we consider deterministic n-dimensional (approximate) balls, each with a fixed reference point O. We write R for the radius of a ball, and assume that it is positive, and Q for the relative distance of the ball's center O' from the reference point O. Up to rotations, a ball is determined by R and Q (that is, we do not consider the direction of the reference point relative to the ball's center) and these quantites are assumed to be random. When a ball containing O is intersected by an IR hyperplane $L^n_{n-1[O]}$, independent of the ball, an $(n-1)$-dimensional ball is obtained almost surely. We write r for the radius of the $(n-1)$-dimensional ball and $q = \frac{1}{r}\|O'|L^n_{n-1[O]}\|$ for the relative distance of its center from O. In analogy to Wicksell's classical problem, we ask if the joint distribution of the *particle parameters* (R, Q) can be determined from the joint distribution of the *profile parameters* (r, q). We refer to this problem as the local version of Wicksell's classical corpuscle problem. As remarked in Section 3.2.2 the local version is trivial when the reference point coincides with the ball's center. When $Q = 0$ the size distributions of balls and section profiles are identical. In Paper A we assume $\mathbb{P}(Q = 0) = 0$. Most of the results can easily be extended to the case $\mathbb{P}(Q = 0) > 0$. We remark that when the reference point of a three-dimensional ball lies on the boundary of the ball, $Q = 1$ a.s., the local Wicksell problem becomes equivalent to the classical Wicksell problem, as the central section can then be considered to be an IUR plane hitting the ball.

The local Wicksell problem shares many similarities with the classical Wicksell problem and in order to describe these, as well as differences between the two, Paper A starts off with a short outline of known results for the classical problem.

It then proceeds with an overview of the main results obtained in the paper but we restate these in the following, concentrating on numerical reconstruction. In the local Wicksell problem there is no size-weighting as in the classical Wicksell problem. Hence, as the radii of the section profiles are smaller than the radii of the respective balls there does not exist a reproducing distribution in the local Wicksell problem (under the assumption $\mathbb{P}(Q > 0) > 0$). The main result of Paper A is that the *joint cumulative distribution function* $F_{(r,q)}$ of the profile parameters can be given in terms of the joint distribution of the particle parameters (R, Q). As one of the profile variables determines the other whenever Q and R are given, there need not exist a *joint probability density function* of (r, q). It is however not difficult to show that the *marginal* distribution functions F_r and F_q always have probability densities. From the integral transform connecting $F_{(r,q)}$ and $F_{(R,Q)}$ it is immediately obtained that F_q *uniquely* determines F_Q. More specifically, F_q and F_Q are connected by an Abel type integral equation which can be inverted explicitly (we give an explicit solution when $n = 3$). Furthermore, when R and Q are independent, $F_{(r,q)}$ can be shown to uniquely determine $F_{(R,Q)}$ but it is still an open problem if this holds when the independence assumption is dropped. When only the marginal distributions F_q and F_r are given this is not the case, as shown by a counterexample.

Many of the results in Paper A require that the particle parameters are independent, that is the size of the particle and the position of its reference point should be independent. There does not appear to be any easy way to check this independence assumption from section profiles, as the profile parameters seem to always be dependent apart from mathematically trivial cases (for instance when $Q = 1$ a.s.). Hence independence is assumed a priori. We believe that this assumption is realistic in many practical applications.

To proof the uniqueness conjecture under the independence assumption, we used the interesting result that the profile radius can be represented as a multiple of R and a random variable Γ, whose density can be given explicitly as a function of Q. This is in analogy to the classical problem (but here R is not size-weighted and the random variable depends on Q). As Γ only depends on (R, Q) through Q, *moment relations* can be obtained when R and Q can be assumed to be independent. If m_k and M_k are the kth moments of r and R, respectively, then $m_k = c_k(Q)M_k$, $k \in \{0, 1, 2, \ldots\}$, and the constants $c_k(Q)$ can be given in terms of F_Q. We show that when $n = 3$, $c_k(Q)$ can also be given in terms of F_q which is very useful in practice as it allows us to access M_k from the section profiles. An extensive simulation study indicates that this estimation procedure is quite stable for moments up to 7th order. This procedure opens up the possibility to determine the parameters in a parametric model of R, thus allowing for a semi-parametric model, where only R, but not Q, needs to follow a parametric model.

It was mentioned in Section 3.2.1 that the size distributions in the classical Wicksell problem belong to the same type of extreme value distributions. This nice result also holds for the marginal distributions in the local setting, given that the particle parameters R and Q are independent.

5.2 Reconstruction methods

Although most of the results in Paper A are theoretical, considerable time was spent on reconstructing the marginal distributions F_R and F_Q when $n = 3$ from given section profiles. Up to date, none of the several suggested methods for the classical problem seems to be superior to all others. We considered three existing distribution-free methods for numerically solving the local problem when the particle parameters are independent. In Paper A we only discuss one of these methods and remark that the other two did not give satisfactory results.

The method that performed well in the local setting is a *Scheil-Schwartz-Saltykov type* method [Sal74]. In [BMN84] six distribution-free methods for solving the classical Wicksell problem were compared. The Scheil-Schwartz-Saltykov method performed well and it is relatively easy to implement. The idea is to group the data and discretize F_Q and F_R. Then the Abel type integral equation relating F_Q and F_q becomes a system of linear equations that can be solved. This gives an estimator for F_Q which can be used to write F_r in terms of $F_{(R,Q)}$ as a system of linear equations which can be solved. The feasibility of the approach is illustrated in a simulation study involving various different distributions and choices of bin width. The method even gives satisfactory results when the profile variables are measured with moderate random multiplicative errors or when small profiles are omitted. These problems are often encountered in practice.

The other two more advanced numerical methods that we studied are *product integration* and *kernel density estimators*. Both of these methods were applied to the integral transform connecting F_Q and F_q (that is, we only reconstructed F_Q from the section profiles). The product integration method is explained in [AJ75] where it is claimed to yield accurate results for the classical Wicksell problem. We used the method on the inverted Abel type integral equation giving F_Q in terms of F_q. The idea of the method is to smooth the sample distribution function with a localised Lagrange interpolation and then to integrate the singularity (in the integral equation) out analytically. The obtained reconstructions of F_Q approximate the true distribution function quite well on average but fluctuate far too much around the true value to be of any use. We also used a quartic kernel smoothing for f_q that allowed to express f_Q in terms of a linear combination of numerous incomplete Beta functions. However, this reconstruction was not stable.

6 Rotational Crofton-type formulae using the invariator principle

The idea of the Morse type surface area estimator is quite simple and it is based on a modification of the area tangent count method, which was discussed in Section 3.1.1 for estimating planar curve length and the integral mean curvature of surfaces. Prompted by a remark of Professor Jan Rataj we decided to use classical *Morse theory* to describe this new estimator, which explains the appellation 'Morse type surface

area estimator'. The analogy of the estimator to the area tangent count method is deferred to Section 7.1. Paper B presents new rotational Crofton formulae, the most important one being a rotational Crofton formula involving Morse theory. The Morse type estimator is derived from a special case of this formula, for objects in arbitrary dimension.

We mentioned earlier that a functional $\alpha(\cdot)$ satisfying (3), where $\beta(X)$ is an intrinsic volume, is obtained by combining the classical Crofton formula and the invariator principle, as shown in [AJ10, Proposition 1] and, independently, in [GACONnB10, Theorem 3.1 with $\lambda = 0$]. As the invariator principle is simply a measure decomposition, analogous results can be obtained using variants of the classical Crofton formula. These variants include a local version of Crofton's formula [Gla97, Theorem 3.4] involving the support measures of polyconvex sets and a Crofton formula for manifolds [Jen98, Proposition 3.7]. These generalizations are treated in Paper B. In [ACZJ12] the invariator principle was combined with a Crofton formula for Minkowski tensors of convex bodies [HSS08, Theorem 2.2].

These rotational Crofton-type formulae do not give an explicit form of the functional $\alpha(\cdot)$ to be measured on the linear section. We give more explicit representations of the measurement function in Paper B. When the volume is sought for, a particularly simple representation for the measurement function is obtained. This representation requires no assumptions on the geometric structure of interest, apart from measurability. Other representations include:

(i) writing the measurement function associated to the curvature measures as an integral over the boundary of the section profile,

(ii) writing a special case of the measurement function associated to the intrinsic volumes in terms of the radial function of the section profile and an angle in the section plane,

(iii) writing a special case of the measurement function associated to the Hausdorff measures, intrinsic volumes, respectively, in terms of so-called critical values of the section profile.

These representations require different regularity assumptions on the object of interest. Representation (i) involves the principal curvatures and the object is therefore assumed to be a convex body with boundary of class C^2. Representation (ii) still requires that the object is convex but the C^2 smoothness assumption can be dropped if O is contained within the interior of the object. Representation (iii) for the Hausdorff measures requires that the object is a compact, smooth manifold while it should be a polyconvex set when the intrinsic volumes are considered. These different representations all play a role when rotational formulae are applied in stereology, a special case of the volume representation is e.g. the *integrated nucleator* whereas a special case of representation (ii) is the integrated surfactor [CO12, Eq. (24)]. In [AJ10, Proposition 3] representation (i) was derived for the intrinsic volumes. Repre-

sentation (iii) is of most interest, as it leads to the Morse type surface area estimator, and we account for it briefly in the following.

6.1 A rotational Crofton formula involving Morse theory

In Paper B we first apply classical Morse theory to the section profile $Y = X \cap L^n_{j+1[O]}$, $j \in \{0, 1, \ldots, n-1\}$, and we therefore require that this profile has a smooth boundary (this is satisfied under the assumption that X is a compact, smooth manifold of dimension $n-j$ that intersects $L^n_{j+1[O]}$ transversely in $\mathbb{R}^n$ for almost all $L^n_{j+1[O]} \in \mathcal{L}^n_{j+1[O]}$). We later show that also non-smooth sets can be allowed. To show this we assume that the section profile is polyconvex (which is satisfied when X is polyconvex), and the Morse indices (to be defined later) have to be replaced by a Hadwiger type index [Had55].

Let X be a compact, smooth manifold of dimension $n-j$ that satisfies the weak regularity condition mentioned above. For $\beta(X) = \mathcal{H}^{n-j}_n(X)$, where $\mathcal{H}^{n-j}_n$ is the $(n-j)$-dimensional Hausdorff measure in $\mathbb{R}^n$, equation (3) holds with

$$\alpha(Y) = c^{n-j+1,n-j}_{n+1,1,1} \int_{S^{n-1} \cap L^n_{j+1[O]}} \int_{-\infty}^{\infty} \chi(Y \cap (ru + u^\perp)) |r|^{n-j-1} \mathrm{d}r \mathrm{d}u^j, \tag{6}$$

where $c^{n-j+1,n-j}_{n+1,1,1}$ is a constant depending on n and j (see (B.1)). We use classical Morse theory to write the Euler characteristic in the above expression in terms of critical values on Y. For $u \in S^{n-1} \cap L^n_{j+1[O]}$ let $f_u(y) = \langle y, u \rangle$ be the height function on Y. We say that a point $p \in Y$ is a *critical point* of f_u if there is a local coordinate system $\phi : U \to Y$, where U is a neighbourhood of O, with $\phi(O) = p$, such that $\frac{\mathrm{d}(f_u \circ \phi)}{\mathrm{d}x}(O) = 0$. If p is a critical point of f_u then $f_u(p)$ is called a *critical value* of f_u. The critical point has *index* one, if the second derivative $\frac{\mathrm{d}^2(f_u \circ \phi)}{\mathrm{d}x^2}(O)$ is negative, and index zero if the second derivative is positive. The main result of Paper B is obtained by writing the Euler characteristic in (6) in terms of the critical values of the section profile. Then the inner integral in (6) can be calculated explicitly and we obtain

$$\alpha(Y) = \tfrac{c^{n-j+1,n-j}_{n+1,1}}{n-j} \int_{S^{n-1} \cap L^n_{j+1[O]}} M(Y, u) \mathrm{d}u^j, \tag{7}$$

where

$$M(Y, u) = \sum_{k=2}^{m} (\mathrm{sgn}(r_k)|r_k|^{n-j} - \mathrm{sgn}(r_{k-1})|r_{k-1}|^{n-j}) \sum_{i=1}^{k-1} v_i \tag{8}$$

depends on all the critical values $r_1 < r_2 < \cdots < r_m$ of the smooth one-dimensional manifold $Y \subseteq L^n_{j+1[O]}$ with respect to the height function f_u. The respective Morse indices are $\lambda_1, \ldots, \lambda_m$ and we abbreviated $v_i = (-1)^{\lambda_i}$, $i = 1, \ldots, m$.

6.2 The Morse type surface area estimator

Let X be a compact, smooth manifold of dimension $n-1$ that satisfies the weak regularity condition (X intersects $L^n_{2[O]}$ transversely in $\mathbb{R}^n$ for almost all $L^n_{2[O]} \in \mathcal{L}^n_{2[O]}$).

Recalling (3), we obtain from (7) with $j = 1$ that the surface area of X can be written as

$$S(X) = c_{2,1}^n \int_{\mathcal{L}_{2[O]}^n} \int_{S^{n-1} \cap L_{2[O]}^n} M(X \cap L_{2[O]}^n, u) \mathrm{d}u^1 \mathrm{d}L_{2[O]}^n, \tag{9}$$

where M is given by (8) with $j = 1$. The integrand presents an unbiased estimator for the surface area of X. The precision of the estimator can be increased by applying angular systematic sampling in the section plane to unbiasedly estimate the inner integral in (9). This gives the Morse type surface area estimator

$$\hat{S}_N = \frac{c_1^n}{N} \sum_{l=0}^{N-1} M(X \cap L_{2[O]}^n, u_{\alpha_0 + l\frac{\pi}{N}}), \tag{10}$$

where u_α is a unit vector making an angle α with a fixed axis in the IR section plane $L_{2[O]}^n \in \mathcal{L}_{2[O]}^n$, α_0 is uniformly distributed in the interval $[0, \pi/N)$ and $N \in \mathbb{N}$ is the number of sampled directions in the section plane.

When it is possible to find critical values for all directions in the section plane (e.g. by automated segmentation of the boundary), equation (9) presents another unbiased surface area estimator which we call the *generalized flower estimator*

$$\hat{S}_{\mathrm{flo}} = c_{2,1}^n \int_{S^{n-1} \cap L_{2[O]}^n} M(X \cap L_{2[O]}^n, u) \mathrm{d}u^1, \tag{11}$$

where $L_{2[O]}^n \in \mathcal{L}_{2[O]}^n$ is IR. We derive a simple computational formula for (11) when $X \subseteq \mathbb{R}^3$ is a simply connected set with interior points that can be represented as the union of finitely many convex polytopes. The formula only requires a list of the vertices of the polygon $X \cap L_{2[O]}^3$.

In Paper B we show that the estimators in (10) and (11) also hold for polyconvex sets X in $\mathbb{R}^n$ (without any extra regularity assumptions) when the Morse indices and critical values in (8) are replaced by Hadwiger type indices and critical values. Furthermore, we show that when $X \subseteq \mathbb{R}^n$ is a compact, topologically regular set ($X = \mathrm{cl}(\mathrm{int} Y)$) with smooth boundary (satisfying the weak regularity condition mentioned earlier), the two definitions of critical values and indices are the same.

6.3 Flower area

When X is a convex body in $\mathbb{R}^n$, equation (8) simplifies and the generalized flower estimator becomes

$$\hat{S}_{\mathrm{flo}} = c_2^n \int_{S^{n-1} \cap L_{2[O]}^n} \mathrm{sgn}(h_{X \cap L_{2[O]}^n}(u)) |h_{X \cap L_{2[O]}^n}(u)|^{n-1} \mathrm{d}u^1, \tag{12}$$

where $\mathrm{sgn}(\cdot)$ is the signum function. As $-h_{X \cap L_{2[O]}^n}(-u) \leq h_{X \cap L_{2[O]}^n}(u)$ for all $u \in S^{n-1} \cap L_{2[O]}^n$, the integrand in (12) is the radial function of some set. We call this set the $(n-1)$-*flower set* of $X \cap L_{2[O]}^n$ and denote it by $H_{X \cap L_{2[O]}^n}^{n-1}$. The flower set of a convex body is only an auxiliary set associated to the section profile and not necessary for the estimation procedure. When $O \in X$, equation (12) with $n = 3$ is

the *flower estimator* for surface area given in [CO05]. The terminology 'flower' is due to [CO05] and comes from the fact that when $X \cap L^3_{2[O]}$ is a planar polygon, $H^1_{X\cap L^3_{2[O]}}$ is a union of finitely many disks and resembles slightly a flower.

For central two-dimensional sections in $\mathbb{R}^3$ the average area of the 1-flower set of a section profile is, up to a factor 4, the surface area of the boundary of the object

$$S(\partial X) = 4 \int_{\mathcal{L}^3_{2[O]}} V_2(H^1_{X\cap L^3_{2[O]}}) \mathrm{d}L^3_{2[O]}.$$

This is in formal analogy with Cauchy's surface area formula [SW08, Eq. (6.12)] that expresses the surface area as mean area of two-dimensional projections

$$S(\partial X) = 4 \int_{\mathcal{L}^3_{2[O]}} V_2(X|L^3_{2[O]}) \mathrm{d}L^3_{2[O]}.$$

This analogy was observed in [GACO09, Section 4.3]. It seems that this analogy is merely a coincidence due to a special choice of dimensions as it only generalizes for very special choices of the dimension of the surrounding space and the dimension of the linear subspace. We did not only treat this analogy for the surface area but for all the intrinsic volumes (and then considered Kubota's formula [SW08, Eq. (6.11)] which generalizes Cauchy's formula).

Paper B also sheds further light on the standing uniqueness conjecture [GACONnB10, Conjecture 4.1] that (3) with $\beta(X) = V_{n-j+m}$, $0 \leq m \leq j$, only holds if the measurement function is of the invariator form

$$\alpha(\cdot) = c^{j+1,n-j+m+1,n-j}_{m+1,n+1,1} \int_{\mathcal{L}^{j+1}_j} V_m(\cdot \cap L^{j+1}_j) d(O, L^{j+1}_j)^{n-j-1} \mathrm{d}L^{j+1}_j.$$

This is inspired by [CO12].

7 The Morse type surfacea area estimator in practice

The goal of Paper C is to advocate the benefits of the Morse type surface area estimator (10) to practical users of stereological tools. In Paper C the object of interest X is either a three-dimensional polyconvex set or a compact subset of $\mathbb{R}^3$ with smooth boundary. If X is a compact set with smooth boundary we have to impose the weak regularity condition mentioned in Section 6.1 to guarantee that the section profile $X \cap L^3_{2[O]}$ has again a smooth boundary.

7.1 A modification of the area tangent count method

The idea of the Morse type estimator is based on a modification of the area tangent count method. The area tangent count method is used to calculate the Euler characteristic in (4) for all $r \in \mathbb{R}$ but as the line in the section plane is weighted, it is not enough to count the number of tangents in the section plane, also their distances from O need to be registered. These distances are the 'critical values' defined in Section 6.1. The procedure is the same as for the tangent count method: a line in the

IR section plane, at a uniformly chosen direction, is swept through the section profile and all translates of the line that are tangent to the section profile are registered, as well as their type (positive or negative tangents, see Section 3.1.1) and critical values. A positive tangent corresponds to a critical point with Morse index zero (and Hadwiger index one) and a negative tangent to a critical point with Morse index one (and Hadwiger index -1).

Tangent counting is derived for ideal smooth objects which is not the case in practice. The boundary of a section profile on a microscopy image can be quite blurry and the (approximate) section profile can therefore appear to have more tangents than the true section profile. This can make tangent counting unstable in practice, as mentioned in [Bad84]. This problem is not a severe practical limitation in our setting as the critical values are used and not only the number of tangents. The modified tangent method splits the integration over the real numbers up into intervals where the Euler characteristic in (4) is constant. The 'wrong' tangents (that is lines that appear to be tangent to the section profile due to the boundary being blurry), for a given direction, are typically very close to 'real' tangents. Therefore, intervals where the 'wrong' Euler characteristic is used are very small and do not contribute much to the estimator.

In Paper C we discuss the precision gain in terms of variance reduction obtained by using the Morse type surface area estimator as compared to earlier approaches (the surfactor and the invariator grid estimator). We generalize the variance decomposition of the invariator estimator (5) to non-convex objects and calculate the different contributions more explicitly (this can be generalized to objects of arbitrary dimension without any extra difficulties). We also mention how these variance contributions simplify for convex objects and in particular for ellipsoids and balls. These variance contributions can be used to express the variance of the Morse type estimator and of the generalized flower estimator (11). To explain the motivation for deriving the Morse type surface area estimator, the results of the simulation study performed in [Thó10] are discussed in Paper C, as already done briefly in Section 4.2.

7.2 Implementation of the Morse type surface area estimator

It was the purpose of Paper C to demonstrate the practicability of the Morse type estimator in a biological application. This required software that allows the user to efficiently sweep a line through a section profile and register tangents. This program was written in [Kal12] and used to estimate the boundary length of planar geometric objects in a more efficient way than the Steinhaus estimator. We adapted this program to our setting for surface area estimation, that is, we used the output of the program to calculate the Morse type surface area estimator. The software is available at the home page `home.imf.au.dk/olofth` and we refer to it as an 'expert-assisted procedure'. In Paper C we give a brief description of this expert-assisted procedure in order to enable stereologists to use it in practice. The procedure is quite simple to use. The input is a section profile, a microscopy image in JPEG

format. When the procedure is run, the user can, on the image, translate a line that is attached to the mouse cursor. The user needs to place all translates of the line that are tangent to the section profile. To distinguish between positive and negative tangents, the user left and right clicks, respectively, with the mouse. It is possible to choose the number of directions N that are to be sampled in the section plane. In the absence of other large sources of variation than the variance from the sampling procedure we recommend using $N = 4$, $N = 2$ if the section profile resembles an ellipse. When there are other sources of variation, which is the case in most real-world applications, we recommend using $N = 2$. These other sources of variation can for example be the true population variance (the variation in surface area among particles) when the aim is to estimate the average surface area in a population of particles. The recommendation concerning the choice of N, when no other major sources of variation are present, was concluded on the basis of a simulation study. The simulation study involved section profiles of various different shapes. For these shapes we also compared the efficiency of $\hat{S}_N$ and the invariator grid estimator $\hat{S}_{\text{grid}}$. The comparison was done by considering the amount of workload needed to obtain a given precision for each of these estimators. It turns out that $\hat{S}_N$ with $N > 1$ should clearly be preferred to $\hat{S}_{\text{grid}}$ and when the expert-assisted procedure is used we always recommend using the Morse type estimator.

We illustrate the application of the Morse type surface area estimator in a study of giant-cell glioblastoma. Although some clinical experts claim that not many objects in practice can be assumed to be convex in shape it turned out to be rather difficult to find particles that could justify the need for extending the pivotal estimator to non-convex particles. However, giant-cell glioblastoma are of interest in medical applications and their nuclei are typically non-convex in shape. The surface area of 51 sampled nuclei was estimated using $\hat{S}_N$ with $N \in \{1, 2, 4\}$. We used these different choices of N, and ignored our own recommendation, to be able to compare the precision of the estimators. The average surface area of the nucleus of a giant-cell glioblastoma was then estimated by taking the average of the empirical estimates of the surface area of the 51 sampled nuclei. Sampling in more directions in the section plane did not noticeably increase the precision of the estimator. When only the variance due to choosing the orientation in a section plane V_{orient}, was studied, for a given nucleus, a large decrease was observed when N was increased. However, this variance contribution is very small compared to the other variance contributions, the variance due to choosing the plane within each nucleus and the true population variance (the variation in surface area among the nuclei). Estimates for the other two variance contributions, V_{plane} and the true population variance, could be obtained by modelling the nuclei. If the nuclei could be modelled by balls (which is not very realistic) the theory in Paper A could be used to obtain these estimates.

The decomposition of the variance of the invariator estimator shows that $V_{\text{plane}} = \mathbb{V}\text{ar}(\hat{S}_{\text{flo}})$ and that the generalized flower estimator has lower variance than $\hat{S}_{\text{inv}}$, $\hat{S}_{\text{grid}}$ and $\hat{S}_N$. As $\hat{S}_{\text{flo}}$ requires finding tangents in all directions in the section plane it is usually not feasible in practice. However, if the boundary of a

section profile can be approximated by a polygon, using automated segmentation, the simple computational formula for $\hat{S}_{\text{flo}}$ mentioned in Section 6.2 (see (B.46)) can be used to obtain $\hat{S}_{\text{flo}}$. Automated segmentation can be of poor quality which leads to a heavily biased estimator (as a 'wrong' section profile is used instead of the true one). *Semi-automatic* procedures have been proposed to deal with this problem. This was done for surface area estimation in [DJ13] and for volume estimation in [HNAJ11]. In semi-automatic procedures, a clinical expert supervises the automated segmentation of the boundary of a given section profile and only intervenes if the segmentation is not satisfactory. If it is satisfactory the surface area is estimated by $\hat{S}_{\text{flo}}$ where the true section profile is replaced by the estimated one. In case of unsatisfactory segmentation, we suggest that the expert performs the necessary measurements in the section plane using the Morse type estimator $\hat{S}_N$. This is most conveniently done by using the expert-assisted procedure.

8 Outlook

In this thesis we derived both results that are interesting from a theoretical point of view and for practical applications in stereology.

We showed a 'local analogue' to the classical Wicksell problem, where we in particular emphasized similarities and differences between the classical and the local problem. In the classical problem, the size distribution of spherical particles can be uniquely determined by the size distribution of its section profiles. It is still an open question if this holds in a local setting, that is, if the joint distribution of the particle parameters can be uniquely determined from the joint distribution of the profile parameters. In the treatment of Wicksell's problem in a local setting we in particular derived stereology of extremes results for the marginal distributions of the parameters. This is presumably only the second study of sterelogy of extremes in a local setting, and the only one where the reference point is arbitrarily positioned inside the particle. Although a population of spheres is a rather restrictive scenario in practical applications, the local Wicksell problem is fascinating and reveals an interesting comparison between local and classical stereological methods. Moreover, there exist particle populations where this assumption is realistic, for example white fat cells [MBBO04]. It would be natural to formulate a local version of Wicksell's problem for ellipsoids like in the classical theory. However, there would be six unknown variables to describe the shape in three-dimensional space and the complicated integral relations between them and their profile counterparts appear to be very complicated and difficult to evaluate.

In the spirit of stereology we combined two seemingly different fields to create a highly useful stereological tool. We intertwined the classical theory of Morse and a Blaschke-Petkantschin type measure decomposition. The result is the Morse type surface area estimator. We argued that the Morse type estimator is the preferred surface area estimator available in local stereology. When automated segmentation is available, we suggested that a semi-automatic procedure should be used to re-

duce the wokload. If the segmentation of a section profile is satisfactory, the simple computational formula for the generalized flower estimator should be used, as the generalized flower estimator is the optimal (with respect to variance) estimator available. If the segmentation is not satisfactory the Morse type estimator, implemented with the expert-assisted procedure, should be used.

The comparison of classical and local stereology also led to new insight of the relation between averaged central sections and projections. Furthermore we derived new rotational Crofton formulae involving critical values and shed further light on the uniqueness conjecture of the measurement function in rotational Crofton formulae. In Paper B we mentioned that it might be possible to extend these rotational Crofton formulae involving critical values to the more general class of sets of positive reach, or even to sets that can be written as certain finite unions of sets of positive reach. This would require an extensive study of the work in [Fu89] but would relax the regularity assumptions required for the application of the Morse type estimator. We remark that these regularity assumptions are typically satisfied in the biological applications, we have in mind. We only considered rotational Crofton formulae involving critical values when the measurement function is of the form (6). That is, we only considered the weighted Euler characteristic of the section profile intersected with an affine line in the IR section, integrated over all possible choices of this line. It is of interest if this can be generalized to other intrinsic volumes than the Euler characteristic. More specifically, it is an open problem if Morse theory and the invariator principle can be combined to derive rotational Crofton formulae in full generality.

Minkowski tensors of convex bodies are a natural extension of the intrinsic volumes and they contain information on size, location, shape and orientation. In [JZ13] local stereological estimators of the Minkowski tensors are presented, both old and new, and their performance is investigated in a simulation study. These estimators are based on the invariator principle and here also the sweeping line idea might prove to be valuable. Tensor valuations will most likely play a decisive role in future research in stereology on size- and orientation-distributions, shape and spatial positioning of arbitrary particles.

Bibliography

[ACZJ12] J. Auneau-Cognacq, J. Ziegel, and E.B.V. Jensen. Rotational integral geometry of tensor valuations. *Adv. Appl. Math.*, 50(3):429–444, 2012.

[AGP03] B.B. Andersen, H.J.G. Gundersen, and B. Pakkenberg. Aging of the human cerebellum: a stereological study. *J. Comp. Neurol.*, 466(3):356–365, 2003.

[AJ75] R.S. Anderssen and A.J. Jakeman. Product integration for functionals of particle size distributions. *Util. Math.*, 8:111–126, 1975.

[AJ10] J. Auneau and E.B.V. Jensen. Expressing intrinsic volumes as rotational integrals. *Adv. Appl. Math.*, 45(1):1–11, 2010.

[Bad84] A.J. Baddeley. Stochastic geometry and image analysis. In *Proceedings of the CWI symposium on mathematics and computer science*. CWI Monographs, 1984.

[BBH03] V. Beneš, K. Bodlák, and D. Hlubinka. Stereology of extremes; bivariate models and computation. *Methodol. Comput. Appl. Probab.*, 5(3):289–308, 2003.

[BJ05] A. Baddeley and E.B.V. Jensen. *Stereology for Statisticians*. Chapman & Hall/CRC, Boca Raton, 2005.

[Bla35] W. Blaschke. Integralgeometrie 1. Ermittlung der Dichten für lineare Unterräume im E_n. *Actualités Scientifiques et Industrielles*, 252:1–22, 1935.

[BMN84] R. Blödner, P. Mühlig, and W. Nagel. The comparison by simulation of solutions of Wicksell's corpuscle problem. *J. Microsc.*, 135:61–74, 1984.

[BS12] C.G. Bowsher and P.S. Swain. Identifying sources of variation and the flow of information in biochemical networks. *Proceedings of the National Academy of Sciences*, 109(20):E1320–E1328, 2012.

[Buf77] G.-L.L. Comte de Buffon. Essai d'arithmétique morale. In *Histoire naturelle, générale et particulière, Supplément 4*, pages 46–123. Imprimerie Royale, Paris, 1777.

[CO76] L.M. Cruz-Orive. Particle size-shape distributions: The general spheroid problem. I. *J. Microsc.*, 107(3):235–253, 1976.

[CO83] L.M. Cruz-Orive. Distribution-free estimation of sphere size distributions from slabs showing overprojection and truncation, with a review of previous methods. *J. Microsc.*, 131:265–290, 1983.

[CO87] L.M. Cruz-Orive. Stereology: recent solutions to old problems and a glimpse into the future. *Acta Stereol.*, 6(3):3–18.5, 1987.

[CO05] L.M. Cruz-Orive. A new stereological principle for test lines in three-dimensional space. *J. Microsc.*, 219(1):18–28, 2005.

[CO08] L.M. Cruz-Orive. Comparative precision of the pivotal estimators of particle size. *Image Anal. Stereol.*, 27(1):17–22, 2008.

[CO09] L.M. Cruz-Orive. Stereology: old and new. In *Proceedings of the 10th European Congress of ISS. The MIRIAM Project Series. Bologna: ESCULAPIO Pub. Co*, pages 3–14, 2009.

[CO12] L.M. Cruz-Orive. Uniqueness properties of the invariator, leading to simple computations. *Image Anal. Stereol.*, 31(2):89–98, 2012.

[Del47] A. Delesse. Procédé mécanique pour déterminer la composition des roches. *Comptes Rendues de l'Académie des Sciences (Paris)*, 25:544–545, 1847.

[Del48] A. Delesse. Procédé mécanique pour déterminer la composition des roches. *Annales des Mines*, 13:379–388, 1848.

[DJ13] J. Dvořák and E.B.V. Jensen. On semiautomatic estimation of surface area. *J. Microsc.*, 250(2):142–157, 2013.

[DM77] P. Davy and R.E. Miles. Sampling theory for opaque spatial specimens. *J. R. Statist. Soc.*, 39:56–65, 1977.

[DR92] H. Drees and R.-D. Reiss. Tail behavior in Wicksell's corpuscle problem. In *Probability Theory and Applications*, pages 205–220. Kluwer, Dordrecht, 1992.

[Fu89] J.H.G. Fu. Curvature measures and generalized Morse theory. *J. Differ. Geom.*, 30:619–642, 1989.

[GACO09] X. Gual-Arnau and L.M. Cruz-Orive. A new expression for the density of totally geodesic submanifolds in space forms, with stereological applications. *Differ. Geom. Appl.*, 27:124–128, 2009.

[GACONnB10] X. Gual-Arnau, L.M. Cruz-Orive, and J.J. Nuño Ballesteros. A new rotational integral formula for intrinsic volumes in space forms. *Adv. Appl. Math.*, 44(3):298–308, 2010.

[Gla97] S. Glasauer. A generalization of intersection formulae of integral geometry. *Geom. Dedicata*, 68(1):101–121, 1997.

[Had51] H. Hadwiger. Beweis eines Funktionalsatzes für konvexe Körper. In *Abh. Math. Sem. Univ. Hamburg*, volume 17, pages 69–76. Springer, Heidelberg, 1951.

[Had52] H. Hadwiger. Additive Funktionale k-dimensionaler Eikörper, I. *Arch. Math.*, 3(6):470–478, 1952.

[Had55] H. Hadwiger. Eulers Charakteristik und kombinatorische Geometrie. *J. Reine Angew. Math.*, 194:101–110, 1955.

[Had57] H. Hadwiger. *Vorlesungen über Inhalt, Oberfläche und Isoperimetrie*, volume 93. Springer, Berlin, 1957.

[HKK+06] C. Hundahl, J. Kelsen, K. Kjær, L.C. Rønn, R.E. Weber, E. Geuens, A. Hay-Schmidt, and J.R. Nyengaard. Does neuroglobin protect neurons from ischemic insult? A quantitative investigation of neuroglobin expression following transient MCAo in spontaneously hypertensive rats. *Brain Research*, 1085(1):19–27, 2006.

[Hlu03a] D. Hlubinka. Stereology of extremes; shape factor of spheroids. *Extremes*, 6(1):5–24, 2003.

[Hlu03b] D. Hlubinka. Stereology of extremes; size of spheroids. *Math. Bohem.*, 128(4):419–438, 2003.

[Hlu06] D. Hlubinka. Extremes of spheroid shape factor based on two dimensional profiles. *Kybernetika*, 42(1):77–94, 2006.

[HNAJ11] L.V. Hansen, J.R. Nyengaard, J.B. Andersen, and E.B.V. Jensen. The semi-automatic nucleator. *J. Microsc.*, 242(2):206–215, 2011.

[HSN07] M. Hosseini-Sharifabad and J.R. Nyengaard. Design-based estimation of neuronal number and individual neuronal volume in the rat hippocampus. *J. Neurosci. Meth.*, 162(1):206–214, 2007.

[HSS08] D. Hug, R. Schneider, and R. Schuster. Integral geometry of tensor valuations. *Adv. Appl. Math.*, 41(4):482–509, 2008.

[Jen84] E.B. Jensen. A design-based proof of Wicksell's integral equation. *J. Microsc.*, 136:345–348, 1984.

[Jen91] E.B.V. Jensen. Recent developments in the stereological analysis of particles. *Ann. Inst. Stat. Math.*, 43:455–468, 1991.

[Jen98] E.B.V. Jensen. *Local Stereology*. World Scientific, Singapore, 1998.

[JK92] E.B.V. Jensen and K. Kiê. A new integral geometric formula of the Blaschke-Petkantschin type. *Math. Nachr.*, 156(1):57–74, 1992.

[JR08] E.B.V. Jensen and J. Rataj. A rotational integral formula for intrinsic volumes. *Adv. Appl. Math.*, 41:530–560, 2008.

[JZ13] E.B.V. Jensen and J.F. Ziegel. Local stereology of tensors of convex bodies. *Methodol. Comput. Appl. Probab.*, 2013.

[Kal12] T. Kallemose. Application of stereological projection formulae for perimeter estimation. Master's thesis, Aarhus University, 2012.

[KCO97] L.M. Karlsson and L.M. Cruz-Orive. Estimation of mean particle size from single sections. *J. Microsc.*, 186(2):121–132, 1997.

[MB99] Y. Murakami and S. Beretta. Small defects and inhomogeneities in fatigue strength: experiments, models and statistical implications. *Extremes*, 2(2):123–147, 1999.

[MBBO04] R.M. Malina, C. Bouchard, and O. Bar-Or. *Growth, Maturation and Physical Activity*. Human Kinetics, United States, 2004.

[MD76] R.E. Miles and P. Davy. Precise and general conditions for the validity of a comprehensive set of stereological fundamental formulae. *J. Microsc.*, 107(3):211–226, 1976.

[MD77] R.E. Miles and P. Davy. On the choice of quadrats in stereology. *J. Microsc.*, 110(1):27–44, 1977.

[Mil71] R.E. Miles. Isotropic random simplices. *Adv. Appl. Probab.*, 3(2):353–382, 1971.

[Mil78a] R.E. Miles. The importance of proper model specification in stereology. In *Geometrical Probability and Biological Structures: Buffon's 200th Anniversary*, pages 115–136. Springer, 1978.

[Mil78b] R.E. Miles. The sampling, by quadrats, of planar aggregates. *J. Microsc.*, 113(3):257–267, 1978.

[Mil79] R.E. Miles. Some new integral geometric formulae, with stochastic applications. *J. Appl. Prob.*, 16:592–606, 1979.

[Paw12] Z. Pawlas. Local stereology of extremes. *Image Anal. Stereol.*, 31:99–108, 2012.

[Pet35] B. Petkantschin. Integralgeometrie 6. Zusammenhänge zwischen den Dichten der linearen Unterräume im n-dimensionalen Raum. In *Abh. Math. Sem. Univ. Hamburg*, volume 11, pages 249–310. Springer, Heidelberg, 1935.

[PMJ+11] L. Palaniyappan, P. Mallikarjun, V. Joseph, T.P. White, and P.F. Liddle. Regional contraction of brain surface area involves three large-scale networks in schizophrenia. *Schizophr. Res.*, 129(2):163–168, 2011.

[Sal74] S.A. Saltykov. *Stereometrische Metallographie.* VEB Deutscher Verlag für Grundstoffindustrie, Leipzig, 1974.

[San04] L.A. Santaló. *Integral geometry and geometric probability*. Cambridge University Press, 2004.

[SKM95] D. Stoyan, W.S. Kendall, and J. Mecke. *Stochastic Geometry and its Applications.* Wiley, New York, 2nd edition, 1995.

[Sto90] D. Stoyan. Stereology and stochastic geometry. *Internat. Statist. Rev.*, 58:227–242, 1990.

[SW08] R. Schneider and W. Weil. *Stochastic and Integral Geometry*. Springer, Heidelberg, 2008.

[TGJ97] T. Tandrup, H.J.G. Gundersen, and E.B.V. Jensen. The optical rotator. *J. Microsc.*, 186(2):108–120, 1997.

[Thó10] Ó. Thórisdóttir. Variance for surface area estimation based on the invariator. Master's thesis, Aarhus University, 2010.

[TK12] Ó. Thórisdóttir and M. Kiderlen. Extended version of "Wicksell's Problem in Local Stereology". Available at `http://csgb.dk/publications/csgbrr/2012/`. 2012.

[WE66a] E.R. Weibel and H. Elias. Introduction to stereologic principles. In *Quantitative Methods in Morphology*, pages 89–98. Springer, Heidelberg, 1966.

[WE66b] E.R. Weibel and H. Elias. Introduction to stereology and morphometry. In *Quantitative Methods in Morphology*, pages 3–19. Springer, Heidelberg, 1966.

[Wic25] S.D. Wicksell. The corpuscle problem I. *Biometrika*, 17:84–99, 1925.

[Wic26] S.D Wicksell. The corpuscle problem. Second memoir. Case of ellipsoidal corpuscles. *Biometrika*, 18:152–172, 1926.

[Zäh90] M. Zähle. A kinematic formula and moment measures of random sets. *Math. Nachr.*, 149(1):325–340, 1990.

Paper A

Wicksell's problem in local stereology

Ó. Thórisdóttir and M. Kiderlen

Department of Mathematics, Aarhus University

Abstract: Wicksell's classical corpuscle problem deals with the retrieval of the size distribution of spherical particles from planar sections. We discuss the problem in a local stereology framework. Each particle is assumed to contain a reference point and the individual particle is sampled with an isotropic random plane through this reference point. Both the size of the section profile and the position of the reference point inside the profile are recorded and used to recover the distribution of the corresponding particle parameters. Theoretical results concerning the relationship between the profile and particle parameters, unfolding of the arising integral equations, uniqueness issues and domain of attraction relations are discussed. We illustrate the approach by reconstructing from simulated data using numerical unfolding algorithms.

Keywords: Wicksell's corpuscle problem; local stereology; inverse problems; numerical unfolding; stereology of extremes.

2010 MSC: 60D05; 45Q05; 65R30; 62G05

A.1 Introduction and account of main results

This work discusses Wicksell's corpuscle problem in a local stereology framework, where the size distribution of spherical particles is recovered from plane sections through reference points. In order to describe similarities and differences of the local and the classical Wicksell problem, we start with a short outline of the latter.

Wicksell's classical corpuscle problem, described very figuratively as 'tomato salad problem' by Günter Bach, asks how to recover the size distribution of random balls in $\mathbb{R}^3$ from the observed size distribution of two-dimensional section profiles. Although the stereological literature often refers to ball-shaped particles as 'spheres', we decided to adopt terminology from pure mathematics, calling the solid particles 'balls', and reserving the word 'sphere' for the boundary of a ball. Assuming that

the "density of the centers and the distribution of the sizes being the same in all parts of the body [where the observation is taken]", Wicksell showed [Wic25] that the density f_r of the profile radii r is given by

$$f_r(x) = \frac{x}{\mathbb{E}R} \int_x^\infty \frac{1}{\sqrt{y^2 - x^2}} \mathrm{d}F_R(y), \tag{A.1}$$

where F_R is the cumulative distribution function of the radius R of the balls in $\mathbb{R}^3$, and $\mathbb{E}R$ is the usual expectation of R. Stoyan & Mecke [MS80] made Wicksell's arguments rigorous showing that (A.1) actually holds for all stationary particle processes of non-overlapping balls, when R has a finite mean. The right hand side of (A.1) is essentially an *Abel integral transform* of F_R. It can be inverted explicitly, and this shows in particular that F_R is determined by the cumulative distribution function F_r of r.

Relation (A.1) is the result of two mutually counteracting sampling effects: As the probability that a ball is hit by the plane is proportional to its radius, the radius distribution of the intersected balls is size weighted, preferring large balls. On the other hand, the profile radius is always smaller than the radius of the intersected ball, as the section plane almost surely misses the ball's center. Already Wicksell was aware of the fact that these two effects can annihilate each other. When R follows a Rayleigh distribution (the distribution of the length of a centered normally distributed two-dimensional vector), r also follows this distribution, with the same parameter. The Rayleigh distribution is the only *reproducing distribution* in this sense; see [DR92]. If R_w denotes the radius-weighted radii distribution with cumulative distribution function

$$F_{R_w}(x) = \frac{1}{\mathbb{E}R} \Big(x F_R(x) - \int_0^x F_R(s) \mathrm{d}s \Big),$$

$x \geq 0$, the two sampling effects can also be expressed by the relation

$$r = \Lambda R_w, \tag{A.2}$$

where Λ is a random variable with Lebesgue-density $s \mapsto \mathbf{1}_{[0,1]}(s) s / \sqrt{1 - s^2}$ that is independent of R_w; see [BJ05]. This also gives the well-known *moment relations*

$$\tilde{m}_k = c_{k+1} \frac{\tilde{M}_{k+1}}{\tilde{M}_1}, \tag{A.3}$$

$k = -1, 0, 1, 2, \ldots$, where $\tilde{m}_k$ and $\tilde{M}_k$ are the kth moments of r and R, respectively, and

$$c_k = \frac{\sqrt{\pi}}{2} \frac{\Gamma\left((k+1)/2\right)}{\Gamma\left(k/2+1\right)}. \tag{A.4}$$

The inversion of the integral equation (A.1) is ill-posed, which can informally be described as 'small deviations of the data can lead to arbitrarily large deviations of the solution'. There exist several methods, both distribution-free (non-parametric) and parametric ones, for numerically solving Wicksell's classical problem. Examples

of distribution-free methods are finite difference methods, spectral differentiation and product integration methods and kernel methods. Parametric methods can be divided into maximum likelihood methods and methods that only use the moment relations. All methods have their advantages and disadvantages and none appears to be generally best. References for the respective methods and an overview of existing ones are given in for example [SKM95, Section 11.4.1], [CO83], [BMN84], [AJ75a] and [ADH90].

Stereology of extremes has received much interest due to applications in material science; see [TS02] for an application to metallurgy. The maximum size of balls in Wicksell's classical problem is studied in [DR92], [TS96], [TS98] and [TS01]. There it is shown that F_R and F_r belong to the same type of extreme value distribution. Extremes of the size and shape parameters of spheroidal particles are studied in [Hlu03a], [Hlu03b], [Hlu06] and [BBH03].

More detailed reviews of the classical Wicksell problem can be found in [SKM95, Section 11.4], [CO83], [OM00, Chapter 6] and earlier contributions, that are listed in these sources.

In the above description of Wicksell's problem, we adopted the common model-based approach, where the particle system is random, and the probe can be taken with an arbitrary (deterministic) plane due to stationarity. Jensen [Jen84] proved that (A.1) also holds in a design-based setting, where the particle system is deterministic – possibly inhomogeneous – but the plane is randomized. In order to obtain a representative sample, it is enough to choose an FUR (*f*ixed orientation *u*niform *r*andom) plane. Inspired by local stereology, we discuss here a design-based sampling scheme, where each particle contains a reference point and the individual particle is sampled with an isotropic plane through that reference point. This design is tailor-made for applications e.g. in biology, where cells often are sampled using a confocal microscope by focusing on the plane through the nucleus or the nucleolus of a cell; see the monograph [Jen98] on local stereology. To our knowledge, the first explicit mention of Wicksell's problem in a local setup is [Jen91], where it is remarked that the problem is trivial whenever the reference point coincides with the ball's center, as the size distributions of balls and section profiles are then identical. This being obvious, we want to show here that the local Wicksell problem is far from trivial if this condition is violated.

Although biological application suggests to restrict considerations to $\mathbb{R}^3$, we will consider particles in n-dimensional space intersected by hyperplanes, as the general theory does not pose any essential extra difficulties. Like in the classical setting, we assume that the particles are (approximate) balls, and in order to incorporate the natural fluctuation, we assume that both the radius of the ball and the position of the reference point in the ball are random. This way, a ball-shaped particle is described by two quantities: firstly its random radius R, the *size of the ball*, and the distance of the reference point from the center of the ball. It turns out to be favorable to work with the *relative distance* $Q \in [0, 1]$ instead, meaning that QR is the distance

of the reference point to the ball's center. The variable Q can be considered as *shape* descriptor. We do not take into account the direction of the reference point relative to the ball's center, as this direction appears to be of minor interest. In addition it cannot be determined from isotropic sections, unless we would also register the orientation of the section plane (which we will not do here). If a ball with a given reference point is intersected by an isotropic hyperplane through the reference point (independent of the ball), an $(n-1)$-dimensional ball is obtained. We let r be its radius and q be the relative distance of the reference point to its center.

Our first result, Theorem A.1, shows that the joint distributions of (r, q) and (R, Q) are connected by an explicit integral transform. Here and in the following we assume that all balls have a positive radius, and that the reference point does almost surely not coincide with the center of a ball, that is, we agree on $\mathbb{P}(Q = 0) = 0$. The last assumption is not essential, and most of our results can be extended to the case $\mathbb{P}(Q = 0) > 0$, as outlined in Remark A.2. Like in the classical Wicksell problem we show that the marginals of r and q always have probability densities f_r and f_q, respectively, and we determine their explicit forms in Corollary A.4. However, the joint distribution of (r, q) need not have a density. Corollary A.4 also shows that f_q only depends on the distribution of Q and not on R, which explains why we are working with *relative* distances. In Proposition A.5 we show that

$$r = \Gamma R \tag{A.5}$$

with a random variable Γ, whose density can be given explicitly. This is in analogy to (A.2) in the classical case. However, there is no size-weighting in our local stereological design, and the variable Γ is now depending on the distribution of Q. Thus, when R and Q are independent, so are R and Γ, and moment relations in analogy to (A.3) are readily obtained: if m_k and M_k are the kth moments of r and R, respectively, then

$$m_k = c_k(Q) M_k, \tag{A.6}$$

$k = 0, 1, 2, \ldots$. The constants $c_k(Q)$ depend on the distribution of Q and are given in Remark A.6. However, (A.6) cannot be applied directly to obtain (estimates of the) moments M_k, as $c_k(Q)$ depends on the shape of the full particle. Corollary A.10 shows that $c_k(Q)$ can be expressed by the distribution of q, making it possible to estimate both m_k and $c_k(Q)$ from the section profiles and thus to access M_k. Simulation studies showed that this estimation procedure is quite stable, as described after Corollary A.10.

We then turn to uniqueness in Section A.4. That the distribution of Q is uniquely determined by the distribution of q follows from the fact that the two distributions are connected by an Abel type integral equation. It can be inverted explicitly; see Proposition A.9 for $n = 3$. Theorem A.7 shows that even the joint distribution of (R, Q) is uniquely determined by the distribution of the profile quantities (r, q), but only under the assumption that R and Q are independent. The two marginals of (r, q) do not uniquely determine (R, Q) without this extra assumption, as shown

by an example after Theorem A.7. It is an open problem whether the *joint distribution of* (r, q) determines the joint distribution of (R, Q) without the independence assumption.

To reconstruct F_R and F_Q from simulated data, when R and Q are independent, we chose to use distribution-free methods. Maximum likelihood methods and method of moments can though also be used as for the classical Wicksell problem. In Section A.6 we describe the implementation of a Scheil-Schwartz-Saltykov type method [Sal74]. Following [CO83], the method can be classified as a finite difference method, more specifically a 'successive subtraction algorithm'. The data is grouped and the distributions F_Q and F_R discretized. Then F_q written in terms of F_Q, F_r written in terms of $F_{R,Q}$, respectively, become systems of linear equations, which can be solved. We carried out a number of simulation studies which illustrate the feasibility of the approach. An example of a reconstruction is reported in Figure A.2.

In Section A.7 we discuss practical examples and then turn to stereology of extremes in Section A.8. Similar results as in the classical case are obtained. Proposition A.15 shows that if the particle parameters, R and Q, are independent, F_R and F_r belong to the same type of extreme value distribution. An analogous result holds for the shape parameters. To our knowledge, stereology of extremes in a local setting has only been treated in [Paw12]. There the shape and size parameters of spheroids are studied but the isotropic section plane is always taken through the center of the spheroid.

As mentioned earlier, a number of results and the implemented reconstruction algorithm depend on the assumption that the particle parameters R and Q are independent. We comment on this assumption in the concluding Section A.9.

A.2 Preliminaries

Throughout we let $\mathbb{R}^n$ denote the n-dimensional Euclidean space and O its origin. The Euclidean scalar product is denoted by $\langle \cdot, \cdot \rangle$ and the Euclidean norm by $\|\cdot\|$. We let e_i be the vector in $\mathbb{R}^n$ with 1 in the ith place and zeros elsewhere. For a set $Y \subseteq \mathbb{R}^n$, we define

$$Y + x = \{y + x \,|\, y \in Y\}, \quad x \in \mathbb{R}^n, \qquad \alpha Y = \{\alpha y \,|\, y \in Y\}, \quad \alpha > 0. \tag{A.7}$$

We use ∂Y for the boundary and $\mathbf{1}_Y$ for the indicator function of Y. The unit ball in $\mathbb{R}^n$ is $B_n = \{x \in \mathbb{R}^n : \|x\| \leq 1\}$ and the boundary of it is the unit sphere (in $\mathbb{R}^n$) S^{n-1}, $S^{n-1} = \{x \in \mathbb{R}^n : \|x\| = 1\}$. A ball in $\mathbb{R}^n$ of radius R centred at O is denoted by RB_n, in accordance to (A.7). We write σ_n for the surface area of the unit ball in $\mathbb{R}^n$, i.e. $\sigma_n = \mathcal{H}_n^{n-1}(S^{n-1})$, where $\mathcal{H}_n^d$ is the d-dimensional *Hausdorff measure* in $\mathbb{R}^n$. When n is clear from the context, we abbreviate $\mathcal{H}_n^d(\mathrm{d}u)$ by $\mathrm{d}u^d$. For $p = 0, 1, \ldots, n$ let

$$\begin{aligned} \mathcal{L}_{p[O]}^n &= \{L_{p[O]}^n \subseteq \mathbb{R}^n \,|\, L_{p[O]}^n \text{ is a } p\text{-dim. linear subspace}\}, \\ \mathcal{L}_p^n &= \{L_p^n \subseteq \mathbb{R}^n \,|\, L_p^n \text{ is a } p\text{-dim. affine subspace}\}, \end{aligned}$$

be the family of all p-dimensional linear, respectively affine, subspaces of $\mathbb{R}^n$. These spaces are equipped with their standard topologies ([SW08]) and we denote their Borel σ-algebras by $\mathcal{B}(\mathcal{L}^n_{p[O]})$, $\mathcal{B}(\mathcal{L}^n_p)$, respectively. The spaces are furthermore endowed with their natural invariant measures, and we write $\mathrm{d}L^n_{p[O]}$ and $\mathrm{d}L^n_p$, respectively, when integrating with respect to these measures. We use the same normalization as in [SW08],

$$\int_{\mathcal{L}^n_{p[O]}} \mathrm{d}L^n_{p[O]} = 1.$$

A random subspace $L^n_{p[O]}$ is called *isotropic random* (IR) if and only if its distribution is given by

$$\mathbb{P}_{L^n_{p[O]}}(A) = \int_{\mathcal{L}^n_{p[O]}} \mathbf{1}_A \mathrm{d}L^n_{p[O]}, \qquad A \in \mathcal{B}(\mathcal{L}^n_{p[O]}).$$

Similarly, a random flat $L^n_p \in \mathcal{L}^n_p$ is called *isotropic uniform random* (IUR) *hitting a compact object* Y if and only if its distribution is given by

$$\mathbb{P}_{L^n_p}(A) = c \int_{\mathcal{L}^n_p} \mathbf{1}_{A \cap \{L^n_p \in \mathcal{L}^n_p \,|\, L^n_p \cap Y \neq \emptyset\}} \mathrm{d}L^n_p, \qquad A \in \mathcal{B}(\mathcal{L}^n_p), \tag{A.8}$$

where c is a normalizing constant. We let $x|L^n_{p[O]}$ be the orthogonal projection of $x \in \mathbb{R}^n$ onto $L^n_{p[O]}$. We furthermore adopt the convention of writing $v^\perp$ for the hyperplane with unit normal $v \in S^{n-1}$. We use $B(z; a, b)$ to denote the *incomplete Beta function*, given by

$$B(z; a, b) = \int_0^z t^{a-1}(1-t)^{b-1}\mathrm{d}t, \qquad 0 < z < 1, \quad a, b > 0.$$

When $z = 1$ we write $B(a, b)$. Note in particular that $B(1/2, (n-1)/2) = \sigma_n/\sigma_{n-1}$. For an arbitrary function f we let $f^+(x) = \max\{f(x), 0\}$ be its positive part. Given a random variable X, its *characteristic function* (or Fourier transform of its distribution) is defined by

$$\varphi_X(t) = \mathbb{E}e^{itX}, \qquad t \in \mathbb{R}.$$

A.3 The direct problem

Consider a random ball in $\mathbb{R}^n$ with positive radius, centered at O' and containing the origin. Let R and Q denote the random variables giving the radius of the ball, and the relative distance of the center of the ball from O, respectively. Intersect the ball with an IR hyperplane, $L^n_{n-1[O]}$, independent of the ball. Then an $(n-1)$-dimensional ball is obtained. Let r be its radius and $q = \frac{1}{r}\|O'|L^n_{n-1[O]}\|$ the relative distance of its center from O, see Figure A.1. Note that r is almost surely positive.

When $Q = 0$ the ball is centered at the origin and all hyperplanes give equivalent $(n-1)$-dimensional balls of radius R. We exclude this throughout, i.e. we assume that

$$\mathbb{P}(Q > 0) = 1. \tag{A.9}$$

This assumption can easily be relaxed, see Remark A.2. The cumulative distribution function $F_{(r,q)}$ of (r, q) is given in the following theorem.

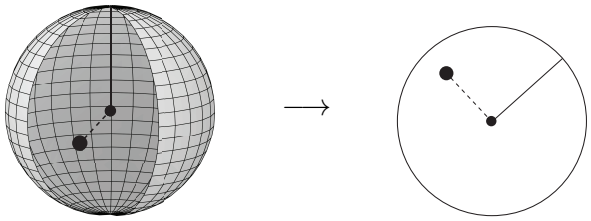

Figure A.1: To the left: $RB_3 + O'$ with reference point (bold). The full line segment has length R and the broken line segment has length RQ. To the right: Section plane with profile. The full line segment and the broken line segment have length r and rq, respectively.

Theorem A.1. *Let $RB_n + O'$ be a random ball in $\mathbb{R}^n$ containing O with $\|O'\| = RQ$, and let*

$$Z = Z(R, Q, x, y) = \frac{1}{Q^2} \max\left\{ \frac{(R^2 - x^2)^+}{R^2}, \frac{(Q^2 - y^2)^+}{1 - y^2} \right\} \tag{A.10}$$

for $x \in [0, \infty)$, $y \in [0, 1)$. If $L^n_{n-1[O]}$ is an IR hyperplane, independent of $RB_n + O'$, we have

$$F_{(r,q)}(x, y) = 1 - \frac{\sigma_{n-1}}{\sigma_n} \mathbb{E}\Big[B\Big(1 - \Big(1 - Z\Big)^+; \frac{1}{2}, \frac{n-1}{2}\Big)\Big], \tag{A.11}$$

for $x \geq 0$ and $0 \leq y < 1$. For $y = 1$, we obtain the marginal distribution function of r by

$$\begin{aligned} F_r(x) &= F_{(r,q)}(x, 1) \\ &= 1 - \frac{\sigma_{n-1}}{\sigma_n} \mathbb{E}\Big[B\Big(1 - \Big(1 - \frac{1}{Q^2 R^2}(R^2 - x^2)^+\Big)^+; \frac{1}{2}, \frac{n-1}{2}\Big)\Big], \end{aligned} \tag{A.12}$$

where $x \geq 0$.

Proof. To avoid confusion we adopt the notation $\mathbb{E}_X$, $\mathbb{E}_{X,Y}$ for the expectation with respect to the random variable X and the pair of random variables (X, Y), respectively. Assume without loss of generality that $O' = RQe_n$. (Otherwise both $RB_n + O'$ and the section plane can be appropriately rotated. As the rotation is independent of the section plane, the rotated plane is still IR.) Let v be an isotropic vector on S^{n-1} representing the unit normal direction of $L^n_{n-1[O]}$. Applying Pythagoras' theorem, we obtain

$$r = R\sqrt{1 - Q^2 \langle e_n, v\rangle^2} \quad \text{and} \quad q = Q\sqrt{\frac{1 - \langle e_n, v\rangle^2}{1 - Q^2 \langle e_n, v\rangle^2}}. \tag{A.13}$$

Using conditional expectation we have for $x \in [0, \infty)$ and $0 \leq y \leq 1$, that

$$\begin{aligned} F_{(r,q)}(x, y) &= \mathbb{E}_{R,Q}\mathbb{E}_v\Big[\mathbf{1}\Big\{R\sqrt{1 - Q^2 \langle e_n, v\rangle^2} \leq x,\ Q\sqrt{\frac{1 - \langle e_n, v\rangle^2}{1 - Q^2 \langle e_n, v\rangle^2}} \leq y\Big\} \,\Big|\, R, Q\Big] \\ &= \mathbb{E}_{R,Q} \frac{1}{\sigma_n} \int_{S^{n-1}} \mathbf{1}\Big\{R\sqrt{1 - Q^2 \langle e_n, v\rangle^2} \leq x,\ \frac{1 - \langle e_n, v\rangle^2}{1 - Q^2 \langle e_n, v\rangle^2} \leq \frac{y^2}{Q^2}\Big\} \mathrm{d}v^{n-1}. \end{aligned}$$

We use cylindrical coordinates [Mül66, p. 1], writing $v = te_n + \sqrt{1 - t^2}\omega$, with $\omega \in S^{n-1} \cap e_n^\perp$ and $t \in [-1, 1]$. Using $\langle e_n, v\rangle = t$ and $\mathcal{H}^{n-2}_{n-1}(S^{n-1} \cap e_n^\perp) = \sigma_{n-1}$, the

cumulative distribution function becomes

$$F_{(r,q)}(x,y) = \mathbb{E}_{R,Q}\frac{\sigma_{n-1}}{\sigma_n}\int_{-1}^{1}\mathbf{1}\Big\{R\sqrt{1-Q^2t^2}\le x,\ \frac{1-t^2}{1-Q^2t^2}\le\frac{y^2}{Q^2}\Big\}\left(1-t^2\right)^{\frac{n-3}{2}}\mathrm{d}t.$$

The integrand is an even function of t. This and rearranging the indicator functions gives

$$F_{(r,q)}(x,y) = \frac{2\sigma_{n-1}}{\sigma_n}\mathbb{E}_{R,Q}\int_0^1\Big(\mathbf{1}\Big\{t\ge\frac{1}{QR}\sqrt{(R^2-x^2)^+},y=1\Big\} + \mathbf{1}\{t\ge\sqrt{Z},y<1\}\Big)\left(1-t^2\right)^{\frac{n-3}{2}}\mathrm{d}t,$$

where Z is given by (A.10). Using the substitution $s=t^2$ the cumulative distribution function of (r,q), under the assumption $0\le y<1$, becomes

$$\begin{aligned}F_{(r,q)}(x,y) &= \frac{\sigma_{n-1}}{\sigma_n}\mathbb{E}_{R,Q}\int_{\min\{1,Z\}}^1 s^{\frac{1}{2}-1}(1-s)^{\frac{n-1}{2}-1}\mathrm{d}s\\ &= 1-\frac{\sigma_{n-1}}{\sigma_n}\mathbb{E}_{R,Q}\Big[B\Big(1-\Big(1-Z\Big)^+;\frac{1}{2},\frac{n-1}{2}\Big)\Big].\end{aligned}$$

Using similar calculations, we obtain (A.12) for the marginal distribution of r. □

Remark A.2. *If $\mathbb{P}(Q>0)<1$, the result of Theorem A.1 and, similarly, results in the subsequent sections can be generalized by conditioning on the event $Q>0$. When $Q=0$, we have $r=R$, and hence*

$$\begin{aligned}F_{(r,q)}(x,y) = \mathbb{P}(Q>0)\Big(1-\frac{\sigma_{n-1}}{\sigma_n}\mathbb{E}\Big[B\Big(1-\Big(1-Z\Big)^+;\frac{1}{2},\frac{n-1}{2}\Big)\Big|Q>0\Big]\Big)\\ +\mathbb{P}(R\le x,Q=0),\end{aligned}$$

when $x\ge 0,\ 0\le y<1$. A similar modification allows to generalize (A.12).

The distribution functions given by (A.11) and (A.12) simplify considerably when $n=3$.

Corollary A.3. *When $n=3$,*

$$F_{(r,q)}(x,y) = \mathbb{E}\Big(1-\sqrt{Z}\Big)^+,\qquad 0\le x,0\le y<1, \tag{A.14}$$

and

$$F_r(x) = \mathbb{E}\Big[\Big(1-\frac{1}{RQ}\sqrt{(R^2-x^2)^+}\Big)^+\Big],\qquad x\ge 0. \tag{A.15}$$

From (A.11) we immediately infer that the marginal distribution of q is given by

$$F_q(y) = 1-\frac{\sigma_{n-1}}{\sigma_n}\mathbb{E}\Big[B\Big(\frac{(Q^2-y^2)^+}{Q^2(1-y^2)};\frac{1}{2},\frac{n-1}{2}\Big)\Big],\qquad 0\le y<1, \tag{A.16}$$

which does not depend on the distribution of R. This is an important fact, which we will use later on. It follows from (A.13) that one of the variables r and q determines the other whenever Q and R are given. This implies that a joint probability

density function of (r, q) need not exist. However, it is elementary to show that the marginal probability density functions exist. Let $\phi(\cdot)$ be any smooth function having a compact support in $(0, \infty)$. Then $\mathbb{E}\phi(X) = \int_0^\infty \phi'(x)(1 - F_X(x))\mathrm{d}x$, where $X = r$, respectively q. Using Fubini and Tonelli arguments, integration by parts and Leibnitz's rule we obtain the following corollary.

Corollary A.4. *Adopt the set-up in Theorem A.1. The probability density functions of r and q exist. The function*

$$f_r(x) = \frac{2\sigma_{n-1}}{\sigma_n}\mathbb{E}\Big[\frac{\boldsymbol{1}\{R\sqrt{1-Q^2} \le x < R\}x}{QR\sqrt{R^2-x^2}}\Big(1 - \frac{R^2-x^2}{Q^2R^2}\Big)^{(n-3)/2}\Big], \tag{A.17}$$

$x \ge 0$, *is a density function of r and*

$$f_q(y) = \frac{2\sigma_{n-1}}{\sigma_n}\mathbb{E}\Big[\boldsymbol{1}\{0 < y < Q\}\Big(\frac{y}{Q}\Big)^{n-2}\frac{(1-Q^2)^{(n-1)/2}}{\sqrt{Q^2-y^2}(1-y^2)^{n/2}}\Big], \tag{A.18}$$

$0 \le y < 1$, *a density function of q.*

We remark that when R and Q are independent and $n = 3$, (A.17) simplifies

$$f_r(x) = x\mathbb{E}_R\Big[\frac{\mathbf{1}\{x < R\}}{R\sqrt{R^2-x^2}}\Big(\mathbb{E}_Q\frac{\mathbf{1}\{R\sqrt{1-Q^2} \le x\}}{Q}\Big)\Big], \qquad x \ge 0. \tag{A.19}$$

According to (A.2) the radius of the section profile can be written as a multiple of the size-weighted radius R_w of the intersected ball in the classical Wicksell problem. A similar result holds in the local Wicksell problem but here the radii of the intersected balls are not size-weighted.

Proposition A.5. *If the assumptions of Theorem A.1 hold, then*

$$r = \Gamma R,$$

where the random variable Γ *has density*

$$f_\Gamma(z) = \frac{2\sigma_{n-1}}{\sigma_n}\mathbb{E}\Big[\boldsymbol{1}\{\sqrt{1-Q^2} \le z < 1\}\frac{z}{Q^{n-2}\sqrt{1-z^2}}(Q^2 - 1 + z^2)^{\frac{n-3}{2}}\Big], \tag{A.20}$$

$z \ge 0$. *If R and Q are independent, then R and* Γ *are independent.*

Proof. Let $h(x|R = R_0)$, $x \ge 0$, be the conditional density of r given that a ball of radius R_0 is cut by the section plane. By (A.17) we have that

$$h(x|R = R_0) = \frac{2\sigma_{n-1}}{\sigma_n}\mathbb{E}\Big[\frac{\mathbf{1}\{R_0\sqrt{1-Q^2} \le x < R_0\}x}{QR_0\sqrt{R_0^2-x^2}}\Big(1 - \frac{R_0^2-x^2}{Q^2R_0^2}\Big)^{\frac{n-3}{2}}\Big|R = R_0\Big],$$

$x \ge 0$, is a version of this density. We note that h satisfies the scaling property

$$h(x|R = R_0) = \frac{1}{R_0}h\Big(\frac{x}{R_0}\Big|R = 1\Big).$$

Let Γ be the random variable defined by $\Gamma = r/R$. Using conditional expectation, conditioning on $R = R_0$, and then a substitution, we obtain

$$\mathbb{P}(\Gamma \leq z) = \mathbb{E}\mathbb{P}(r \leq zR_0 | R = R_0) = \mathbb{E}[\int_0^z R_0 h(sR_0 | R = R_0) \mathrm{d}s],$$

for $z \geq 0$. Applying the scaling property and conditional expectation we see that a density of Γ is given by (A.20). When Q and R are independent, R and Γ are independent by construction. □

The cumulative distribution function of the random variable Γ in Proposition A.5 is immediately obtained using (A.12) with $R = 1$,

$$F_\Gamma(z) = 1 - \frac{\sigma_{n-1}}{\sigma_n} \mathbb{E}\Big[B\Big(1 - \Big(1 - \frac{(1-z^2)}{Q^2}\Big)^+; \frac{1}{2}, \frac{n-1}{2}\Big)\Big], \quad 0 \leq z < 1. \tag{A.21}$$

Remark A.6. *As the distribution of Γ in Proposition A.5 only depends on (R, Q) through Q we may write $c_k(Q) = \mathbb{E}\Gamma^k$, $k = 0, 1, 2, \ldots$, for the kth moment of Γ. These moments are given by*

$$c_k(Q) = \frac{2\sigma_{n-1}}{\sigma_n} \mathbb{E}\Big[\frac{1}{Q^{n-2}} \int_{\sqrt{1-Q^2}}^1 \frac{z^{k+1}}{\sqrt{1-z^2}} (Q^2 - 1 + z^2)^{(n-3)/2} \mathrm{d}z\Big], \tag{A.22}$$

for $k = 0, 1, 2, \ldots$. In particular for $n = 3$, the substitution $x = z^2$, yields

$$c_k(Q) = \frac{1}{2} \mathbb{E}\Big[\frac{1}{Q}\Big(\frac{\sigma_{k+3}}{\sigma_{k+2}} - B\Big(1 - Q^2, \frac{k+2}{2}, \frac{1}{2}\Big)\Big)\Big]. \tag{A.23}$$

Denote the kth moment of R by M_k, and that of r by m_k. When R and Q are independent, Proposition A.5 gives us the following moment relation

$$m_k = c_k(Q) M_k, \tag{A.24}$$

where $c_k(Q)$ is given by (A.22).

A.4 Uniqueness

The distribution F_q uniquely determines F_Q. This can be seen from (A.18), which can be rewritten as

$$f_q(y) = \frac{2\sigma_{n-1} y^{n-2}}{\sigma_n (1-y^2)^{n/2}} \mathbf{1}\{y > 0\} \int_y^1 \frac{(1-s^2)^{\frac{n-1}{2}}}{s^{n-2}\sqrt{s^2 - y^2}} \mathrm{d}F_Q(s).$$

This is essentially an Abel transform of the positive measure $(1-s^2)^{\frac{n-1}{2}} / s^{n-2} \mathrm{d}F_Q(s)$. The Abel transform has a unique solution, see e.g. [GV91, Section 1.2], and hence F_q uniquely determines F_Q. An explicit solution is given in Proposition A.9 for $n = 3$.

When the spatial parameters R and Q are independent, we also can show that F_r determines F_R uniquely.

Theorem A.7. *Adopt the set-up in Theorem A.1. If R and Q are independent, $F_{(r,q)}$ uniquely determines $F_{(R,Q)}$.*

Proof. From Proposition A.5 we have that $r = \Gamma R$ and thus $\log r = \log \Gamma + \log R$. When R and Q are independent, Γ and R are independent and hence the characteristic functions obey

$$\varphi_{-\log r}(t) = \varphi_{-\log \Gamma}(t)\varphi_{-\log R}(t), \quad t \in \mathbb{R}. \tag{A.25}$$

We want to show that the characteristic function $\varphi_{-\log \Gamma}$ is an analytic function. We note that $F_{-\log \Gamma}(z) = 1 - F_\Gamma(e^{-z})$. Using the dominated convergence theorem, we get $\lim_{z\to 0} f_\Gamma(z) = 0$. Hence, applying l'Hopital's rule, we obtain

$$\lim_{z\to\infty} \frac{1 - F_{-\log \Gamma}(z)}{e^{-z}} = \lim_{z\to 0} \frac{F_\Gamma(z)}{z} = \lim_{z\to 0} f_\Gamma(z) = 0,$$

that is $1 - F_{-\log \Gamma}(z) = o(e^{-z})$ as $z \to \infty$. As $F_{-\log \Gamma}(-z) = 0$ when $z \geq 0$, we have

$$1 - F_{-\log \Gamma}(z) + F_{-\log \Gamma}(-z) = o(e^{-z}).$$

Therefore $\varphi_{-\log \Gamma}$ is an analytic function [Luk60, p.137]. This implies that $\varphi_{-\log \Gamma}$ has only countably many zeros. Therefore, in view of (A.25), $\varphi_{-\log r}$ uniquely determines the continuous function $\varphi_{-\log R}$. It then follows from the Fourier uniqueness theorem that F_r determines F_R uniquely. As F_q uniquely determines F_Q, this finishes the proof. □

It is of interest to ask if the same holds without the independence assumption: Does the joint distribution $F_{(r,q)}$ uniquely determine $F_{(R,Q)}$ when the independence assumption is dropped? This is an open question, but the following example shows that the answer is negative if only the marginals F_q and F_r are given.

Example A.8. Assume $n = 3$ and let the joint density of (R, Q) be given by

$$f_{(R,Q)}(t, s) = 3s\,\mathbf{1}\{0 < t < s < 1\}. \tag{A.26}$$

Then the two marginals are

$$f_Q(s) = 3s^2\,\mathbf{1}\{0 < s < 1\}, \quad f_R(t) = \tfrac{3}{2}(1 - t^2)\,\mathbf{1}\{0 < t < 1\}.$$

We now show that there is another pair (R', Q') of size and shape variables which are independent, but lead to the same section marginals F_q and F_r as does the pair (R, Q) with density (A.26). As $F_{Q'}$ is uniquely determined by F_q, we necessarily have $F_{Q'} = F_Q$. If we assume that R' has a density $f_{R'}$, this and (A.17) imply that this density must satisfy

$$f_r(x) = \tfrac{3}{2}x^3 \int_x^\infty \frac{f_{R'}(s)}{s^3\sqrt{s^2 - x^2}}\,\mathrm{d}s. \tag{A.27}$$

Solving this Abel transform (see e.g. [GV91, p.35]), we get

$$f_{R'}(s) = -\frac{4s^4}{3\pi} \int_s^\infty \frac{\frac{\mathrm{d}}{\mathrm{d}x}(f_r(x)x^{-3})}{\sqrt{x^2 - s^2}}\,\mathrm{d}x. \tag{A.28}$$

Hence, we would define $f_{R'}$ by (A.28) if we can guarantee that this function is a density. By (A.26) and (A.17), f_r is explicitly known. With this f_r the right hand side of (A.28) indeed is non-negative and integrates to one; see [TK12, p.12-13] for details. Hence $f_{R'}$ is a density. We thus have shown that populations of balls with size-shape parameters (R, Q) and (R', Q'), respectively, lead to the same size-shape distributions of their profiles, although $F_{(R,Q)} \neq F_{(R',Q')}$. ∎

A.5 The unfolding problem

We mentioned in the introduction that there exists a reproducing distribution for the radii in the classical Wicksell problem (the Rayleigh distribution). In the local Wicksell problem a reproducing radii distribution does typically not exist. When the balls are not a.s. centered at O, the radii of the section profiles are smaller than the radii of the respective balls with positive probability. This implies that there does not exist a reproducing distribution in the local Wicksell problem under the assumption $\mathbb{P}(Q > 0) > 0$.

In the previous section we saw that under the assumption that R and Q are independent, $F_{(r,q)}$ uniquely determines $F_{(R,Q)}$. In this section we will present analytical unfolding formulae and moment relations. In order to avoid technicalities, we restrict attention to the three-dimensional case, which is most relevant for practical applications. The following proposition gives F_Q in terms of F_q.

Proposition A.9. *If the assumptions of Theorem A.1 hold, and $n = 3$, then*

$$1 - F_Q(y) = -\frac{2y^3}{\pi}\Big(\int_y^1 \frac{(s^2-2)(1-F_q(s))}{s^3\sqrt{1-s^2}\sqrt{s^2-y^2}}\mathrm{d}s - \int_y^1 \frac{\sqrt{1-s^2}}{s^2\sqrt{s^2-y^2}}\mathrm{d}F_q(s)\Big), \quad \text{(A.29)}$$

$y \in [0, 1)$.

Proof. Let $0 \leq y < 1$. From (A.16) we know that the distributions of Q and q are connected by

$$F_q(y) = 1 - \mathbb{E}\Big[\frac{\sqrt{(Q^2-y^2)^+}}{Q\sqrt{1-y^2}}\Big].$$

Using integration by parts and rearranging, we obtain

$$1 - F_q(y) = \frac{y^2}{\sqrt{1-y^2}} \int_y^1 \frac{1}{s^2\sqrt{s^2-y^2}}(1-F_Q(s))\mathrm{d}s. \quad \text{(A.30)}$$

Define

$$h(y) = \frac{\sqrt{1-y^2}}{y^2}(1-F_q(y)) \quad \text{and} \quad g(s) = \frac{1-F_Q(s)}{s^2}. \quad \text{(A.31)}$$

Equation (A.30) is an Abel transform of $g(s)$ with solution given by

$$g(y) = -\frac{2}{\pi}\frac{\mathrm{d}}{\mathrm{d}y}\int_y^1 \frac{sh(s)}{\sqrt{s^2-y^2}}\mathrm{d}s = -\frac{2y}{\pi}\int_y^1 \frac{h'(s)}{\sqrt{s^2-y^2}}\mathrm{d}s; \quad \text{(A.32)}$$

see for instance [GV91, p.35]. Inserting for g and the derivative of h, (A.29) is obtained. □

Using similar arguments as in the proof of Proposition A.9, we obtain that when Q has a density f_Q, it is given by

$$f_Q(s) = \frac{8s^2}{\pi}\frac{\mathrm{d}^2}{\mathrm{d}(s^2)^2}\int_s^1 \frac{t\sqrt{1-t^2}}{\sqrt{t^2-s^2}}(1-F_q(t))\mathrm{d}t, \qquad 0 \le s < 1. \tag{A.33}$$

We can use (A.32) to write the moments of Γ in Proposition A.5 as functions of q only.

Corollary A.10. *Adopt the set-up in Theorem A.1. For $n = 3$ the moments of the random variable Γ in Proposition A.5, can be written as*

$$\mathbb{E}\Gamma^k = 1 - \frac{k}{\pi}\mathbb{E}[\tilde{\Gamma}(q)], \qquad k = 0, 1, 2, \ldots, \tag{A.34}$$

where

$$\tilde{\Gamma}(y) = \int_0^y \frac{\sqrt{1-s^2}}{s}\int_0^{s^2} \frac{\sqrt{t}(1-t)^{\frac{k-2}{2}}}{\sqrt{s^2-t}}\mathrm{d}t\mathrm{d}s. \tag{A.35}$$

Proof. Using (A.21) with $n = 3$ we note that the distribution function of Γ can be written as

$$F_\Gamma(z) = \mathbb{E}\Big[\Big(1 - \frac{1}{Q}\sqrt{1-z^2}\Big)^+\Big] = \sqrt{1-z^2}\int_{\sqrt{1-z^2}}^1 g(s)\mathrm{d}s, \quad 0 \le z < 1,$$

where $g(s)$ is given by (A.31). Using the first equality in (A.32) and substituting $t = 1 - z^2$, the moments of Γ are given by

$$\mathbb{E}\Gamma^k = \int_0^1 kz^{k-1}(1-F_\Gamma(z))\mathrm{d}z = 1 - \frac{k}{\pi}\int_0^1 (1-t)^{\frac{k-2}{2}}\sqrt{t}\int_{\sqrt{t}}^1 \frac{yh(y)}{\sqrt{y^2-t}}\mathrm{d}y\mathrm{d}t.$$

Inserting h and using Tonelli's theorem we arrive at

$$\begin{aligned}\mathbb{E}\Gamma^k &= 1 - \frac{k}{\pi}\int_0^1 \frac{\sqrt{1-y^2}}{y}(1-F_q(y))\int_0^{y^2} \frac{\sqrt{t}(1-t)^{\frac{k-2}{2}}}{\sqrt{y^2-t}}\mathrm{d}t\mathrm{d}y \\ &= 1 - \frac{k}{\pi}\mathbb{E}[\tilde{\Gamma}(q)],\end{aligned}$$

where $\tilde{\Gamma}$ is given by (A.35). □

If $k = 2m$, $m \ge 1$, equation (A.34) simplifies to

$$\mathbb{E}\Gamma^{2m} = 1 - \frac{m}{\pi}\sum_{j=0}^{m-1}\binom{m-1}{j}(-1)^j\frac{\sigma_{2j+4}}{\sigma_{2j+3}}\mathbb{E}\Big[B\Big(q^2; j+1, \frac{3}{2}\Big)\Big],$$

and in particular

$$\mathbb{E}\Gamma^2 = \tfrac{1}{3}(2 + \mathbb{E}[(1-q^2)^{3/2}]).$$

Thus the average surface area of balls in $\mathbb{R}^3$ can be estimated ratio unbiasedly by

$$\frac{\frac{12\pi}{N}\sum_{i=1}^{N} r_i^2}{2+\frac{1}{N}\sum_{i=1}^{N}(1-q_i^2)^{3/2}},$$

where $(r_1, q_1), \ldots, (r_N, q_N)$ are N independent observations of profile parameters.

When Q has a density, similar arguments as applied in the proof of (A.33) can be used to show that the moments of Γ can be written as

$$\mathbb{E}\Gamma^k = \frac{1}{2\pi}\mathbb{E}[\tilde{\Gamma}_1(q^2)] + \frac{1}{\pi}\mathbb{E}[\tilde{\Gamma}_2(q^2)], \tag{A.36}$$

where

$$\tilde{\Gamma}_1(y) = \int_0^y \frac{(1-t)^{k/2}}{\sqrt{t}} B\Big(\frac{y-t}{1-t}, \frac{1}{2}, \frac{1}{2}\Big)\mathrm{d}t, \quad \tilde{\Gamma}_2(y) = \sqrt{1-y}\int_0^y \frac{(1-t)^{k/2}}{\sqrt{t}\sqrt{y-t}}\mathrm{d}t.$$

By (A.24) and Corollary A.10, the moments of R can be estimated from the section profiles when R and Q are independent. A number of stochastic simulation studies were carried out, varying F_Q, F_R and the number of observations. The function `quad` in the language and interactive environment `Matlab` was used to determine $\tilde{\Gamma}_1$ and $\tilde{\Gamma}_2$ numerically. We used (A.36) instead of the more general expression given in Corollary A.10 as it is more straight-forward to implement. Then M_k was estimated by dividing the crude Monte Carlo (CMC) estimate of m_k by the CMC estimate obtained for $\mathbb{E}\Gamma^k$ using (A.36). The simulations suggest that the estimation procedure is quite stable for moments up to 7th order. The difference between the coefficient of error of this estimator and of M_k estimated by CMC, using the simulated particle radii, is typically less than 10% for $k = 1, \ldots, 7$. This seems to be true irrespective of the choice of F_Q and even after adding moderate measurement errors to r and q.

A.6 Reconstruction

In this section we will discuss the estimation of F_R and F_Q from data. We assume throughout this section that R and Q are independent, and that $n = 3$. To assure this independence, a priori knowledge on the particles is required. There are, however, cases, where this independence holds trivially. We refer to the concluding Section A.9 for a discussion. As mentioned in the introduction, there exist various methods for numerically solving Wicksell's classical problem but none of these seems to be superior to all the others. In [BMN84] six distribution-free methods are compared using several error criteria as well as studying their numerical stability and sensitivity to underlying distributions. Considering all criteria, the Scheil-Schwartz-Saltykov method (S^3M) from [Sal74] is favoured, in particular when the underlying distribution is smooth. The method can be classified as a finite difference method, a class of methods which are relatively easy to implement. We therefore chose to implement a variation of S^3M. The method and its advantages and disadvantages are discussed in [BMN84]. Although this method is rather crude,

we obtain satisfactory results. We have also studied the product integration method explained in [AJ75b]. The method has been claimed to yield accurate results for Wicksell's classical problem, but our reconstruction of F_Q based on Proposition A.9 is not satisfactory. The reconstruction $\hat{F}_Q$ is not monotonic and fluctuates far too much around F_Q to be of any use. We have also implemented kernel density estimators for obtaining $\hat{F}_Q$ but without obtaining stable results.

In the following we describe the implementation of S^{3}M in our setup. We start using S^{3}M to obtain a discrete approximation of F_Q based on the Abel-type relation (A.30). By discretizing F_Q, the integral becomes a finite sum. This produces a system of linear equations that can be solved. After having obtained an estimate $\hat{F}_Q$ we can apply S^{3}M again, this time discretizing F_R to solve (A.15) numerically (where $\hat{F}_Q$ is substituted for the unknown F_Q). We used `Matlab` for all simulations and for generating Figure A.2.

Assume that we observe N pairs $(r_1, q_1), \dots, (r_N, q_N)$ of size and shape variables in independent sections of (independent) particles. Assume further that all observed r's, are less than or equal to a constant c. Divide the intervals $(0, 1]$ and $(0, c]$ into classes of constant width. Let k_1 denote the number of classes for q, k_2 the number of classes for Q, k_3 for r and k_4 for R. Different to [BMN84] we allow k_1, k_3, to be greater than k_2, k_4, respectively. Define $\Delta_i = 1/k_i$, $i = 1, 2$, $\Delta_i = c/k_i$, $i = 3, 4$. Let $n_i = \mathbb{P}(q \in ((i-1)\Delta_1, i\Delta_1])$ be the probability that q is in class $i \in \{1, \dots, k_1\}$, $N_j = \mathbb{P}(Q \in ((j-1)\Delta_2, j\Delta_2])$ the probability that Q is in class $j \in \{1, \dots, k_2\}$, $m_a = \mathbb{P}(r \in ((a-1)\Delta_3, a\Delta_3])$ the probability that r is in class $a \in \{1, \dots, k_3\}$, and $M_b = \mathbb{P}(R \in ((b-1)\Delta_4, b\Delta_4])$ the probability that R is in class $b \in \{1, \dots, k_4\}$.

The S^{3}M method approximates $F_Q(u)$ by the step function

$$u \mapsto \sum_{j:\Delta_2 j \le u} N_j.$$

Note that we use the standard definition of a cumulative distribution function and hence the notation is slightly different from [BMN84] where left continuous distribution functions are considered. Inserting the approximation for F_Q in (A.30) and simplifying, we obtain

$$1 - F_q(i\Delta_1) \approx \frac{1}{\sqrt{1 - i^2\Delta_1^2}\Delta_2} \sum_{j=1}^{k_2} N_j \mathbf{1}\{i\Delta_1 < j\Delta_2\} \frac{\sqrt{j^2\Delta_2^2 - i^2\Delta_1^2}}{j},$$

where the approximation is exact if and only if Q only has mass in the points $\Delta_2 j$, $j = 1, \dots, k_2$. Hence n_i can be approximated by

$$n_i = (1 - F_q((i-1)\Delta_1)) - (1 - F_q(i\Delta_1)) \approx \sum_{j=1}^{k_2} b_{ij} N_j, \tag{A.37}$$

for $i = 1, \dots, k_1$, where the constants b_{ij} depend only on Δ_1 and Δ_2; see [TK12, p.17] for an explicit formula. If F_q in (A.37) is replaced by its empirical cumulative distribution function we obtain $\hat{n}_i = \frac{1}{N} \sum_{j=1}^{N} \mathbf{1}\{q_j \in ((i-1)\Delta_1, i\Delta_1]\}$ as approximations of

the left hand side of (A.37). Using these and solving the corresponding linear system yields therefore approximations $\hat{N}_j$ of the unknown probabilities N_j, $j = 1, \ldots, k_2$. The function

$$\hat{F}_Q(u) = \sum_{j:\Delta_2 j \leq u} \hat{N}_j \tag{A.38}$$

is then the estimator for F_Q.

In a second step (A.15) is inverted using S^{3}M and the estimator $\hat{F}_Q$. This is in analogy to the treatment of F_Q and the derivation is deferred to the appendix.

In our simulations, we used N independent realizations of (r_i, q_i) to estimate $\hat{n}_i$, $i = 1, \ldots, k_1$ and $\hat{m}_a$, $a = 1, \ldots, k_3$. Then we solved (A.37) using constrained minimum least squares, `lsqlin` in `Matlab`. To ensure that the estimated distribution functions are non-decreasing, we required that $\hat{N}_j \geq 0$, $j = 1, \ldots, k_2$, $\hat{M}_b \geq 0$, $b = 1, \ldots, k_4$. Non-negativity constraints have also been suggested in [Tay83] for the classical S^{3}M. The distribution function F_Q is then estimated by (A.38). Using the estimate $\hat{F}_Q$, the linear system of equations involving the relative frequencies $\hat{m}_a$ in terms of $\hat{M}_b$ (equation (A.40)) can be solved for $\hat{M}_b$, $b = 1, \ldots, k_4$, in exactly the same way and F_R is then estimated by $\hat{F}_R(u) = \sum_{b:\Delta_4 b \leq u} \hat{M}_b$.

The simulations in [BMN84] show that classes with overestimation of the distribution function are usually close to classes with underestimation and the authors refer to this phenomenon quite intuitively as *waves*. In order to decrease the occurrence of waves, we allowed k_1, k_3, to be greater than k_2, k_4, respectively. However, this does not seem to be of great importance in our setting. We ran two types of simulations, one with the number of classes equal and another one with the number of classes unequal. Then the Kullback Leibler divergence between the true probability distribution and each of the estimated ones was calculated using `KLDiv` in `Matlab`. The difference was negligible (even after adding independent measurement errors to r_j and q_j). Therefore we chose the number of classes equal in the figure presented below.

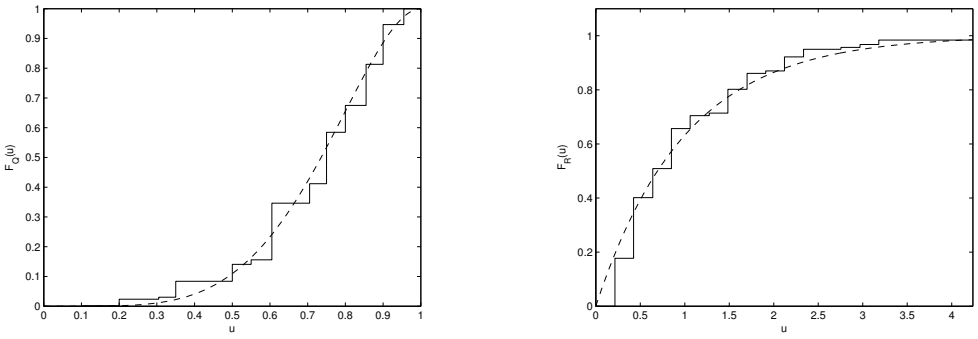

Figure A.2: The dashed curves are the true distribution functions $F_Q(u)$ (to the left) and $F_R(u)$ (to the right) when $Q \sim \text{Beta}(5, 2)$ and $R \sim \text{e}(1)$ whereas the step functions are the estimated ones. Parameter choice: $k_1 = k_2 = k_3 = k_4 = 20$, $N = 100$.

In Figure A.2 true and reconstructed distribution functions of Q (left) and R (right) are compared, where Q follows the Beta distribution with parameters 5 and

2 while R is exponentially distributed with mean one. The number of classes were chosen to be 20 for all four variables and 100 observations were used.

These results indicate that the S^{3}M method works well for reconstructing F_R and F_Q from simulated data. This is true even when the profile variables are measured with random multiplicative errors. The errors were chosen to be independent, lognormally (truncated lognormal in the case of q) distributed variables with mean one and moderate variance. Even with variance $1/2$ the mean Kullback Leibler divergence between the true probability distribution and the one obtained using the perturbed profile variables did not differ from the corresponding mean Kullback Leibler divergence using the unperturbed profile variables.

In practice, for instance in a confocal microscopy image, the boundary of an object can be quite blurry and it can therefore be difficult to evaluate profile variables when the reference point is close to the boundary and the IR section is such that it produces a small profile. We analysed how this influenced the reconstructions by omitting small profiles obtained when $Q > 1 - 0.1/R$ and $0 < r < 0.5$. Otherwise the setup was like in Figure A.2, again with 100 valid observations. This did not influence the reconstruction of F_Q, but to obtain a satisfactory reconstruction of F_R a similar recommendation as in [BMN84] applies: the sample size should be large (more than 400 profile sections) but the number of classes small (around 7).

A.7 Examples

For illustration we discuss some special cases and variants of the above general theory. We restrict attention to the three-dimensional case. Recall that we considered Q to be a variable describing the 'shape' of the random ball under consideration. We first show that the formulae simplify if Q is (almost surely) the same for all particles, meaning that all reference points have the same relative distance from their respective ball centers.

Example A.11. Assume that $Q = Q_0$ a.s., $Q_0 > 0$. Then the marginal distribution function of q given by (A.30) becomes

$$F_q(y) = 1 - \mathbf{1}\{y < Q_0\} \frac{\sqrt{Q_0^2 - y^2}}{Q_0 \sqrt{1 - y^2}}.$$

Furthermore, the moments of Γ in (A.23) simplify to

$$c_k(Q) = \frac{1}{2Q_0} \Big(\frac{\sigma_{k+3}}{\sigma_{k+2}} - B\Big(1 - Q_0^2, \frac{k+2}{2}, \frac{1}{2}\Big)\Big).$$

For $k = 1, 2$, we obtain

$$c_1(Q) = \frac{\pi}{4Q_0} - \frac{\sin^{-1}(\sqrt{1 - Q_0^2})}{2Q_0} + \frac{\sqrt{1 - Q_0^2}}{2}, \quad c_2(Q) = 1 - \frac{Q_0^2}{3}. \qquad \blacksquare$$

The formulae simplify in particular if the reference point lies on the boundary of the object, that is, when $Q_0 = 1$.

Example A.12. Let the reference point be located on the boundary of the ball $RB_3 + O'$. Then $Q = 1$ a.s. and we immediately obtain from Example A.11 that $q = 1$ a.s. and $c_k(Q) = \sigma_{k+3}/(2\sigma_{k+2})$. Note that this constant is the same as c_{k+1} given by (A.4), which can be explained by the fact that the section plane is an IUR plane hitting the ball, as shown in Example A.14. The moments of Γ can in fact be calculated explicitly in n-dimensional space and (A.24) becomes

$$m_k = \frac{\sigma_{n-1}\sigma_{k+n}}{\sigma_n\sigma_{k+n-1}} M_k.$$

Furthermore (A.19) becomes an Abel transform of the positive measure $\mathbb{P}_R(\mathrm{d}t)/t$. Hence, when R has a density function f_R, it is given by

$$\begin{aligned} f_R(t) &= -\frac{2t^2}{\pi} \int_t^\infty \frac{1}{\sqrt{x^2 - t^2}} \frac{\mathrm{d}}{\mathrm{d}x} \Big(\frac{f_r(x)}{x} \Big) \mathrm{d}x \\ &= -\frac{2t}{\pi} \frac{\mathrm{d}}{\mathrm{d}t} \int_t^\infty \frac{f_r(x)}{\sqrt{x^2 - t^2}} \mathrm{d}x; \end{aligned}$$

see for instance [GV91, p.35]. ∎

In practice a particle may have an easily identifiable kernel that cannot be treated as a mathematical point. Thus one has to work with a reference set of positive volume. In general, our methods do not apply in this case, but whenever the reference set is (approximately) ball-shaped, concentric with the whole particle, and has a radius proportional to the particle size, our method can be used. We suggest in the following examples two possible schemes for this situation.

Example A.13. Assume that the particle $RB_3 + O'$ contains a reference set $Q_0 RB_3 + O'$, $Q_0 \in (0, 1]$. The first sampling design we suggest is the choice of an isotropic plane through a uniformly chosen boundary point of the reference set. Let $L^3_{2[O]}$ be an IR plane and z a uniformly distributed point on the boundary of the reference set, chosen independently of $L^3_{2[O]}$. Define $L = L^3_{2[O]} + z$ and adopt L as the section plane, that is (r, q) refers to the parameters of the disk $(RB_3 + O') \cap L$. By construction (r, q) can thus be interpreted as section variables from a local IR plane through the reference point z, which has relative distance Q_0 from the ball's center. Hence, we can use the local Wicksell theory directly with $Q = Q_0$. The simplifications in Example A.11 apply. ∎

Example A.14. As in Example A.13 assume that the particle $RB_3 + O'$ contains a reference set $Q_0 RB_3 + O'$, $Q_0 \in (0, 1]$. In contrast to Example A.13 we now use an IUR section plane L^3_2 hitting the reference set. By definition, the distribution of L^3_2 is

$$\mathbb{P}_{L^3_2}(A) = \frac{1}{2\sigma_3 Q_0} \int_{S^2} \int_{-Q_0}^{Q_0} \mathbf{1}_A(ru + u^\perp) \mathrm{d}r \mathrm{d}u^2, \qquad A \in \mathcal{B}(\mathcal{L}^3_2).$$

Using cylindrical coordinates, we have, equivalently,

$$\mathbb{P}_{L_2^3}(A) = \frac{1}{\sigma_3^2} \int_{S^2} \int_{S^2} \mathbf{1}_A(Q_0 v + u^\perp) \mathrm{d}u^2 \mathrm{d}v^2, \qquad \blacksquare$$

so L_2^3 is an isotropic plane through the (independent) point $z = Q_0 v$, which is uniform on the boundary of the reference set. Concluding, we see that L_2^3 has the same distribution as L in Example A.13. Hence, the two designs lead to the same sample distribution, and, again, Wicksell's local theory with $Q = Q_0$ applies.

The last two (coinciding) sampling schemes can in particular be applied when the reference set is taken to be the whole ball. This is equivalent to choosing $Q_0 = 1$ and the formulae in Example A.12 can be applied in this case.

A.8 Stereology of extremes

In some practical applications, for instance when studying damage of materials [MB99], the distribution of the maximal size parameter is of more interest than the whole distribution. When extremal parameters are studied based on lower dimensional sections we speak of stereology of extremes. We will here discuss stereology of extremes in the context of the local Wicksell problem.

The reader is referred to [Haa70] for results in extreme value theory. Following the notation in [Haa70] we write $F \in \mathcal{D}(L)$ if F is in the domain of attraction of the distribution function L. Up to affine transformations, L must be one of the extreme value distributions: Fréchet $L_{1,\gamma}$, Weibull $L_{2,\gamma}$ and Gumbel L_3, where $\gamma > 0$ is a parameter.

We assume that R and Q are independent and that $n = 3$. Given independent observations $(r_1, q_1), \ldots, (r_N, q_N)$ we are interested in the distribution of the extremal particle radius. Therefore relations between the domains of attraction of the distributions of the size parameters are of interest. These are given in the following theorem.

Proposition A.15. *Let $n = 3$, $\gamma > 0$, and assume that R and Q are independent and have probability densities. The following statements hold*

- *if $F_R \in \mathcal{D}(L_{1,\gamma})$, then $F_r \in \mathcal{D}(L_{1,\gamma})$,*
- *if $F_R \in \mathcal{D}(L_{2,\gamma})$, then $F_r \in \mathcal{D}(L_{2,\gamma+1/2})$,*
- *if $F_R \in \mathcal{D}(L_3)$, then $F_r \in \mathcal{D}(L_3)$.*

A proof of this proposition can be found in [TK12, p.22-24]. Using similar arguments, an analogous result for the shape parameters can be shown: $F_Q \in \mathcal{D}(L_{2,\gamma})$ implies $F_q \in \mathcal{D}(L_{2,\gamma+1/2})$ and $F_Q \in \mathcal{D}(L_3)$ implies $F_q \in \mathcal{D}(L_3)$.

In order to use these results in practical applications, the normalizing constants for both F_r and F_R are required. They can be estimated by a semi-parametric approach as in the classical Wicksell problem: First a parametric model for F_R is chosen.

We know from Proposition A.15 that F_R and F_r belong to the same domain of attraction. Hence normalizing constants based on $(r_1, q_1), \ldots, (r_N, q_N)$ can be found, for example using maximum likelihood estimators based on the k largest observations; cf. [Wei78]. One then has to derive normalizing constants for F_R from the estimated normalizing constants for F_r. Methods regarding this are discussed in e.g. [Hlu03b] and [Tak87]. When normalizing constants for F_R have been obtained, they can be used to approximate the distribution of the extremal particle radius.

A.9 Conclusion

The present paper gives a detailed survey of Wicksell's famous corpuscle problem in a local setting. We have derived several results analogous to the ones existing for the classical problem and described differences between the two. We have in particular given the distributions and marginal densities of the profile parameters in terms of the particle parameters, derived moment relations, uniqueness results and domain of attraction relations as well as given some examples and reconstructions of the particle distributions from experimental data. Many of these results require that the particle parameters are independent. Given experimental data, one might hope that the independence assumption of the particle parameters could be assured by cheking if the profile parameters can be assumed to be independent. However, this is not possible as the profile parameters are always dependent apart from mathematically trivial cases, for instance when $Q = 1$ a.s. Nevertheless, we believe that in many practical applications it is not unrealistic to assume a priori that the relative position of the reference point does not depend on the size of the object.

It should be mentioned that also the case $Q = 1$ a.s. (certainly implying the independence of R and Q) is relevant for applications. For instance, white fat cells are spherical in shape and have their nucleus at the cell's periphery; see [MBBO04, p. 163]. Using this nucleus as reference point allows to use the formulae in Example A.12 and the S^3M algorithm to estimate moments or even the distribution of R. As we have seen in Example A.14, the local formulae can even be applied when there is no natural reference point, but the section planes are just chosen to be IUR hitting the particle under consideration.

Acknowledgement

Both authors have been supported by the Centre for Stochastic Geometry and Advanced Bioimaging, funded by the Villum Foundation.

Appendix: S^3M for F_R

We have described shortly in the main text how S^3M can be used to invert (A.30). The following inversion of (A.15) is slightly more involved, as it is based on the approximation $\hat{F}_Q$. We therefore give some additional details here. We note that

(A.15) can be rewritten as

$$F_r(x) = (1 - F_R(x)) + \mathbb{E}\Big[\mathbf{1}\{x < R\}\frac{\sqrt{R^2 - x^2}}{R}\int_{\frac{1}{R}\sqrt{R^2-x^2}}^{1}\frac{1}{s^2}(1 - F_Q(s))\mathrm{d}s\Big],$$

for $x \in [0, \infty)$. Approximating F_Q by $\hat{F}_Q$ given by (A.38) we find

$$\begin{aligned}\mathbb{E}\Big[\mathbf{1}\{x < R\}\frac{\sqrt{R^2 - x^2}}{R}\int_{\frac{1}{R}\sqrt{R^2-x^2}}^{1}\frac{1}{s^2}(1 - \hat{F}_Q(s))\mathrm{d}s\Big]&\\ = 1 - \sum_{j=1}^{k_2-1}\hat{N}_j\frac{1}{\Delta_2 j}\int_x^{x/\sqrt{1-\Delta_2^2 j^2}}\frac{x^2}{t^2\sqrt{t^2 - x^2}}(1 - F_R(t))\mathrm{d}t&\\ - F_R(x) - \hat{N}_{k_2}\frac{1}{\Delta_2 k_2}\int_x^{\infty}\frac{x^2}{t^2\sqrt{t^2 - x^2}}(1 - F_R(t))\mathrm{d}t.&\end{aligned}$$

Hence

$$\begin{aligned}F_r(x) \approx \frac{1}{3}\Big(2 - \sum_{j=1}^{k_2-1}\hat{N}_j\frac{1}{\Delta_2 j}\int_x^{x/\sqrt{1-\Delta_2^2 j^2}}\frac{x^2}{t^2\sqrt{t^2 - x^2}}(1 - F_R(t))\mathrm{d}t&\\ - \hat{N}_{k_2}\frac{1}{\Delta_2 k_2}\int_x^{\infty}\frac{x^2}{t^2\sqrt{t^2 - x^2}}(1 - F_R(t))\mathrm{d}t\Big).&\end{aligned} \tag{A.39}$$

Recall that m_a is the probability that r is in class a, $a = 1, \ldots, k_3$, and M_b the probability that R is in class b, $b = 1, \ldots, k_4$. The S^{3}M method approximates $F_R(u)$ by

$$u \mapsto \sum_{b:\Delta_4 b \le u} M_b.$$

Using this in (A.39) we obtain, again using elementary calculations, that

$$\begin{aligned}F_r(a\Delta_3) \approx -\frac{1}{3}\Big(\sum_{j=1}^{k_2-1}\hat{N}_j\frac{1}{\Delta_2 j}\sum_{b=1}^{k_4}M_b\mathbf{1}\{\Delta_4 b \ge a\Delta_3\}\sqrt{1 - \Big(\min\Big\{\frac{\Delta_4^2 b^2}{a^2\Delta_3^2}, \frac{1}{1 - \Delta_2^2 j^2}\Big\}\Big)^{-1}}&\\ + \hat{N}_{k_2}\frac{1}{\Delta_2 k_2}\sum_{b=1}^{k_4}M_b\mathbf{1}\{\Delta_4 b \ge a\Delta_3\}\sqrt{1 - \frac{a^2\Delta_3^2}{\Delta_4^2 b^2}} - 2\Big).&\end{aligned}$$

We are thus lead to the linear system

$$\hat{m}_a = \hat{F}_r(a\Delta_3) - \hat{F}_r((a-1)\Delta_3) = \sum_{b=1}^{k_4} c_{ab}\hat{M}_b, \tag{A.40}$$

$a = 1, \ldots, k_3$, involving the relative frequencies $\hat{m}_a = \frac{1}{N}\sum_{j=1}^{N}\mathbf{1}\{r_j \in ((a-1)\Delta_3, a\Delta_3]\}$. Here

$$\begin{aligned}c_{ab} = \frac{1}{3}\sum_{j=1}^{k_2-1}\hat{N}_j\frac{1}{\Delta_2 j}\Big(\mathbf{1}\{\Delta_4 b \ge (a-1)\Delta_3\}\sqrt{1 - \Big(\min\Big\{\frac{\Delta_4^2 b^2}{(a-1)^2\Delta_3^2}, \frac{1}{1 - \Delta_2^2 j^2}\Big\}\Big)^{-1}}&\\ - \mathbf{1}\{\Delta_4 b \ge a\Delta_3\}\sqrt{1 - \Big(\min\Big\{\frac{\Delta_4^2 b^2}{a^2\Delta_3^2}, \frac{1}{1 - \Delta_2^2 j^2}\Big\}\Big)^{-1}}\Big)&\\ + \frac{\hat{N}_{k_2}}{3\Delta_2 k_2}\Big(\mathbf{1}\{\Delta_4 b \ge (a-1)\Delta_3\}\sqrt{1 - \frac{(a-1)^2\Delta_3^2}{\Delta_4^2 b^2}} - \mathbf{1}\{\Delta_4 b \ge a\Delta_3\}\sqrt{1 - \frac{a^2\Delta_3^2}{\Delta_4^2 b^2}}\Big)&\end{aligned}$$

for $a = 1, \ldots, k_3$, $b = 1, \ldots, k_4$, depends only on Δ_3, Δ_4, $(\hat{N}_1, \ldots, \hat{N}_{k_2})$ and Δ_2. The linear system of equations can be solved for the unknown $\hat{M}_b$ approximating M_b, $b = 1, \ldots, k_4$.

Bibliography

[ADH90] R.S. Anderssen and F.R. De Hoog. Abel integral equations. In *Numerical solution of integral equations*, volume 42, pages 373–410. Plenum Press, New York, 1990.

[AJ75a] R.S. Anderssen and A.J. Jakeman. Abel type integral equations in stereology. II. Computational methods of solution and the random spheres approximation. *J. Microsc.*, 105:135–153, 1975.

[AJ75b] R.S. Anderssen and A.J. Jakeman. Product integration for functionals of particle size distributions. *Util. Math.*, 8:111–126, 1975.

[BBH03] V. Beneš, K. Bodlák, and D. Hlubinka. Stereology of extremes; bivariate models and computation. *Methodol. Comput. Appl. Probab.*, 5(3):289–308, 2003.

[BJ05] A. Baddeley and E.B.V. Jensen. *Stereology for Statisticians*. Chapman & Hall/CRC, Boca Raton, 2005.

[BMN84] R. Blödner, P. Mühlig, and W. Nagel. The comparison by simulation of solutions of Wicksell's corpuscle problem. *J. Microsc.*, 135:61–74, 1984.

[CO83] L.M. Cruz-Orive. Distribution-free estimation of sphere size distributions from slabs showing overprojection and truncation, with a review of previous methods. *J. Microsc.*, 131:265–290, 1983.

[DR92] H. Drees and R.-D. Reiss. Tail behavior in Wicksell's corpuscle problem. In *Probability Theory and Applications*, pages 205–220. Kluwer, Dordrecht, 1992.

[GV91] R. Gorenflo and S. Vessella. *Abel Integral Equations. Analysis and Applications.* Springer, Heidelberg, 1991.

[Haa70] L. Haan. *On Regular Variation and Its Application to the Weak Convergence of Sample Extremes*. Mathematisch Centrum, 1970.

[Hlu03a] D. Hlubinka. Stereology of extremes; shape factor of spheroids. *Extremes*, 6(1):5–24, 2003.

[Hlu03b] D. Hlubinka. Stereology of extremes; size of spheroids. *Math. Bohem.*, 128(4):419–438, 2003.

[Hlu06] D. Hlubinka. Extremes of spheroid shape factor based on two dimensional profiles. *Kybernetika*, 42(1):77–94, 2006.

[Jen84] E.B. Jensen. A design-based proof of Wicksell's integral equation. *J. Microsc.*, 136:345–348, 1984.

[Jen91] E.B.V. Jensen. Recent developments in the stereological analysis of particles. *Ann. Inst. Stat. Math.*, 43:455–468, 1991.

[Jen98] E.B.V. Jensen. *Local Stereology.* World Scientific, Singapore, 1998.

[KM06] S. Kötzer and I. Molchanov. On the domain of attraction for the lower tail in Wicksell's corpuscle problem. In *Proceedings S4G. International Conference on Stereology, Spatial Statistics and Stochastic Geometry. Prague, June 26-29, 2006*, pages 91–96, 2006.

[Luk60] E. Lukacs. *Characteristic Functions.* Charles Griffin & Company Limited, London, 1960.

[MB99] Y. Murakami and S. Beretta. Small defects and inhomogeneities in fatigue strength: experiments, models and statistical implications. *Extremes*, 2(2):123–147, 1999.

[MBBO04] R.M. Malina, C. Bouchard, and O. Bar-Or. *Growth, Maturation and Physical Activity*. Human Kinetics, United States, 2004.

[MS80] J. Mecke and D. Stoyan. Stereological problems for spherical particles. *Math. Nachr.*, 96:311–317, 1980.

[Mül66] C. Müller. *Spherical Harmonics.* Springer, Heidelberg, 1966.

[OM00] J. Ohser and F. Mücklich. *Statistical Analysis of Microstructures in Materials Science*. John Wiley & Sons, New York, 2000.

[Paw12] Z. Pawlas. Local stereology of extremes. *Image Anal. Stereol.*, 31:99–108, 2012.

[Sal74] S.A. Saltykov. *Stereometrische Metallographie.* VEB Deutscher Verlag für Grundstoffindustrie, Leipzig, 1974.

[SKM95] D. Stoyan, W.S. Kendall, and J. Mecke. *Stochastic Geometry and its Applications.* Wiley, New York, 2nd edition, 1995.

[SW08] R. Schneider and W. Weil. *Stochastic and Integral Geometry*. Springer, Heidelberg, 2008.

[Tak87] R. Takahashi. Normalizing constants of a distribution which belongs to the domain of attraction of the Gumbel distribution. *Stat. Probab. Lett.*, 5(3):197–200, 1987.

[Tay83] C.C. Taylor. A new method for unfolding sphere size distributions. *J. Microsc.*, 132:57–66, 1983.

[TK12] Ó. Thórisdóttir and M. Kiderlen. Extended version of "Wicksell's Problem in Local Stereology". Available at `http://csgb.dk/publications/csgbrr/2012/`. 2012.

[TS96] R. Takahashi and M. Sibuya. The maximum size of the planar sections of random spheres and its application to metallurgy. *Ann. Inst. Stat. Math.*, 48(1):127–144, 1996.

[TS98] R. Takahashi and M. Sibuya. Prediction of the maximum size in Wicksell's corpuscle problem. *Ann. Inst. Stat. Math.*, 50(2):361–377, 1998.

[TS01] R. Takahashi and M. Sibuya. Prediction of the maximum size in Wicksell's corpuscle problem, II. *Ann. Inst. Stat. Math.*, 53(3):647–660, 2001.

[TS02] R. Takahashi and M. Sibuya. Metal fatigue, Wicksell transform and extreme values. *Appl. Stoch. Models Bus. Ind.*, 18(3):301–312, 2002.

[Wei78] I. Weissman. Estimation of parameters and larger quantiles based on the k largest observations. *J. Am. Stat. Assoc.*, 73:812–815, 1978.

[Wic25] S.D. Wicksell. The corpuscle problem I. *Biometrika*, 17:84–99, 1925.

Supplementary material

For the reader's convenience we give here the parts of the extended version [TK12] that are referred to in Paper A.

A.I Extended version of Example A.8

Example A.16. Assume $n = 3$ and let the joint density of (R, Q) be given by

$$f_{(R,Q)}(t,s) = 3s\,\mathbf{1}\{0 < t < s < 1\}. \tag{A.41}$$

Then the two marginals are

$$f_Q(s) = 3s^2\,\mathbf{1}\{0 < s < 1\}, \quad f_R(t) = \tfrac{3}{2}(1-t^2)\,\mathbf{1}\{0 < t < 1\}.$$

Inserting (A.41) into (A.17) and using elementary but tedious calculations, we obtain that f_r is given by

$$\begin{aligned} f_r(x) = {} & 3\,\mathbf{1}\{x<1\}\tan^{-1}\Big(\sqrt{1-x^2}/x\Big) \\ & - \mathbf{1}\{1/2 < x < 1\}3x(\log(1+\sqrt{1-x^2}) - \log x) \\ & - \mathbf{1}\{x < 1/2\}3x\Big[\log\Big(\sqrt{(1-\sqrt{1-4x^2})/2} + \sqrt{(1-\sqrt{1-4x^2})/2 - x^2}\Big) \\ & + \log(1+\sqrt{1-x^2}) - \log x \\ & - ((1+\sqrt{1-4x^2})/2)^{-1/2} + ((1-\sqrt{1-4x^2})/2)^{-1/2} \\ & - \log\Big(\sqrt{(1+\sqrt{1-4x^2})/2} + \sqrt{(1+\sqrt{1-4x^2})/2 - x^2}\Big)\Big]. \end{aligned} \tag{A.42}$$

We now show that there is another pair (R', Q') of size and shape variables which are independent, but lead to the same section marginals F_q and F_r as does the pair (R, Q) with density (A.41). As $F_{Q'}$ is uniquely determined by F_q, we necessarily have $F_{Q'} = F_Q$. If we assume that R' has a density $f_{R'}$, this and (A.17) imply that this density must satisfy

$$f_r(x) = \tfrac{3}{2}x^3 \int_x^\infty \frac{f_{R'}(s)}{s^3\sqrt{s^2-x^2}}\mathrm{d}s. \tag{A.43}$$

Define

$$h(x) = \frac{2}{3x^3} f_r(x) \quad \text{and} \quad g(s) = \frac{f_{R'}(s)}{s^3}.$$

Equation (A.43) is an Abel transform of $g(s)$ with solution given by

$$f_{R'}(s) = -\frac{2s^4}{\pi} \int_s^\infty \frac{h'(x)}{\sqrt{x^2 - s^2}} \mathrm{d}x, \tag{A.44}$$

see e.g. [GV91, p.35]. Hence, we would define $f_{R'}$ by (A.44) if we can guarantee that this function is a density. Inserting f_r given by (A.42) it can be shown that the function $h'(x)$ is negative for all x. Furthermore, using Tonelli's theorem, we obtain

$$\begin{aligned} \int_0^\infty f_{R'}(s)\mathrm{d}s &= -\frac{2}{\pi} \int_0^\infty h'(x) \int_0^x \frac{s^4}{\sqrt{x^2 - s^2}} \mathrm{d}s\mathrm{d}x \\ &= -\frac{3}{8} \int_0^\infty h'(x) x^4 \mathrm{d}x. \end{aligned}$$

Using partial integration and inserting for h, we find that $f_{R'}$ integrates to one. Hence $f_{R'}$ is a density. We thus have shown that populations of balls with size-shape parameters (R, Q) and (R', Q'), respectively, lead to the same size-shape distributions of their profiles, although $F_{(R,Q)} \neq F_{(R',Q')}$. ∎

A.II The constants in (A.37)

The constants b_{ij} in (A.37) are given explicitly by

$$b_{ij} = \frac{1}{j\Delta_2} \left(\mathbf{1}\{(i-1)\Delta_1 < j\Delta_2\} \frac{\sqrt{j^2\Delta_2^2 - (i-1)^2\Delta_1^2}}{\sqrt{1 - (i-1)^2\Delta_1^2}} - \mathbf{1}\{i\Delta_1 < j\Delta_2\} \frac{\sqrt{j^2\Delta_2^2 - i^2\Delta_1^2}}{\sqrt{1 - i^2\Delta_1^2}} \right),$$

for $j = 1, \ldots, k_2$, $i = 1, \ldots, k_1 - 1$, and

$$b_{k_1 j} = \frac{1}{j\Delta_2} \mathbf{1}\{(k_1-1)\Delta_1 < j\Delta_2\} \frac{\sqrt{j^2\Delta_2^2 - (k_1-1)^2\Delta_1^2}}{\sqrt{1 - (k_1-1)^2\Delta_1^2}}, \qquad j = 1, \ldots, k_2.$$

A.III Proof of Proposition A.15

Let $\omega_F = \sup\{x : F(x) < 1\}$ be the right endpoint of a distribution function F. There are sufficient and necessary conditions for $F \in \mathcal{D}(L)$. These conditions are ($\gamma > 0$)

- $F \in \mathcal{D}(L_{1,\gamma}) \Leftrightarrow \omega_F = \infty$, $\lim_{x\to\infty} \frac{1-F(yx)}{1-F(x)} = y^{-\gamma}$ for all $y > 0$.
- $F \in \mathcal{D}(L_{2,\gamma}) \Leftrightarrow \omega_F < \infty$, $\lim_{x\to 0+} \frac{1-F(\omega_F - yx)}{1-F(\omega_F - x)} = y^{\gamma}$ for all $y > 0$.
- $F \in \mathcal{D}(L_3) \Leftrightarrow \lim_{x\to\omega_F -} \frac{1-F(x+yb(x))}{1-F(x)} = e^{-y}$ for all $y \in \mathbb{R}$. The function b is some auxiliary function (it can be chosen such that it is differentiable for $x < \omega_F$ with $\lim_{x\to\omega_F -} b'(x) = 0$ and $\lim_{x\to\infty} b(x)/x = 0$ if $\omega_F = \infty$, or $\lim_{x\to\omega_F -} b(x)/(\omega_F - x) = 0$ if $\omega_F < \infty$).

The proof of Proposition A.15 uses the following lemma. The lemma is a slight generalisation of [Haa70, Lemma 1.2.1] and the proof is analogous to the one given there. A similar result can be found in [KM06, Lemma 2.4].

Lemma A.17. *Let f and g be positive functions on $\mathbb{R}^2$ and $a \in \mathbb{R}$, such that*

$$\int_a^\omega f(s,t)\mathrm{d}t < \infty, \quad \int_a^\omega g(s,t)\mathrm{d}t < \infty$$

for some $\omega \in (a, \infty]$ and all $s \geq a$. If

$$\lim_{\substack{(s,t)\to(\omega,\omega)\\ s\leq t<\omega}} \frac{f(s,t)}{g(s,t)} = c, \quad \text{where } c \in [0,\infty]. \tag{A.45}$$

then

$$\lim_{s\to\omega-} \frac{\int_s^\omega f(s,t)\mathrm{d}t}{\int_s^\omega g(s,t)\mathrm{d}t} = c.$$

An analogous result holds when s approaches ω from the right.

Proof of Proposition A.15. Writing out (A.15) explicitly gives

$$1 - F_r(x) = \int_x^\infty \Big(\frac{\sqrt{t^2-x^2}}{t} \int_{\frac{1}{t}\sqrt{t^2-x^2}}^1 \frac{f_Q(s)}{s}\mathrm{d}s + F_Q\Big(\frac{1}{t}\sqrt{t^2-x^2}\Big)\Big) f_R(t)\mathrm{d}t.$$

Applying integration by parts on the outer integral, we find that

$$1 - F_r(x) = \int_x^\infty \frac{x^2}{t^2\sqrt{t^2-x^2}}(1-F_R(t)) \int_{\frac{1}{t}\sqrt{t^2-x^2}}^1 \frac{f_Q(s)}{s}\mathrm{d}s\mathrm{d}t, \qquad x > 0. \tag{A.46}$$

We see from (A.13) that $\omega_{F_R} = \omega_{F_r}$ and we will call this common value ω. Let $y > 0$ and assume first that $F_R \in \mathcal{D}(L_{1,\gamma})$ and this implies $\omega = \infty$. Using (A.46) and then the substitution $t = yz$ in the numerator, we obtain after some simplification

$$\lim_{x\to\infty} \frac{1-F_r(yx)}{1-F_r(x)} = \lim_{x\to\infty} \frac{\int_x^\infty \frac{x^2}{t^2\sqrt{t^2-x^2}}(1-F_R(yt)) \int_{\frac{1}{t}\sqrt{t^2-x^2}}^1 \frac{f_Q(s)}{s}\mathrm{d}s\mathrm{d}t}{\int_x^\infty \frac{x^2}{t^2\sqrt{t^2-x^2}}(1-F_R(t)) \int_{\frac{1}{t}\sqrt{t^2-x^2}}^1 \frac{f_Q(s)}{s}\mathrm{d}s\mathrm{d}t}.$$

We note that

$$\lim_{\substack{(x,t)\to(\infty,\infty)\\ x\leq t<\infty}} \frac{\frac{1}{t^2\sqrt{t^2-x^2}}(1-F_R(yt)) \int_{\frac{1}{t}\sqrt{t^2-x^2}}^1 \frac{1}{s} f_Q(s)\mathrm{d}s}{\frac{1}{t^2\sqrt{t^2-x^2}}(1-F_R(t)) \int_{\frac{1}{t}\sqrt{t^2-x^2}}^1 \frac{1}{s} f_Q(s)\mathrm{d}s} = \lim_{x\to\infty} \frac{1-F_R(yx)}{1-F_R(x)}.$$

Hence using Lemma A.17, and $F_R \in \mathcal{D}(L_{1,\gamma})$, we find

$$\lim_{x\to\infty} \frac{1-F_r(yx)}{1-F_r(x)} = \lim_{x\to\infty} \frac{1-F_R(yx)}{1-F_R(x)} = y^{-\gamma},$$

that is $F_r \in \mathcal{D}(L_{1,\gamma})$.

Let us now assume that $F_R \in \mathcal{D}(L_{2,\gamma})$ implying in particular that $0 < \omega < \infty$. From (A.46) we have

$$\lim_{x\to 0+} \frac{1-F_r(\omega-yx)}{1-F_r(\omega-x)} = \lim_{x\to 0+} \frac{y\int_0^x \frac{(\omega-yx)^2(1-F_R(\omega-zy))}{(\omega-zy)^2\sqrt{(\omega-zy)^2-(\omega-yx)^2}} \int_{\frac{1}{(\omega-zy)}}^1 \sqrt{(\omega-zy)^2-(\omega-yx)^2}\,\frac{f_Q(s)}{s}\mathrm{d}s\mathrm{d}z}{\int_0^x \frac{(\omega-x)^2(1-F_R(\omega-z))}{(\omega-z)^2\sqrt{(\omega-z)^2-(\omega-x)^2}} \int_{\frac{1}{(\omega-z)}}^1 \sqrt{(\omega-z)^2-(\omega-x)^2}\,\frac{f_Q(s)}{s}\mathrm{d}s\mathrm{d}z},$$

where we have substituted $t = \omega - zy$ in the numerator and $t = \omega - z$ in the denominator. As

$$\lim_{\substack{(x,z)\to(0,0)\\ 0<z\le x}} \frac{\frac{(\omega-yx)^2(1-F_R(\omega-zy))}{(\omega-zy)^2\sqrt{(\omega-zy)^2-(\omega-yx)^2}} \int_{\frac{1}{(\omega-zy)}}^1 \sqrt{(\omega-zy)^2-(\omega-yx)^2}\,\frac{f_Q(s)}{s}\mathrm{d}s}{\frac{(\omega-x)^2(1-F_R(\omega-z))}{(\omega-z)^2\sqrt{(\omega-z)^2-(\omega-x)^2}} \int_{\frac{1}{(\omega-z)}}^1 \sqrt{(\omega-z)^2-(\omega-x)^2}\,\frac{f_Q(s)}{s}\mathrm{d}s} = \lim_{x\to 0+} \frac{1}{\sqrt{y}} \frac{(1-F_R(\omega-xy))}{(1-F_R(\omega-x))}$$

we have, using Lemma A.17 and $F_R \in \mathcal{D}(L_{2,\gamma})$, that

$$\lim_{x\to 0+} \frac{1-F_r(\omega-yx)}{1-F_r(\omega-x)} = y \lim_{x\to 0+} \frac{1}{\sqrt{y}} \frac{(1-F_R(\omega-xy))}{(1-F_R(\omega-x))} = y^{\gamma+1/2}.$$

Thus, $F_r \in \mathcal{D}(L_{2,\gamma+1/2})$.

Assume next that $F_R \in \mathcal{D}(L_3)$ and let the auxiliary function b be differentiable for $x < \omega$ with $\lim_{x\to\omega-} b'(x) = 0$ and $\lim_{x\to\infty} b(x)/x = 0$ if $\omega = \infty$ or $\lim_{x\to\omega-} b(x)/(\omega - x) = 0$ if $\omega < \infty$. Using (A.46) we have

$$\lim_{x\to\omega-} \frac{1-F_r(x+yb(x))}{1-F_r(x)} = \lim_{x\to\omega-} \frac{\int_{x+yb(x)}^\omega \frac{(x+yb(x))^2(1-F_R(t))}{t^2\sqrt{t^2-(x+yb(x))^2}} \int_{\sqrt{1-(x+yb(x))^2/t^2}}^1 \frac{1}{s} f_Q(s)\mathrm{d}s\mathrm{d}t}{\int_x^\omega \frac{x^2(1-F_R(t))}{t^2\sqrt{t^2-x^2}} \int_{\sqrt{1-(x/t)^2}}^1 \frac{1}{s} f_Q(s)\mathrm{d}s\mathrm{d}t}.$$

Due to the properties of b there exists an $x_0 \in (0,\omega)$ such that $g : x \mapsto x + yb(x)$ is a strictly increasing function on $[x_0,\omega)$; see for instance [DR92]. Using the substitution $t = z + yb(z)$ in the numerator and noting that from the properties of b we have $\lim_{x\to\omega-} g^{-1}(\omega) = \omega$, we obtain

$$\lim_{x\to\omega-} \frac{1-F_r(x+yb(x))}{1-F_r(x)} = \lim_{x\to\omega-} \Big(1+y\frac{b(x)}{x}\Big)^2 \frac{\int_x^\omega \frac{(1-F_R(z+yb(z)))\int_{\sqrt{1-(x+yb(x))^2/(z+yb(z))^2}}^1 \frac{1}{s} f_Q(s)\mathrm{d}s}{(z+yb(z))^2\sqrt{(z+yb(z))^2-(x+yb(x))^2}}(1+yb'(z))\mathrm{d}z}{\int_x^\omega \frac{(1-F_R(z))}{z^2\sqrt{z^2-x^2}} \int_{\sqrt{1-(x/z)^2}}^1 \frac{1}{s} f_Q(s)\mathrm{d}s\mathrm{d}z}.$$

Considering the quotient of the integrands, we have

$$\lim_{\substack{(x,z)\to(\omega,\omega)\\ x\le z<\omega}} \frac{\frac{(1-F_R(z+yb(z)))\int_{\sqrt{1-(x+yb(x))^2/(z+yb(z))^2}}^1 \frac{1}{s} f_Q(s)\mathrm{d}s}{(z+yb(z))^2\sqrt{(z+yb(z))^2-(x+yb(x))^2}}(1+yb'(z))}{\frac{(1-F_R(z))}{z^2\sqrt{z^2-x^2}}\int_{\sqrt{1-(x/z)^2}}^1 \frac{1}{s} f_Q(s)\mathrm{d}s}$$

$$= \lim_{\substack{(x,z)\to(\omega,\omega)\\ x\le z<\omega}} \left(1-\left(\frac{x}{z}\right)^2\right)^{\frac{1}{2}} \left(1+y\frac{b(z)}{z}\right)^{-3} \left(1-\left(\frac{x}{z}\right)^2\left(\frac{1+yb(x)/x}{1+yb(z)/z}\right)^2\right)^{-\frac{1}{2}}$$

$$\times \frac{1-F_R(z+yb(z))}{1-F_R(z)} \frac{\int_{\sqrt{1-(\frac{x}{z})^2(\frac{1+yb(x)/x}{1+yb(z)/z})^2}}^1 \frac{1}{s} f_Q(s)\mathrm{d}s}{\int_{\sqrt{1-(\frac{x}{z})^2}}^1 \frac{1}{s} f_Q(s)\mathrm{d}s}(1+yb'(z)).$$

Using the properties of the function b, applying Lemma A.17 and using $F_R \in \mathcal{D}(L_3)$, we find

$$\lim_{x\to\omega-} \frac{1-F_r(x+yb(x))}{1-F_r(x)} = \lim_{x\to\omega-} \frac{1-F_R(x+yb(x))}{1-F_R(x)} = e^{-y}.$$

Hence $F_r \in \mathcal{D}(L_3)$, which finishes the proof. □

Paper B

The invariator principle in convex geometry

Ó. Thórisdóttir and M. Kiderlen

Department of Mathematics, Aarhus University

Abstract: The invariator principle is a measure decomposition that was rediscovered in local stereology in 2005 and has since been used widely in the stereological literature. We give an exposition of invariator related results where existing formulae are generalized and new ones proposed. In particular, we look at rotational Crofton-type formulae that are obtained by combining the invariator principle and classical Crofton formulae. This results in geometrical quantities represented as averages over weighted Crofton-type integrals in linear sections. We refer to these weighted integrals as measurement functions and derive several, more explicit representations of these functions. In particular, we use Morse theory to write the measurement functions in terms of critical values of the sectioned object. This is very useful for surface area estimation.

Keywords: Local stereology; invariator principle; rotational Crofton-type formulae; Morse theory; Hadwiger's index; surface area estimation.

2010 MSC: 60D05; 52A22; 58E05

B.1 Introduction

The invariator [CO05] is a powerful principle for generating a hyperplane in an isotropic random subspace that is motion invariant in n-dimensions. It is a special case of a classical result [Pet35] that was rediscovered in local stereology and used for applications in [CO05]. Since then it has received much interest in the stereological literature. It was generalized in [GACO09] to Riemannian manifolds with constant sectional curvature. In [GACO09] and, independently, in [AJ10], the invariator principle was combined with the classical Crofton formula to obtain new rotational Crofton-type formulae which yield new stereological estimators of geometrical quantities. The purpose of this survey is to give an overview of invariator related results in Euclidean space and to include natural generalizations that apparently have not been treated in the literature yet.

Crofton's formula is an important result of integral geometry as it relates properties on flat sections of a spatial structure to geometrical quantities of the original structure. Rotational versions of Crofton's formula only use sections with linear subspaces, that is, subspaces through a fixed reference point, which usually is assumed to be the origin. They express certain geometrical quantities as averages of measurements in the linear sections. The average is taken with respect to a rotation invariant measure, therefore the word *rotational*. Techniques that are based on sections through a fixed reference point are often called *local*; see the monograph [Jen98] on local stereology. In integral geometry the term 'local' is used when so-called local versions of the intrinsic volumes are considered, that is when also normals and position of boundary points of an object of interest are taken into account. In the following we use the latter notion of the word.

The major new contribution of the present paper is to combine the invariator and concepts from Morse theory for obtaining a new rotational Crofton formula. What is different and appealing with this new formula is that the measurement functional on the section of the object is written entirely in terms of so-called critical points. This proves to be very useful for applications where the surface area is sought for.

The paper is written self-contained. It is organized as follows. In Section B.2 we introduce the notation and recall some important concepts. The first result, Proposition B.2 in Section B.3, is a rotational Crofton formula for the support measures obtained by combining the invariator principle and a local Crofton formula. It has as a special case the rotational Crofton formula for intrinsic volumes derived in [GACO09] and [AJ10]. The combination of the invariator principle and the classical Crofton formula does not yield an explicit form of the functional to be measured on the section. This functional will be called the *measurement function* from now on, and we will present more explicit representations of this measurement function in Section B.4. We start by generalizing the results of [AJ10]. In [AJ10] the measurement function involving the intrinsic volumes is written as an integral over the object's boundary and we extend this to curvature measures. Then we show that when the object of interest is convex, the measurement function can be written in terms of the radial function of the sectioned object and an angle in the section plane. The main result can be found in Section B.4.3. Here we give a very basic introduction to Morse theory before presenting the new rotational Crofton formula for smooth manifolds in Theorem B.6. This theorem is formulated for smooth manifolds as we want to apply classical Morse theory. As shown in Theorem B.7 an analogous result holds for polyconvex sets, where Hadwiger's index [Had55], an index closely related to the Morse index, is used for determining critical points. When the geometrical quantity of interest is the surface area of a topologically regular set with smooth boundary, the two theorems coincide. In Section B.4.4 we discuss the formal analogy of the new formula with Kubota's formula and give a simple computational formula for the measurement function when the object of interest is a polytope. We conclude the paper with a discussion on stereological applications of these rotational formulae, both old and new.

B.2 Preliminaries

Throughout, $\mathbb{R}^n$ denotes the n-dimensional Euclidean space and O its origin. The Euclidean scalar product is denoted by $\langle \cdot, \cdot \rangle$ and the Euclidean norm by $\|\cdot\|$. For a topological space E we let $\mathcal{B}(E)$ be the Borel σ-algebra in E. We furthermore write $\mathcal{H}_n^d$ for the d-dimensional *Hausdorff measure* in $\mathbb{R}^n$ [SW08, p. 634]. When n is clear from the context, $\mathcal{H}_n^d(\mathrm{d}u)$ is abbreviated to $\mathrm{d}u^d$. For a set $Y \subseteq \mathbb{R}^n$, we define

$$Y + x = \{y + x \,|\, y \in Y\},\ x \in \mathbb{R}^n, \qquad \alpha Y = \{\alpha y \,|\, y \in Y\},\ \alpha > 0.$$

We use ∂Y for the boundary, $\mathrm{int} Y$ for the interior, $\mathrm{cl} Y$ for the closure and $\mathbf{1}_Y$ for the indicator function of Y. When we want to emphasize the geometric meaning, we write $S(Y) = \mathcal{H}_n^{n-1}(Y)$ for the *surface area* of a Borel-set Y. Whenever defined, $\chi(Y)$ denotes the *Euler characteristic* of Y. If $Y \subseteq \mathbb{R}^1$ is compact $\chi(Y)$ is the number of connected components of Y. The unit ball in $\mathbb{R}^n$ is $B_n = \{x \in \mathbb{R}^n \mid \|x\| \leq 1\}$ and the boundary of it is the unit sphere (in $\mathbb{R}^n$) $S^{n-1} = \{x \in \mathbb{R}^n \mid \|x\| = 1\}$. The volume of B_n is given by

$$\kappa_n = \pi^{n/2} \Gamma(1 + \tfrac{n}{2})^{-1}$$

and the surface area of its boundary by

$$\sigma_n = n\kappa_n = 2\pi^{n/2} \Gamma(\tfrac{n}{2})^{-1}.$$

To simplify later expressions, we write

$$c_{j_1, j_2 \ldots, j_k}^{i_1, i_2, \ldots, i_{k'}} = \frac{\sigma_{i_1} \sigma_{i_2} \cdots \sigma_{i_{k'}}}{\sigma_{j_1} \sigma_{j_2} \cdots \sigma_{j_k}}. \tag{B.1}$$

For $\alpha, \beta, \gamma \in \mathbb{R}, \gamma \notin \{0, -1, -2, \ldots\}$, we write $F(\alpha, \beta, \gamma; \cdot)$ for the hypergeometric function

$$F(\alpha, \beta; \gamma; z) = \sum_{k=0}^{\infty} \frac{(\alpha)_k (\beta)_k}{(\gamma)_k} \frac{z^k}{k!}, \qquad z \in [-1, 1],$$

where $(x)_k$ is the Pochhammer symbol

$$(x)_k = \begin{cases} \frac{\Gamma(x+k)}{\Gamma(x)}, & x > 0, \\ (-1)^k \frac{\Gamma(-x+1)}{\Gamma(-x-k+1)}, & x \leq 0. \end{cases}$$

Let $X \subseteq \mathbb{R}^n$ be a nonempty, compact set which is *star-shaped* at O (i.e. every line through O that hits X does so in a (possibly degenerate) line segment). The *radial function* of X, ρ_X, is defined by

$$\rho_X(x) = \sup\{\alpha \in \mathbb{R} \,|\, \alpha x \in X\},$$

for $x \in \mathbb{R}^n \setminus \{O\}$. The set X is uniquely determined by ρ_X. We use $\mathcal{K}^n$ for the family of all *convex bodies* (compact, convex sets) of $\mathbb{R}^n$; cf. [Sch93] for the theory of convex bodies. If $X \in \mathcal{K}^n$ and ∂X does not contain any line segment X is called *strictly convex*. For $X \in \mathcal{K}^n$ its *support function*, h_X, is given by

$$h_X(u) = \max_{x \in X} \langle u, x \rangle, \qquad u \in S^{n-1}.$$

The value $h_X(u)$ is the signed distance from O to the supporting hyperplane to X with outer unit normal vector u. For $q > 0$ we define the *q-flower set* H_X^q of $X \in \mathcal{K}^n$ by

$$\rho_{H_X^q}(u) = \operatorname{sgn}(h_X(u))|h_X(u)|^q, \qquad u \in S^{n-1}, \tag{B.2}$$

where $\operatorname{sgn}(\cdot)$ is the *signum function*. Note that the right hand side of (B.2) is always the radial function of some set, as $-h_X(-u) \leq h_X(u)$ for all $u \in S^{n-1}$. When $q = 1$, H_X^1 is the set whose radial function is the support function of X and is referred to as the support set of X in [CO05]. When X is a planar polygon, H_X^1 is a union of finitely many disks and resembles slightly a flower and was called the flower of X in [CO11]. As already mentioned, we extend that terminology and speak of a q-flower set, see Section B.4.4 for its relevance in connection with the invariator principle.

We let $\mathcal{R}^n$ be the family of all *polyconvex sets* (sets that can be expressed as finite unions of convex bodies) of $\mathbb{R}^n$. A support element of $\emptyset \neq X \in \mathcal{K}^n$ is a pair $(x, u) \in \Sigma = \mathbb{R}^n \times S^{n-1}$, where $x \in \partial X$ and u is an outer unit normal vector of X at x. More formally $(x, u) \in \Sigma$ is a support element of X if and only if $x \in X$ satisfies $h_X(u) = \langle u, x \rangle$. We let $\operatorname{Nor} X$ be the set of all support elements of X. As in [Gla97, p. 109] we extend this definition to polyconvex sets. For $X \in \mathcal{R}^n$ let $R(X)$ be the set of all sequences $(X_i)_{i\in\mathbb{N}}$ in $\mathcal{K}^n$ with $X = \cup_{i=1}^{\infty} X_i$ and $X_i = \emptyset$ for almost all $i \in \mathbb{N}$ and let $S(\mathbb{N})$ be the set of all nonempty subsets of $\mathbb{N}$. Then we define

$$\operatorname{Nor} X = \cap_{(X_i)\in R(X)} \cup_{v\in S(\mathbb{N})} \operatorname{Nor}(\cap_{i\in v} X_i). \tag{B.3}$$

We follow the notation in [Sch93, 4.2] and write $\Xi_m(X, \cdot)$, $0 \leq m \leq n-1$, for the support measures of $X \in \mathcal{R}^n$ on $\mathcal{B}(\Sigma)$. They are concentrated on $\operatorname{Nor} X$. We obtain the curvature measures by the specialization $\Phi_m(X, A) = \Xi_m(X, A \times S^{n-1})$, $A \in \mathcal{B}(\mathbb{R}^n)$, and the area measures by $\Psi_m(X, B) = \Xi_m(X, \mathbb{R}^n \times B)$, $B \in \mathcal{B}(S^{n-1})$, $m \in \{0, 1, \ldots, n-1\}$. For $m = n$, only the curvature measure is defined. We put $\Phi_n(X, \cdot) = \mathcal{H}_n^n(X \cap \cdot)$, so $\Phi_n(X, \cdot)$ is the restriction of the Lebesgue measure to X. The intrinsic volumes are the total measures $V_m(X) = \Xi_m(X, \Sigma)$. Of special interest will be the volume V_n, the surface area $2V_{n-1}$ and the Euler characteristic $V_0 = \chi$. For $X \in \mathcal{K}^n$, integers $r, s \geq 0$ and $m \in \{0, 1, \ldots, n-1\}$, we write

$$\Phi_{m,r,s}(X) = \frac{\sigma_{n-m}}{r!s!\sigma_{n-m+s}} \int_{\Sigma} x^r u^s \Xi_m(X, \mathrm{d}(x, u)),$$

for the *Minkowski tensors*. Here $x^r u^s$ is the symmetric tensor product of rank $r + s$ of the symmetric tensors x^r and u^s. For $s = 0$ we obtain the volume tensor of rank r

$$\Phi_{m,r,0}(X) = \frac{1}{r!} \int_X x^r \Phi_m(X, \mathrm{d}x),$$

which is also defined for $m = n$. Note also that $\Phi_{m,0,0}(X) = V_m(X)$. For an introduction to Minkowski tensors see [HSS08] and references therein.

For $j = 0, 1, \ldots, n$ we let

$$\mathcal{L}_{j[O]}^n = \{L_{j[O]}^n \subseteq \mathbb{R}^n \mid L_{j[O]}^n \text{ is a } j\text{-dim. linear subspace}\},$$
$$\mathcal{L}_j^n = \{L_j^n \subseteq \mathbb{R}^n \mid L_j^n \text{ is a } j\text{-dim. affine subspace}\}$$

be the families of all j-dimensional linear and affine subspaces of $\mathbb{R}^n$, respectively. For $0 \leq j \leq r \leq n$ and a fixed $L^n_{r[O]} \in \mathcal{L}^n_{r[O]}$ we write $\mathcal{L}^r_j$ for the family of all j-dimensional affine subspaces L^r_j within this linear subspace, despite the fact that this notation does not reflect the surrounding linear space. These spaces are equipped with their standard topologies and endowed with their natural invariant measures; see [SW08]. We write $\mathrm{d}L^n_{j[O]}$, and $\mathrm{d}L^r_j$, respectively, when integrating with respect to these invariant measures. We use the same normalization as in [SW08]:

$$\int_{\mathcal{L}^n_{j[O]}} \mathrm{d}L^n_{j[O]} = 1 \quad \text{and} \quad \int_{\{L^r_j \in \mathcal{L}^r_j \,|\, L^r_j \cap B_n \neq \emptyset\}} \mathrm{d}L^r_j = \kappa_{r-j}.$$

A random subspace $L^n_{j[O]}$ is called *isotropic random* (IR) if and only if its distribution is given by

$$\mathbb{P}_{L^n_{j[O]}}(A) = \int_{\mathcal{L}^n_{j[O]}} \mathbf{1}_A \, \mathrm{d}L^n_{j[O]}, \quad A \in \mathcal{B}(\mathcal{L}^n_{j[O]}).$$

Similarly, a random flat $L^n_j \in \mathcal{L}^n_j$ is called *isotropic uniform random* (IUR) *hitting a compact object* Y if and only if its distribution is given by

$$\mathbb{P}_{L^n_j}(A) = c \int_{\mathcal{L}^n_j} \mathbf{1}_{A \cap \{L^n_j \in \mathcal{L}^n_j \,|\, L^n_j \cap Y \neq \emptyset\}} \, \mathrm{d}L^n_j, \qquad A \in \mathcal{B}(\mathcal{L}^n_j),$$

where c is a normalizing constant. We write $(L^n_j)^\perp \in \mathcal{L}^n_{n-j[O]}$ for the linear subspace orthogonal to $L^n_{j[O]} \in \mathcal{L}^n_{j[O]}$ and $x|L^n_{j[O]}$ for the orthogonal projection of $x \in \mathbb{R}^n$ onto $L^n_{j[O]} \in \mathcal{L}^n_{j[O]}$. We furthermore adopt the convention of writing $u^\perp$ for the orthogonal complement of the line through O with direction $u \in S^{n-1}$. For $\eta \subseteq \Sigma$ and $L^n_j \in \mathcal{L}^n_j$, $j \in \{0, \ldots, n-1\}$, we define

$$\begin{aligned} \eta \wedge L^n_j = \{(x,u) \in \Sigma \,|\, &\text{there are } u_1, u_2 \in S^{n-1} \text{ with } (x,u_1) \in \eta, \\ &x \in L^n_j, u_2 \in (L^n_j)^\perp, u \in \operatorname{pos}\{u_1, u_2\}\}, \end{aligned}$$

where $\operatorname{pos}\{u_1, u_2\} = \{\lambda_1 u_1 + \lambda_2 u_2 \,|\, \lambda_1, \lambda_2 \geq 0\}$ is the positive hull of the set $\{u_1, u_2\}$. For $B \in \mathcal{B}(S^{n-1})$ we let

$$\begin{aligned} B \wedge L^n_j = \{u \in S^{n-1} \,|\, &\text{there are } u_1, u_2 \in S^{n-1} \text{ with } u_1 \in B, \\ &u_2 \in (L^n_j)^\perp, u \in \operatorname{pos}\{u_1, u_2\}\}. \end{aligned}$$

A generalization of the classical Crofton formula is the following local Crofton formula for polyconvex sets.

Proposition B.1. *[Gla97, Theorem 3.4] Let $X \in \mathcal{R}^n$ and j, m be integers satisfying $0 \leq m < j \leq n-1$. Then for $\eta \in \mathcal{B}(\mathrm{Nor}X)$*

$$\Xi_{n-j+m}(X, \eta) = c^{j+1,n-j+m+1}_{m+1,n+1} \int_{\mathcal{L}^n_j} \Xi_m(X \cap L^n_j, \eta \wedge L^n_j) \mathrm{d}L^n_j. \tag{B.4}$$

We use the word *smooth* to mean differentiable of class C^∞ and refer to [Bre93, 2.1. Definition p. 68] for a definition of an m-dimensional smooth manifold in $\mathbb{R}^n$. For a manifold $X \subseteq \mathbb{R}^n$ of class C^1 let $T_x(X)$ be the vector space of all tangent vectors to X at a point $x \in X$. For two manifolds $X_1, X_2 \subseteq \mathbb{R}^n$ of class C^1 we write $X_1 \pitchfork X_2$ in $\mathbb{R}^n$, and say that X_1 intersects X_2 *transversely* in $\mathbb{R}^n$, if whenever $x \in X_1 \cap X_2$, we have $T_x(X_1) + T_x(X_2) = T_x(\mathbb{R}^n)$. This is standard notation in differential geometry [Bre93, 7.6. Definition p. 84]. Correspondingly, for $X \in \mathcal{R}^n$ and $L^n_{j[O]} \in \mathcal{L}^n_{j[O]}$ we write $\partial X \pitchfork L^n_{j[O]}$ in $\mathbb{R}^n$ if any supporting hyperplane of X at any point in $\partial X \cap L^n_{j[O]}$, together with $L^n_{j[O]}$, spans $\mathbb{R}^n$, that is

$$(x, u) \in \mathrm{Nor} X, x \in L^n_{j[O]} \Rightarrow u \not\perp L^n_{j[O]}.$$

When $X \in \mathcal{R}^n$ and $O \notin \partial X$, we have $\partial X \pitchfork L^n_{j[O]}$ in $\mathbb{R}^n$ for almost all $L^n_{j[O]} \in \mathcal{L}^n_{j[O]}$. This was shown for $X \in \mathcal{K}^n$ in [JR08, Prop. 1] and generalizes to polyconvex sets using (B.3). Furthermore, if X_1 and X_2 are embedded submanifolds of $\mathbb{R}^n$, in the sense of [Bre93, 5.7. Definition p. 79], and $X_1 \pitchfork X_2$ in $\mathbb{R}^n$, then $X_1 \cap X_2$ is a submanifold of $\mathbb{R}^n$ of dimension $\dim(X_1) + \dim(X_2) - n$ [Bre93, 7.7. Theorem p. 84].

B.3 Invariator principle and rotational Crofton formulae

The goal of rotational integral geometry is to find analogs of (B.4) where the motion invariant integration over all affine flats is replaced by rotation invariant integration over all linear subspaces. In its most general form, a rotational Crofton formula is thus

$$\beta(X) = \int_{\mathcal{L}^n_{j+1[O]}} \alpha(X \cap L^n_{j+1[O]}) \mathrm{d}L^n_{j+1[O]}, \tag{B.5}$$

$j = 0, 1, \ldots, n-1$, for suitable X and functionals $\alpha(\cdot)$ and $\beta(\cdot)$. We consider here only the stereologically motivated question how $\alpha(\cdot)$ should be chosen in order to obtain a desired geometric characteristic $\beta(X)$ of X. For the question of how $\beta(X)$ can be explicitly calculated, when $\alpha(\cdot)$ is given (e.g. an intrinsic volume) see [JR08].

In [AJ10, Proposition 1] and [GACONnB10, Theorem 3.1 with $\lambda = 0$] a functional $\alpha(\cdot)$ was given such that (B.5) holds where $\beta(X) = V_m(X)$, $m = n - j, \ldots, n$. The key idea is to combine the classical Crofton formula with a Blaschke-Petkantschin-type result, which is often called the *invariator principle* in stereology. In stereological terminology, this relation states how a j-dimensional flat in an isotropic $(j+1)$-dimensional subspace must be chosen in order to obtain an IUR flat in $\mathbb{R}^n$. For all non-negative measurable functions f on $\mathcal{L}^n_j$ and $j \in \{0, 1, \ldots, n-1\}$

$$\int_{\mathcal{L}^n_j} f(L^n_j) \mathrm{d}L^n_j = c_1^{n-j} \int_{\mathcal{L}^n_{j+1[O]}} \int_{\mathcal{L}^{j+1}_j} f(L^{j+1}_j) d(O, L^{j+1}_j)^{n-j-1} \mathrm{d}L^{j+1}_j \mathrm{d}L^n_{j+1[O]}, \tag{B.6}$$

where $d(O, L^{j+1}_j)$ is the Euclidean distance from O to L^{j+1}_j and the constant c_1^{n-j} is given by (B.1). This follows from [GACO09, Corollary 3.1 when $\lambda = 0$] where different normalizations of the invariant measures have been used. The same approach leads also to a rotational Crofton formula for support measures by combining Proposition B.1 with (B.6).

Proposition B.2. *Let $X \in \mathcal{R}^n$, $j \in \{1,\dots,n-1\}$, $m \in \{0,\dots,j-1\}$ and $\eta \in \mathcal{B}(NorX)$. For $\beta(X) = \Xi_{n-j+m}(X,\eta)$, equation* (B.5) *holds with*

$$\alpha(\cdot) = c_{m+1,n+1,1}^{j+1,n-j+m+1,n-j} \int_{\mathcal{L}_j^{j+1}} \Xi_m(\cdot \cap L_j^{j+1}, \eta \wedge L_j^{j+1}) d(O, L_j^{j+1})^{n-j-1} \mathrm{d}L_j^{j+1},$$

with the leading constant given by (B.1).

The proposition holds in particular for the marginal measures of the support measures and their total masses, the intrinsic volumes. Explicitly, taking $\eta = A \times S^{n-1}$ in Proposition B.2, with $A \in \mathcal{B}(\mathbb{R}^n)$, it follows that for $\beta(X) = \Phi_{n-j+m}(X,A)$, equation (B.5) holds with

$$\alpha(\cdot) = c_{m+1,n+1,1}^{j+1,n-j+m+1,n-j} \int_{\mathcal{L}_j^{j+1}} \Phi_m(\cdot \cap L_j^{j+1}, A \cap L_j^{j+1}) d(O, L_j^{j+1})^{n-j-1} \mathrm{d}L_j^{j+1}, \quad \text{(B.7)}$$

$0 \le m \le j \le n-1$. Similarly for $\beta(X) = \Psi_{n-j+m}(X,B)$, $B \in \mathcal{B}(S^{n-1})$, equation (B.5) holds with

$$\alpha(\cdot) = c_{m+1,n+1,1}^{j+1,n-j+m+1,n-j} \int_{\mathcal{L}_j^{j+1}} \Psi_m(\cdot \cap L_j^{j+1}, B \wedge L_j^{j+1}) d(O, L_j^{j+1})^{n-j-1} \mathrm{d}L_j^{j+1}, \quad \text{(B.8)}$$

$0 \le m < j \le n-1$. As already stated in [AJ10, Proposition 1] and [GACONnB10, Theorem 3.1 with $\lambda = 0$] for more general set classes, taking $\eta = \Sigma$, equation (B.5) with $\beta(X) = V_{n-j+m}(X)$ holds for

$$\alpha(\cdot) = c_{m+1,n+1,1}^{j+1,n-j+m+1,n-j} \int_{\mathcal{L}_j^{j+1}} V_m(\cdot \cap L_j^{j+1}) d(O, L_j^{j+1})^{n-j-1} \mathrm{d}L_j^{j+1}, \quad \text{(B.9)}$$

$0 \le m \le j \le n-1$. This relation will be of particular interest when the Euler characteristic occurs on the right hand side. Taking $m = 0$ in (B.9), applying the duality result [Jen98, Proposition 3.3] and an invariance argument, we note that $\beta(X) = V_{n-j}(X)$ and

$$\alpha(\cdot) = c_{n+1,1,1}^{n-j+1,n-j} \int_{S^{n-1} \cap L_{j+1[O]}^n} \int_{-\infty}^{\infty} \chi(\cdot \cap (ru + u^\perp)) |r|^{n-j-1} \mathrm{d}r \mathrm{d}u^j \quad \text{(B.10)}$$

satisfy (B.5). When the section profile $Y = X \cap L_{j+1[O]}^n$ is convex, the Euler characteristic of $Y \cap (ru + u^\perp)$ equals one if the hyperplane $ru + u^\perp$ hits Y, and zero otherwise. Clearly, for a given $u \in S^{n-1} \cap L_{j+1[O]}^n$, $ru + u^\perp$ hits Y if and only if $-h_{X \cap L_{j+1[O]}^n}(-u) \le r \le h_{X \cap L_{j+1[O]}^n}(u)$. Hence, we can calculate the inner integral in (B.10) explicitly and obtain, using the reflection invariance of the Hausdorff measure,

$$\alpha(\cdot) = \frac{c_{n+1,1}^{n-j+1,n-j}}{n-j} \int_{S^{n-1} \cap L_{j+1[O]}^n} \mathrm{sgn}(h_{(\cdot)}(u)) |h_{(\cdot)}(u)|^{n-j} \mathrm{d}u^j. \quad \text{(B.11)}$$

If furthermore X contains O, the expression becomes

$$\alpha(\cdot) = \frac{c_{n+1,1}^{n-j+1,n-j}}{n-j} \int_{S^{n-1} \cap L_{j+1[O]}^n} h_{(\cdot)}^{n-j}(u) \mathrm{d}u^j. \quad \text{(B.12)}$$

For a smooth manifold $X \subseteq \mathbb{R}^n$ of dimension m, equation (B.5) holds with $\beta(X) = \mathcal{H}_n^m(X)$ and

$$\alpha(\cdot) = c_{j+m-n+1,n+1,1}^{m+1,j+1,n-j} \int_{\mathcal{L}_j^{j+1}} \mathcal{H}_n^{m-n+j}(\cdot \cap L_j^{j+1}) d(O, L_j^{j+1})^{n-j-1} \mathrm{d}L_j^{j+1}, \tag{B.13}$$

where j is an integer satisfying $n - m \leq j \leq n - 1$. This follows by combining (B.6) with the Crofton formula for manifolds [Jen98, Proposition 3.7].

When $X \in \mathcal{K}^n$ a classical Crofton formula for Minkowski tensors [HSS08, Theorem 2.2] (see also [SS02] for special cases) can be combined with the invariator principle to obtain rotational Crofton formulae for Minkowski tensors. The derivation of these formulae is straightforward, but we do not report them here as the function $\beta(\cdot)$ occurring in these formulae is typically a linear combination of several Minkowski tensors also involving the metric tensor and complicated coefficients. In [ACZJ12] the notion of Minkowski tensors was extended to so-called integrated Minkowski tensors obtained as certain tensor averages of flat sections of X. This extended class has the appealing property to be closed under rotational Crofton integrals: if $\alpha(\cdot)$ in (B.5) is an integrated Minkowski tensor, then $\beta(\cdot)$ is an integrated Minkowski tensor, too [ACZJ12, Proposition 4.1]. The proof is based on a measure decomposition that generalizes (B.6); see (B.16) below. A special case of this result, particularly important for applications, is obtained in [ACZJ12, Corollary 4.4 with $q = 1$]: For $r \in \mathbb{N}_0$ and $s \in \{0, 1\}$ equation (B.5) holds with $\beta(X) = \Phi_{n+m-j-1,r,s}(X)$ and

$$\alpha(\cdot) = c \int_{\mathcal{L}_j^{j+1}} \Phi_{m-1,r,s}^{(L_j^{j+1})}(\cdot \cap L_j^{j+1}) d(O, L_j^{j+1})^{n-j-1} \mathrm{d}L_j^{j+1}. \tag{B.14}$$

Here $0 < m \leq j \leq n - 1$, $\Phi_{m-1,r,s}^{(L_j^{j+1})}$ is the Minkowski tensor relative to L_j^{j+1} and

$$c = \tfrac{(m-1)!(n-1)!}{(j-1)!(n+m-1-j)!} c_{n-j+m+s+1,j,1}^{n,s+m+1,n-j}.$$

Furthermore, for $j \in \{0, 1, \ldots, n-1\}$ and any non-negative integer r, equation (B.5) with $\beta(X) = \Phi_{n,r,0}(X)$ holds for

$$\alpha(\cdot) = c_1^{n-j} \int_{\mathcal{L}_j^{j+1}} \Phi_{j,r,0}^{(L_j^{j+1})}(\cdot \cap L_j^{j+1}) d(O, L_j^{j+1})^{n-j-1} \mathrm{d}L_j^{j+1}. \tag{B.15}$$

It is not a limitation of the results of this section that they are obtained using (B.6) instead of the more general measure decomposition [SW08, p. 285]

$$\int_{\mathcal{L}_r^n} f(L_r^n) \mathrm{d}L_r^n = c(n, j, r) \int_{\mathcal{L}_{j+1[O]}^n} \int_{\mathcal{L}_r^{j+1}} f(L_r^{j+1}) d(O, L_r^{j+1})^{n-j-1} \mathrm{d}L_r^{j+1} \mathrm{d}L_{j+1[O]}^n, \tag{B.16}$$

where $f \geq 0$ is a measurable function on $\mathcal{L}_r^n$, $0 \leq r \leq j \leq n - 1$ and $c(n, j, r)$ is a constant depending on n, j and r. Combining this measure decomposition with Crofton's formula produces expressions of the form (B.5) where the measurement functions are integrals over $\mathcal{L}_r^{j+1}$ instead of $\mathcal{L}_j^{j+1}$. These functionals do though not

depend on r, as was shown for the intrinsic volumes in [AC10, Proposition 2]. The proofs for the cases where $\beta(\cdot)$ is a support measure (in $\eta \subseteq \mathrm{Nor}X$), a Hausdorff measure or $\Phi_{k,r,s}$, where $1 \leq k \leq n-1$, r a non-negative integer and $s \in \{0,1\}$, are almost identical to the one given there and are based on an application of Crofton's formula in L_r^{j+1}.

B.4 Representations of the measurement function

The measurement function $\alpha(\cdot)$ in Proposition B.2 and the special cases given in (B.7)–(B.9), as well as (B.13), are difficult to evaluate as they involve a weighted Crofton-type integration in the section plane $L^n_{j+1[O]}$. More explicit representations for the measurement function are known, in particular when X has a C^2 boundary or is a polytope. We will now give different representations of the measurement function, which all play a role when applying rotational formulae in stereology.

A particularly simple representation is obtained for the volume functional $\beta(\cdot) = \mathcal{H}^n_n(\cdot)$. In this case, no assumptions on X, apart from measurability, are required.

Proposition B.3. *For any $X \in \mathcal{B}(\mathbb{R}^n)$, $\beta(X) = \mathcal{H}^n_n(X)$ and*

$$\alpha(\cdot) = c^n_{j+1} \int_{(\cdot)} \|z\|^{n-j-1} \mathrm{d}z^{j+1}$$

satisfy (B.5) *for any $0 \leq j \leq n-1$.*

Proposition B.3 follows from a twofold application of spherical coordinates and an invariance argument; see also [AJ10, Proposition 2] for an alternative proof. It implies in particular that $\beta(X) = \Phi_n(X, A)$ and

$$\alpha(\cdot) = c^n_{j+1} \int_{(\cdot)\cap A} \|z\|^{n-j-1} \mathrm{d}z^{j+1} \tag{B.17}$$

satisfy (B.5) for any $X \in \mathcal{R}^n$, $A \in \mathcal{B}(\mathbb{R}^n)$.

B.4.1 The measurement function as an integral over the profile boundary

We show that the measurement function associated to the curvature measures can be written as an integral over the boundary of the section profile. As this integral involves principal curvatures, we assume that $X \in \mathcal{K}^n$ has a boundary of class C^2. For $L^n_j \in \mathcal{L}^n_j$, $j \in \{1, \ldots, n-1\}$, let $\partial'(X \cap L^n_j)$ be the relative boundary of $X \cap L^n_j$, i.e. its boundary as a subset of L^n_j. As $\partial X \pitchfork L^n_j$ for almost all $L^n_j \in \mathcal{L}^n_j$, the principal curvatures $\kappa'_1(x), \ldots, \kappa'_{j-1}(x)$ of $\partial'(X \cap L^n_j) \subseteq L^n_j$ at $x \in \partial'(X \cap L^n_j)$, as well as the normalized elementary symmetric functions of the principal curvatures of $\partial'(X \cap L^n_j)$, $H_0 = 1$,

$$H_m(x, L^n_j) = \binom{j-1}{m}^{-1} \sum_{1 \leq i_1 < \cdots < i_m \leq j-1} \kappa'_{i_1}(x) \cdots \kappa'_{i_m}(x),$$

$m = 1, \dots, j-1$, exist almost surely. In addition, we write $n'(x)$ for the (almost surely unique) outer unit normal of $X \cap L^n_j$ at $x \in \partial'(X \cap L^n_j)$.

Proposition B.4. *Let $X \in \mathcal{K}^n$ with boundary of class C^2, $A \in \mathcal{B}(\mathbb{R}^n)$ and let j, m be integers with $0 \le m < j \le n-1$. Then $\beta(X) = \Phi_{n-j+m}(X, A)$ and*

$$\alpha(X \cap L^n_{j+1[O]}) = c^{j+1,n-j+m+1,n-j}_{m+1,n+1,j-m,1} \int_{\partial'(X \cap L^n_{j+1[O]}) \cap A} h_m(X \cap L^n_{j+1[O]}, x) \mathrm{d}x^j \tag{B.18}$$

satisfy (B.5)*, where*

$$\begin{aligned} &h_m(X \cap L^n_{j+1[O]}, x) \\ &\quad = \binom{j-1}{m} \int_{\mathcal{L}^{j+1}_{j[O]}} H_{j-m-1}(x, L^{j+1}_{j[O]} + x) \|n'(x)| L^{j+1}_{j[O]}\| \|x| (L^{j+1}_{j[O]})^{\perp}\|^{n-j-1} \mathrm{d}L^{j+1}_{j[O]}. \end{aligned}$$

The proof of Proposition B.4 uses the representation [SW08, p. 607] of $\Phi_{n-j+m}(X, \cdot)$ as integral involving principal curvatures and follows otherwise the proof of [AJ10, Proposition 3] where (B.18) is shown for $A = \mathbb{R}^n$ without the convexity assumption.

For $m = j-1$, the function $h_{j-1}(X \cap L^n_{j+1[O]}, \cdot)$ does not depend on the principal curvatures, and was determined in [AJ10, Proposition 4]. In view of (B.18) and using this simplification, $\beta(X) = \Phi_{n-1}(X, A)$ and

$$\begin{aligned} &\alpha(X \cap L^n_{j+1[O]}) \\ &\quad = c^n_{j+1,1} \int_{\partial'(X \cap L^n_{j+1[O]}) \cap A} \|z\|^{n-j-1} F(-\tfrac{1}{2}, -\tfrac{n-j-1}{2}; \tfrac{j}{2}; \sin^2 \angle(n'(z), z)) \mathrm{d}z^j \end{aligned} \tag{B.19}$$

satisfy (B.5). The special cases $A = \mathbb{R}^n$ of (B.18) and (B.19) yield the known rotational Crofton formula [AJ10, Proposition 3 and p. 6] for intrinsic volumes.

Note that (B.19) can be written using the j-th support measure $\Xi'_j(Y, \cdot)$ of $Y = X \cap L^n_{j+1[O]}$ with respect to $L^n_{j+1[O]}$; see for instance [HSS08, p. 488]. Hence $\beta(X) = \Phi_{n-1}(X, A)$ and

$$\begin{aligned} \alpha(X \cap L^n_{j+1[O]}) = &c^n_{j+1,1} \int_{(A \cap L^n_{j+1[O]}) \times (S^{n-1} \cap L^n_{j+1[O]})} \|z\|^{n-j-1} \\ &F(-\tfrac{1}{2}, -\tfrac{n-j-1}{2}; \tfrac{j}{2}; \sin^2 \angle(u, z)) \Xi'_j(X \cap L^n_{j+1[O]}, \mathrm{d}(z, u)) \end{aligned} \tag{B.20}$$

satisfy (B.5). As support measures are weakly continuous [Sch93, Theorem 4.2.1] and any convex body can be approximated by a decreasing sequence of convex bodies with boundary of class C^2 [Sch93, pp. 159–160], equation (B.20) is a solution of (B.5) with $\beta(X) = \Phi_{n-1}(X, A)$ for arbitrary convex bodies, as long as $\Phi_{n-1}(X, \partial A) = 0$. In particular, the choice $A = \mathbb{R}^n$ gives a rotational integral formula for $V_{n-1}(X)$ for all $X \in \mathcal{K}^n$.

B.4.2 The measurement function as an integral over the sphere

When $\beta(X)$ in (B.5) is the surface area of $X \in \mathcal{K}^n$, the measurement function can be written in terms of the radial function of the section profile and an angle in the section plane. This is obtained by using representation (B.20) derived in the preceding section for $m = j-1$ and the coarea formula.

Proposition B.5. *For $X \in \mathcal{K}^n$ with $O \in \operatorname{int} X$ and $L^n_{j+1[O]} \in \mathcal{L}^n_{j+1[O]}$ let $Y = X \cap L^n_{j+1[O]}$. Then $\beta(X) = V_{n-1}(X)$ and*

$$\alpha(Y) = c^n_{j+1,1} \int_{S^{n-1} \cap L^n_{j+1[O]}} \rho_Y^{n-1}(u) \frac{1}{\cos \alpha} F(-\tfrac{1}{2}, -\tfrac{n-j-1}{2}; \tfrac{j}{2}; \sin^2 \alpha) \mathrm{d}u^j \tag{B.21}$$

satisfy (B.5)*, where α is the angle between the (almost surely unique) outer unit normal of Y in $L^n_{j+1[O]}$ at $\rho_Y(u)u$ and the line connecting this boundary point with O.*

Proof. We assume first that X has a unique outer unit normal in every boundary point. This is equivalent to saying that ∂X is a C^1-surface; see e.g. [Sch93, p. 104]. Then (B.19) with $A = \mathbb{R}^n$ gives

$$\alpha(Y) = c^n_{j+1,1} \int_{\partial' Y} \|z\|^{n-j-1} F(-\tfrac{1}{2}, -\tfrac{n-j-1}{2}; \tfrac{j}{2}; \sin^2 \alpha) \mathrm{d}z^j.$$

In the following, we identify $L^n_{j+1[O]}$ with $\mathbb{R}^{j+1}$ (and hence assume $Y \subseteq \mathbb{R}^{j+1}$). The claim then follows for X with boundary of class C^1 if we can show the transformation formula

$$\int_{S^j} g(f(u)) Jf(S^j; u) \mathrm{d}u^j = \int_{\partial Y} g(z) \mathrm{d}z^j \tag{B.22}$$

with

$$\begin{aligned} f : \mathbb{R}^{j+1} \setminus \{O\} &\to \partial Y \\ x &\mapsto \rho_Y(x) x, \end{aligned}$$

and Jacobian $Jf(S^j; u) = \rho_Y^j(u) / \cos \alpha$, for arbitrary measurable $g \geq 0$.

Equation (B.22) follows from an application of the coarea formula [Jen98, Theorem 2.1] by calculation of the Jacobian. We have

$$Df(x) = \Big(\frac{\partial f_i}{\partial x_k} \Big)_{i,k=1,\dots,j+1} = x(\nabla \rho_Y(x))^t + \rho_Y(x) I_{j+1},$$

where I_k is the $(k \times k)$-identity matrix. If u denotes the outer unit normal of Y at $\rho_Y(x)x$, the directional derivative of f in direction $y \neq O$ must be a vector in the tangent space $\rho_Y(x)x + u^\perp$, so $(Df(x)y)^t u = 0$. More explicitly, $y^t \nabla \rho_Y(x) x^t u + \rho_Y(x) y^t u = 0$. Choosing $y \in u^\perp$ arbitrary, and then $y = u$ gives $\nabla \rho_Y(x) = -\frac{\rho_Y(x)}{\cos \alpha} u$, so

$$Df(x) = \rho_Y(x)(I_{j+1} - \tfrac{1}{\cos \alpha} x u^t)$$

when $x \in S^j$. The Jacobian is given by

$$Jf(S^j; x) = \sqrt{\det(EDf(x)^t (EDf(x)^t)^t)}$$

where the rows of the matrix E consist of an orthonormal basis of $x^\perp$. This gives

$$\begin{aligned} Jf(S^j; x) &= \rho_Y^j(x) \sqrt{\det(I_{j+1} + \tfrac{1}{\cos^2 \alpha} Eu(Eu)^t)} \\ &= \rho_Y^j(x)(1 + \tfrac{\|Eu\|^2}{\cos^2 \alpha})^{1/2} \\ &= \frac{\rho_Y^j(x)}{\cos \alpha}, \end{aligned}$$

as required. Using the continuity of the intrinsic volumes and Lebesgue's dominated convergence theorem the C^1-assumption can be omitted, as outlined in the following. If Y has a unique outer unit normal in $L^n_{j+1[O]}$ at $y \in \partial Y$ we say that y is a regular point of Y. Let $\operatorname{reg} Y$ be the set of regular points of Y, $S_Y = \{u \in S^{n-1} \cap L^n_{j+1[O]} \,|\, \rho_Y(u)u \notin \operatorname{reg} Y\}$ and define

$$\begin{aligned} g : \partial Y \setminus \operatorname{reg} Y &\to S_Y \\ x &\mapsto \frac{x}{\|x\|}. \end{aligned}$$

As [Sch93, Theorem 2.2.4.] implies $\mathcal{H}^j_{j+1}(\partial Y \setminus \operatorname{reg} Y) = 0$ and g is a Lipschitz mapping, we have $\mathcal{H}^j_{j+1}(S_Y) = 0$. We therefore only consider $u \in S^{n-1} \cap L^n_{j+1[O]} \setminus S_Y$ in the following.

Let $X_i = X + i^{-1}B_n$ be the parallel body of X at distance i^{-1}. Then ∂X_i is a C^1-surface. As $X_i \searrow X$ for $i \to \infty$ we have that $Y_i = X_i \cap L^n_{j+1[O]}$ converges to $Y = X \cap L^n_{j+1[O]}$ and, by continuity of the radial function, $\rho_{Y_i}(u)u \to \rho_Y(u)u$, as $i \to \infty$. By the fact that $\rho_Y(u)u \in \operatorname{reg} Y$, we conclude that $\alpha_i \to \alpha$ for $i \to \infty$, where α_i is the angle between the outer unit normal of Y_i at $\rho_{Y_i}(u)u$ and the line connecting this boundary point with O. As $O \in \operatorname{int} X$, there exists α' such that $\alpha_i < \alpha' < \pi/2$ for all i and hence $\cos\alpha_i > \cos\alpha' > 0$. This implies that the hypergeometric function $F(-\frac{1}{2}, -\frac{n-j-1}{2}; \frac{j}{2}; \sin^2\alpha_i)$ can be written as an absolutely convergent power series in $\sin^2\alpha_i$ and is therefore a continuous function on $[0, \alpha']$. Therefore, there exists a finite constant $C = C(Y, n, j)$ such that

$$\rho^{n-1}_{Y_i}(u)\frac{1}{\cos\alpha_i}F(-\tfrac{1}{2}, -\tfrac{n-j-1}{2}; \tfrac{j}{2}; \sin^2\alpha_i) < C$$

for all $u \in S^{n-1} \cap L^n_{j+1[O]}$ and all i. Furthermore, we have shown pointwise convergence of the integrand

$$\rho^{n-1}_{Y_i}(u)\frac{1}{\cos\alpha_i}F(-\tfrac{1}{2}, -\tfrac{n-j-1}{2}; \tfrac{j}{2}; \sin^2\alpha_i) \to \rho^{n-1}_{Y}(u)\frac{1}{\cos\alpha}F(-\tfrac{1}{2}, -\tfrac{n-j-1}{2}; \tfrac{j}{2}; \sin^2\alpha)$$

for $u \in S^{n-1} \cap L^n_{j+1[O]} \setminus S_Y$. Hence Lebesgue's dominated convergence theorem can be applied and the result follows without assuming that ∂X is a C^1-surface. □

We remark that the proposition also holds without assuming $O \in \operatorname{int} X$ but then the assumptions that X is strictly convex and that ∂X is a C^1-surface have to be added. Then (B.21) becomes

$$\alpha(Y) = c^n_{j+1,1}\int_{\{u \in S^{n-1} \cap L^n_{j+1[O]} \,|\, \exists \beta \in \mathbb{R} : \beta u \in Y\}} \rho^{n-1}_Y(u)\frac{1}{\cos\alpha}F(-\tfrac{1}{2}, -\tfrac{n-j-1}{2}; \tfrac{j}{2}; \sin^2\alpha)\mathrm{d}u^j.$$

The hypergeometric function in (B.21) simplifies when $n = 3$, $j = 1$ [Jen98, Example 5.10]

$$F(-\tfrac{1}{2}, -\tfrac{1}{2}; \tfrac{1}{2}; \sin^2\alpha) = \cos\alpha + \alpha\sin\alpha. \tag{B.23}$$

Hence, according to Proposition B.5, for $X \in \mathcal{K}^3$ with $O \in \mathrm{int}X$, equation (B.5) with $\beta(X) = V_2(X)$ is satisfied by

$$\alpha(X \cap L^3_{2[O]}) = \int_{S^2 \cap L^3_{2[O]}} \rho^2_{X \cap L^3_{2[O]}}(u)(1 + \alpha \tan \alpha)\mathrm{d}u.$$

This integral equation is the basis of the well-known surfactor, see Section B.5.

B.4.3 Morse type representation

In the derivation of (B.11), we have seen that a measurement function depending on the Euler characteristic of hyperplane sections can be expressed by means of the support function when X is convex. The values of the support function can be thought of as critical values of the section profiles. We now show that the use of critical values of the section profiles can be extended to more general sets. We first formulate the result for smooth manifolds and then for polyconvex sets.

In order to obtain the counting measure on the right hand side of (B.13) we consider an $(n-j)$-dimensional manifold X. If we assume that $X \pitchfork L^n_{j+1[O]}$ in $\mathbb{R}^n$ for almost all $L^n_{j+1[O]} \in \mathcal{L}^n_{j+1[O]}$, then $Y = X \cap L^n_{j+1[O]}$ is almost surely a one-dimensional smooth manifold; see the discussion at the end of Section B.2. To discuss critical values of the manifold Y we use classical Morse theory. This theory studies the topology of manifolds in terms of functions defined on the manifolds. For the convenience of the reader we give here the basics of Morse theory for one-dimensional manifolds and refer to [Mil63] for more general results. We describe Morse theory in $\mathbb{R}^n$, but will later apply it to the section plane $L^n_{j+1[O]}$. For the purposes of stating results from Morse theory we introduce *CW-complexes*. The notion of a CW-complex is due to [Whi49]. We will assume that X is compact and therefore only need to consider finite CW-complexes. A finite CW complex Y is a topological space such that there is $n \in \mathbb{N}_0$ and a finite nested sequence

$$\emptyset \subseteq Y_0 \subseteq Y_1 \subseteq \cdots \subseteq Y_n = Y, \tag{B.24}$$

such that the following two conditions hold

(i) Y_0 is finite,

(ii) for each $d \in \{1, \ldots, n\}$, Y_d is obtained from Y_{d-1} by attaching finitely many d-cells, as described in [LW69, p. 47], where a d-cell is the image of a continuous function $\phi : B_d \to X$ that is injective on $\mathrm{int}B_d$.

The number n in the above nested sequence is the *dimension* of the CW-complex Y. If n_0 is the number of elements in Y_0, and n_d is the number of d-cells attached to Y_{d-1} to obtain Y_d, the Euler characteristic of Y is given by [Lee00, p. 373]

$$\chi(Y) = \sum_{d=0}^{n} (-1)^d n_d. \tag{B.25}$$

In the present work only CW-complexes of dimension one play a role, and they will be used only as a tool to determine the Euler-characteristic of hyperplane sections and sublevel sets of one-dimensional smooth manifolds.

Let $Y \subseteq \mathbb{R}^n$ be a compact smooth manifold of dimension one and let $f : Y \to \mathbb{R}$ be a smooth function. A point $p \in Y$ is a *critical point* of f if there is a local coordinate system $\phi : U \to Y$, where U is a neighbourhood of O, $\phi(O) = p$, such that $\bar{f} = f \circ \phi$ has a usual critical point at O:

$$\frac{\mathrm{d}\bar{f}}{\mathrm{d}x}(O) = 0.$$

If furthermore

$$\frac{\mathrm{d}^2\bar{f}}{\mathrm{d}x^2}(O) \neq 0$$

we say that p is a *non-degenerate* critical point. The definition of a critical point and non-degeneracy does not depend on the choice of the local coordinate system ϕ. If p is a critical point of f then $f(p)$ is called a *critical value* of f. We say that a function f is a *Morse function* if all of its critical points are non-degenerate and with different critical values. It is shown in [Fu89, Section 5] that the height function $f_u(y) = \langle y, u \rangle$ is a Morse function for almost all $u \in S^{n-1}$, even under the weaker assumption that Y is a set of positive reach. A set $X \subseteq \mathbb{R}^n$ is said to be of positive reach if there exists $r > 0$ such that for all $x \in X + rB_n$ there exists a unique point of X nearest to x.

If the second derivative at a non-degenerate critical point is negative, the critical point is said to have index one, otherwise it has index zero. Again, the index does not depend on the local coordinate system chosen. According to the Morse Lemma [Mil63, Lemma 2.2] the behaviour of f in a neighbourhood of a non-degenerate critical point p can be completely described by its index: There exists a chart y in a neighbourhood U of p with $y(p) = 0$ and such that

$$f = f(p) + (-1)^\lambda y^2$$

holds throughout U, where $\lambda \in \{0, 1\}$ is the index of f at p. From this it follows that a non-degenerate critical point is isolated.

In the following we will apply Morse theory only to height functions f_u, where $u \in S^{n-1}$ is chosen such that f_u is a Morse function for a given manifold Y. For a given $r \in \mathbb{R}$ and $u \in S^{n-1}$ we define the sub- and superlevel sets

$$Y_{\leq r} = \{y \in Y \mid f_u(y) \leq r\},$$
$$Y_{\geq r} = \{y \in Y \mid f_u(y) \geq r\}.$$

According to [Bre93, 7.4. Corollary p. 84] (with θ the height function on Y) and the fact that f_u is a Morse function for almost all u, the set $Y \cap (ru + u^\perp)$ is an embedded submanifold of Y for almost all $r \in \mathbb{R}$ and almost all $u \in S^{n-1}$. Therefore we can use the additivity of the Euler characteristic for manifolds, to write

$$\chi(Y \cap (ru + u^\perp)) = \chi(Y_{\leq r}) + \chi(Y_{\geq r}) - \chi(Y). \tag{B.26}$$

Let $r_1, r_2 \in \mathbb{R}$ with $r_1 < r_2$ and assume that the set $\{y \in Y \mid r_1 \leq f_u(y) \leq r_2\}$ contains no critical points of f_u. Then, by [Mil63, Theorem 3.1], $Y_{\leq r_2}$ and $Y_{\leq r_1}$ are homotopy

equivalent. Furthermore if f_u has no degenerate critical points, Y has the homotopy type of a CW-complex with one cell of dimension λ for each critical point of index λ [Mil63, Theorem 3.5]. According to [Mil63, Remark on p. 24], for all $r \in \mathbb{R}$ the set $Y_{\leq r}$ has the homotopy type of a finite CW-complex, with one cell of dimension λ for each critical point of index λ in $Y_{\leq r}$. This holds even if r is a critical value. In particular, both have the same Euler characteristic. Let now $m = m(u)$ be the number of critical points of the height function f_u on Y and $r_i = r_i(u)$, $i = 1, \ldots, m$, their critical values. We assume without loss of generality that the critical points are enumerated such that $r_1 < r_2 < \cdots < r_m$. Then, if $\lambda_i = \lambda_i(u)$, $i = 1, \ldots, m$, are the indices of the respective critical points, it follows from (B.25) with $n = 1$ that

$$\chi(Y_{\leq r}) = \sum_{i:r_i \leq r} (-1)^{\lambda_i}. \tag{B.27}$$

Applying the same argument with the function f_{-u} and constant $-r$, we obtain the Euler characteristic of the superlevel sets

$$\chi(Y_{\geq r}) = \sum_{i:r_i \geq r} (-1)^{1-\lambda_i}. \tag{B.28}$$

From (B.27) and (B.28) we get

$$\chi(Y) = \sum_{i=1}^{m} (-1)^{\lambda_i} = \sum_{i=1}^{m} (-1)^{1-\lambda_i}, \tag{B.29}$$

so $\chi(Y) = 0$. Inserting (B.27)–(B.29) into (B.26) gives

$$\begin{aligned} \chi(Y \cap (ru + u^{\perp})) &= \sum_{i:r_i \leq r} (-1)^{\lambda_i} - \sum_{i:r_i \geq r} (-1)^{\lambda_i} \\ &= 2 \sum_{i:r_i \leq r} (-1)^{\lambda_i} - \sum_{i:r_i = r} (-1)^{\lambda_i}. \end{aligned} \tag{B.30}$$

We are now equipped with the necessary terminology and results for writing the measurement function associated to the Hausdorff measures in (B.13) with $m = n - j$ in terms of critical points of the height function on the section profile.

Theorem B.6. *Let $X \subseteq \mathbb{R}^n$ be a compact smooth manifold of dimension $n - j$, where $j \in \{0, 1, \ldots, n-1\}$. Assume that $X \pitchfork L^n_{j+1[O]}$ for almost all $L^n_{j+1[O]} \in \mathcal{L}^n_{j+1[O]}$. Then for $\beta(X) = \mathcal{H}^{n-j}_n(X)$, equation* (B.5) *holds with*

$$\alpha(\cdot) = \tfrac{c^{n-j+1,n-j}_{n+1,1}}{n-j} \int_{S^{n-1} \cap L^n_{j+1[O]}} M(\cdot, u) \mathrm{d}u^j, \tag{B.31}$$

where

$$M(Y, u) = \sum_{k=2}^{m} (\operatorname{sgn}(r_k)|r_k|^{n-j} - \operatorname{sgn}(r_{k-1})|r_{k-1}|^{n-j}) \sum_{i=1}^{k-1} v_i \tag{B.32}$$

depends on all the critical values $r_1 < r_2 < \cdots < r_m$ of the smooth one-dimensional manifold $Y \subseteq L^n_{j+1[O]}$ with respect to the function $f_u(x) = \langle x, u \rangle$. The respective Morse indices are $\lambda_1, \ldots, \lambda_m$ and we abbreviated $v_i = (-1)^{\lambda_i}$, $i = 1, \ldots, m$.

Proof. Taking $m = n - j$ in (B.13) and using the results leading to (B.10) ([Jen98, Proposition 3.3] and an invariance argument), the expression becomes

$$\alpha(X \cap L^n_{j+1[O]}) = c^{n-j+1,n-j}_{n+1,1,1} \int_{S^{n-1} \cap L^n_{j+1[O]}} \int_{-\infty}^{\infty} \mathcal{H}^0_n(X \cap L^n_{j+1[O]} \cap (ru + u^\perp)) \, |r|^{n-j-1} \mathrm{d}r \mathrm{d}u^j. \tag{B.33}$$

Due to the assumption of transversality, $X \cap L^n_{j+1[O]}$ is a one-dimensional embedded submanifold of $\mathbb{R}^n$ for almost all $L^n_{j+1[O]} \in \mathcal{L}^n_{j+1[O]}$; see the discussion at the end of Section B.2. As f_u is a Morse function on $X \cap L^n_{j+1[O]}$ for almost all $u \in S^{n-1} \cap L^n_{j+1[O]}$, $(X \cap L^n_{j+1[O]}) \cap (ru + u^\perp)$ is a finite set for almost all $u \in S^{n-1} \cap L^n_{j+1[O]}$ and $r \in \mathbb{R}$. Hence, the counting measure in (B.33) can be replaced by the Euler characteristic and the theorem follows by inserting (B.30) into (B.33) and calculating the inner integral explicitly. □

We remark that it might be possible to generalize Theorem B.6 to sets of positive reach by using [Fu89], where the classical Morse theory is extended to sets of positive reach. We do not consider this here but give an analogous result for not necessarily smooth polyconvex sets using Hadwiger's index, an index closely related to the Morse index. For $Y \in \mathcal{R}^n$ and $u \in S^{n-1}$ let

$$g^*_u(Y; r) = \lim_{\varepsilon \to 0+} (\chi(Y \cap (ru + u^\perp)) - \chi(Y \cap ((r - \varepsilon)u + u^\perp))), \tag{B.34}$$

$r \in \mathbb{R}$, be the index function given by [Had55, Eq. (9)]. The index function is non-zero for only finitely many r. Hadwiger [Had55] showed that

$$\chi(Y) = \sum_r g^*_u(Y; r) \tag{B.35}$$

holds for all $u \in S^{n-1}$. We use this index to represent the measurement function (B.10) associated to the intrinsic volumes entirely in terms of critical values in the section profile. For $u \in S^{n-1}$ let

$$g_u(r) = g^*_u(Y; r) - g^*_{-u}(Y; r), \quad r \in \mathbb{R}. \tag{B.36}$$

We note that g_u also depends on Y but decided not to overload the notation. For a given $u \in S^{n-1}$ we say that $r \in \mathbb{R}$ is a *critical value* of Y in direction u if $g_u(r) \neq 0$.

In order to parallel the formulation to Theorem B.6 in the following result for polyconvex sets, we choose $\beta(X) = 2V_{n-j}(X)$ for the left hand side of (B.5). That the factor two is natural here, can be seen in the case $j = 1$, as $2V_{n-1}(X) = \mathcal{H}^{n-1}_n(\partial X)$ for any convex body X with interior points.

Theorem B.7. *Let $X \in \mathcal{R}^n$ and $j \in \{0, 1, \ldots, n-1\}$. Then for $\beta(X) = 2V_{n-j}(X)$, equation* (B.5) *holds with*

$$\alpha(\cdot) = \frac{c^{n-j+1,n-j}_{n+1,1}}{n-j} \int_{S^{n-1} \cap L^n_{j+1[O]}} M(\cdot, u) \mathrm{d}u^j, \tag{B.37}$$

where

$$M(Y,u) = \sum_{k=2}^{m} (\operatorname{sgn}(r_k)|r_k|^{n-j} - \operatorname{sgn}(r_{k-1})|r_{k-1}|^{n-j}) \sum_{i=1}^{k-1} v_i \tag{B.38}$$

depends on all the critical values $r_1 < r_2 < \cdots < r_m$ of $Y \subseteq L^n_{j+1[O]}$ in direction u with respective indices $v_i = g_u(r_i)$, $i = 1, \ldots, m$, where g_u is given by (B.36).

Proof. For $L^n_{j+1[O]} \in \mathcal{L}^n_{j+1[O]}$ the set $Y = X \cap L^n_{j+1[O]}$ is polyconvex. Fix $u \in S^{n-1} \cap L^n_{j+1[O]}$. Using (B.35), we have $\chi(Y) = \sum_{i=1}^{m} g^*_u(Y; r_i)$. Furthermore, as the sublevel set $Y_{\leq r}$, $r \in \mathbb{R}$, is polyconvex and

$$g^*_u(Y; r') = g^*_u(Y_{\leq r}; r')$$

for $r' \leq r$, its Euler characteristic can be written as

$$\chi(Y_{\leq r}) = \sum_{i: r_i \leq r} g^*_u(Y; r_i), \qquad r \in \mathbb{R}.$$

Similarly, we can write the Euler characteristic of the superlevel set

$$\chi(Y_{\geq r}) = \sum_{i: r_i \geq r} g^*_{-u}(Y; r_i), \qquad r \in \mathbb{R}.$$

As (B.26) also holds when Y is a polyconvex set, this gives

$$\chi(Y \cap (ru + u^\perp)) = \sum_{i: r_i \leq r} (g^*_u(Y; r_i) - g^*_{-u}(Y; r_i)) + \sum_{i: r_i = r} g^*_{-u}(Y; r_i).$$

Inserting this into (B.10) and calculating the inner integral explicitly, the result follows. □

As already noted in (B.11) and at the beginning of this section, when $X \in \mathcal{K}^n$ there are two critical values for any given direction $u \in S^{n-1} \cap L^n_{j+1[O]}$, and these are $h_{X \cap L^n_{j+1[O]}}(u)$ and $-h_{X \cap L^n_{j+1[O]}}(-u)$. Using that $-h_{X \cap L^n_{j+1[O]}}(-u) \leq h_{X \cap L^n_{j+1[O]}}(u)$, that $v_1 = 1$ for all $u \in S^{n-1} \cap L^n_{j+1[O]}$ and all $L^n_{j+1[O]} \in \mathcal{L}^n_{j+1[O]}$, and that the Hausdorff measure is reflection invariant, it follows that (B.37) simplifies to (B.11) and furthermore to (B.12) if X contains O. This shows in particular that when $X \in \mathcal{K}^n$ has a smooth boundary, the M-functions in (B.32) and (B.38) with $j = 1$ coincide, which implies that Theorem B.6, applied to ∂X, is equivalent to Theorem B.7. The M-functions agree for more general classes of sets than smooth convex sets. Let X be a compact, topologically regular set, i.e. $X = \operatorname{cl}(\operatorname{int} X)$. If ∂X is a smooth manifold of dimension $n-1$ and $\partial X \pitchfork L^n_{2[O]}$, then the boundary of $Y = X \cap L^n_{2[O]}$ is a one-dimensional smooth manifold. We formulate the result for Y and identify $L^n_{2[O]}$ with $\mathbb{R}^2$.

Proposition B.8. *Let $Y \subseteq \mathbb{R}^2$ be compact, topologically regular and such that ∂Y is a one-dimensional smooth manifold. Then, for almost all $u \in S^1$, r is a critical value of ∂Y with respect to the height function f_u, in the sense of classical Morse theory, if and only if $g_u(r) \neq 0$ for Y. Furthermore, if λ is the Morse index of a non-degenerate critical point with critical value r, then*

$$g_u(r) = (-1)^\lambda. \tag{B.39}$$

Proof. Let $u \in S^1$ be such that f_u is a Morse function. If r is not a critical value in the sense of Morse theory, (B.30) implies that $\chi(X \cap (tu + u^\perp))$ is constant for all t in a neighbourhood of r. This implies $g_u(r) = 0$, so r is not a critical value in the Hadwiger sense.

Now assume that r is a critical value in the sense of Morse theory. To simplify notation, we assume that $u = (0, 1)$ and $r = 0$ holds. Hence, the x-axis is a tangent to ∂Y at some point p, which we may assume to be O. As f_u is a Morse function, the origin is non-degenerate and isolated from all other critical points. Assume first that the index of O is $\lambda = 0$. Then there is an $\varepsilon > 0$ and a neighbourhood U of O in the x-axis such that $\partial Y \cap \varepsilon B_2 = \text{graph}\gamma$ for some convex function $\gamma : U \to \mathbb{R}$. As Y is topologically regular, either $M_+ = \text{epi}\gamma \cap \varepsilon B_2 = \{(x, y) \in \varepsilon B_2 \mid x \in U, \gamma(x) \leq y\}$ or $M_- = \text{cl}(\varepsilon B_2 \setminus M_+)$ coincides with $Y \cap \varepsilon B_2$.

Consider the case $Y \cap \varepsilon B_2 = M_-$. As all other critical values are at positive distance from $r = 0$, (B.30) shows that $\chi(X \cap (tu + u^\perp))$ does not change for small $t \leq 0$ implying $g_u^*(Y; 0) = 0$. However, for small $t > 0$, $\chi(X \cap (tu + u^\perp)) = \chi(X \cap u^\perp) + 1$ and $g_{-u}^*(Y; 0) = -1$. This gives $g_u(0) = 1 = (-1)^\lambda$, as required. The case $Y \cap \varepsilon B_2 = M_+$ is treated in a similar way, and the case $\lambda = 1$ can be reduced to the above by replacing u with $-u$. Summarizing, the definition of critical value is the same for both, Morse and Hadwiger theory, and (B.39) holds. □

B.4.4 The generalized flower volume and projection formulae

The invariator principle was first used in [CO05] to estimate volume and surface area of objects in $\mathbb{R}^3$ from 2-dimensional flat sections. Up to a factor 2, the surface area of $X \in \mathcal{K}^3$ is $V_2(X)$ and it follows from (B.11) and the definition (B.2) of the q-flower set that

$$V_2(X) = 2 \int_{\mathcal{L}^3_{2[O]}} V_2(H^1_{X \cap L^3_{2[O]}}) \mathrm{d}L^3_{2[O]}. \tag{B.40}$$

For $O \in X$ this was observed in [CO05]. An analogous result holds in all dimensions.

Lemma B.9. *Let $X \in \mathcal{K}^n$ be given. Then, for $j \in \{1, \ldots, n-1\}$,*

$$V_{n-j}(X) = c^{n-j+1,n-j}_{n+1,1} \tfrac{j+1}{n-j} \int_{\mathcal{L}^n_{j+1[O]}} V_{j+1}(H^{\frac{n-j}{j+1}}_{X \cap L^n_{j+1[O]}}) \mathrm{d}L^n_{j+1[O]}. \tag{B.41}$$

Proof. Equation (B.11) and the definition (B.2) of the q-flower set imply

$$V_{n-j}(X) = \tfrac{c^{n-j+1,n-j}_{n+1,1}}{n-j} \int_{\mathcal{L}^n_{j+1[O]}} \Big(\int_{\{u \in S^{n-1} \cap L^n_{j+1[O]} \mid h_{X \cap L^n_{j+1[O]}}(u) \geq 0\}} \rho^{j+1}_{H^q_{X \cap L^n_{j+1[O]}}}(u) \mathrm{d}u^j$$
$$- \int_{\{u \in S^{n-1} \cap L^n_{j+1[O]} \mid h_{X \cap L^n_{j+1[O]}}(u) \leq 0\}} |\rho_{H^q_{X \cap L^n_{j+1[O]}}}(u)|^{j+1} \mathrm{d}u^j \Big) \mathrm{d}L^n_{j+1[O]},$$

where $q = (n-j)/(j+1)$. Introducing spherical coordinates in $L^n_{j+1[O]}$ shows that the inner integrals yield the $(j+1)$-dimensional volume of $H^q_{X \cap L^n_{j+1[O]}}$ up to a factor $j+1$. □

In [GACO09, Section 4.3] the formal analogy of (B.40) with Kubota's formula [SW08, Eq. (6.11)] was remarked. Kubota's formula expresses intrinsic volumes of $X \in \mathcal{K}^n$ by orthogonal projections $X|L^n_{n-j[O]}$ of X onto $L^n_{n-j[O]} \in \mathcal{L}^n_{n-j[O]}$:

$$V_{n-j}(X) = c^{n-j+1,j+1}_{n+1,1} \int_{\mathcal{L}^n_{n-j[O]}} V_{n-j}(X|L^n_{n-j[O]}) \mathrm{d}L^n_{n-j[O]}. \tag{B.42}$$

The special case $n = 3, j = 1$ reads

$$V_2(X) = 2 \int_{\mathcal{L}^3_{2[O]}} V_2(X|L^3_{2[O]}) \mathrm{d}L^3_{2[O]}, \tag{B.43}$$

so the surface area of X is proportional to the average area of all its projections on isotropic hyperplanes. Similarly (B.40) expresses $V_2(X)$ as average of areas associated to sections with isotropic hyperplanes, where now, areas of the associated 1-flower set $H^1_{X \cap L^3_{2[O]}}$ have to be taken. Lemma B.9 shows that this analogy breaks down in general dimensions for two reasons: the $(n-j)$th intrinsic volume of X requires $(j+1)$-dimensional sections, and a $(n-j)/(j+1)$-flower set has to be considered instead of a 1-flower set. Only when n is odd and $j = (n-1)/2$ the formal analogy between (B.42) and (B.41) holds, like in the special case $n = 3, j = 1$. It is thus questionable if (B.40) should be considered as a 'dual' of (B.43) in the spirit of the dual theory of convex geometry. It appears that this analogy is a coincidence due to a special choice of dimensions.

It should also be noted that formulae like (B.41) trivially hold for *some* associated set replacing the $(n-j)/(j+1)$-flower set of X, as any non-negative number α is the volume of e.g. a $(j+1)$-dimensional ball with radius $(\alpha/\kappa_{j+1})^{1/(j+1)}$.

Due to the relevance for applications, we return to the analogy of the special cases (B.40) and (B.43). In [Sch88] it was shown (in arbitrary dimension) that (B.43) still holds for $X \in \mathcal{R}^3$, if the integrand on the right hand side of

$$V_2(X|L^3_{2[O]}) = \int_{L^3_{2[O]}} \mathbf{1}_{X|L^3_{2[O]}}(z) \mathrm{d}z^2$$

is replaced by the integral of the orthogonal projections of X on $L^3_{2[O]}$ with multiplicities. This is also true for (B.40), if the indicator in

$$V_2(H^1_{X \cap L^3_{2[O]}}) = \int_{L^3_{2[O]}} \mathbf{1}_{H^1_{X \cap L^3_{2[O]}}}(z) \mathrm{d}z^2$$

is replaced by $\chi(X \cap L^3_{2[O]} \cap (z + z^\perp))$. The latter function only takes integer values and could be interpreted as 'indicator function of $H^1_{X \cap L^3_{2[O]}}$ with multiplicities'. The next proposition determines this function more explicitly when X is a finite union of polytopes in $\mathcal{K}^3$. We write $Y = X \cap L^3_{2[O]}$ and identify $L^3_{2[O]}$ with $\mathbb{R}^2$. We restrict attention to topologically regular sets $Y \subseteq \mathbb{R}^2$.

Proposition B.10. *Let $Y \subseteq \mathbb{R}^2$ be topologically regular, bounded and polygonal. Then ∂Y consists of finitely many closed polygonal Jordan paths $p^{(1)}, p^{(2)}, \ldots, p^{(k)} \subseteq \mathbb{R}^2$ such*

that $p^{(i)} \cap p^{(j)}$ is empty or finite for all $1 \le i < j \le k$. If $y_1^{(i)}, \dots, y_{m_i}^{(i)}$ are the consecutive vertices when walking along $p^{(i)}$, then

$$\chi(Y \cap (z + z^\perp)) = \sum_{i=1}^{k} \sum_{j=1}^{m_i} \mathbf{1}_{B(y_j^{(i)}) \setminus B(y_{j+1}^{(i)})}(z)$$

for $\mathcal{H}_2^2$-almost all $z \in \mathbb{R}^2$, where $B(y) = \frac{y}{2} + \frac{\|y\|}{2} B_2$ and $y_{m_i+1}^{(i)} := y_1^{(i)}$.

Proof. For $\mathcal{H}_2^2$-almost all $z \in \mathbb{R}^2$ we have

$$\begin{aligned} \chi(Y \cap (z + z^\perp)) &= \frac{1}{2} \chi(\partial Y \cap (z + z^\perp)) \\ &= \sum_{i=1}^{k} \frac{1}{2} \sum_{j=1}^{m_i} \chi\big([y_j^{(i)}, y_{j+1}^{(i)}] \cap (z + z^\perp)\big), \end{aligned} \tag{B.44}$$

where $[y, y']$ is the line segment with endpoints $y, y' \in \mathbb{R}^2$. By Pythagoras' theorem, we have $[0, y] \cap (z + z^\perp) \neq \emptyset$ if and only if $z \in B(y)$ and hence, for $\mathcal{H}_2^2$-almost all $z \in \mathbb{R}^2$,

$$[y, y'] \cap (z + z^\perp) \neq \emptyset \Leftrightarrow z \in (B(y) \setminus B(y')) \cup (B(y') \setminus B(y)).$$

Thus, for almost all z,

$$\begin{aligned} \frac{1}{2} \sum_{j=1}^{m_i} \chi\big([y_j^{(i)}, y_{j+1}^{(i)}] \cap (z + z^\perp)\big) &= \frac{1}{2} \sum_{j=1}^{m_i} (\mathbf{1}_{B(y_j^{(i)}) \setminus B(y_{j+1}^{(i)})}(z) + \mathbf{1}_{B(y_{j+1}^{(i)}) \setminus B(y_j^{(i)})}(z)) \\ &= \sum_{j=1}^{m_i} \mathbf{1}_{B(y_j^{(i)}) \setminus B(y_{j+1}^{(i)})}(z). \end{aligned}$$

Inserting this into (B.44) gives the assertion. □

When $Y \subseteq \mathbb{R}^2$ is a simply connected, polygonal set with interior points, and $y_1, \dots, y_m$ are its consecutive vertices, then

$$\chi(Y \cap (z + z^\perp)) = \sum_{i=1}^{m} \mathbf{1}_{B(y_i) \setminus B(y_{i+1})}(z)$$

for $\mathcal{H}_2^2$-almost all $z \in \mathbb{R}^2$. In other words, $\chi(Y \cap (z + z^\perp))$ can be read from the vector $v = (\mathbf{1}_{B(y_1)}(x), \mathbf{1}_{B(y_2)}(x), \dots, \mathbf{1}_{B(y_m)}(x)) \in \{0,1\}^m$ by counting the number of blocks with consecutive 1's (in a cyclic manner). For instance, when $v = (1,1,0,1,1,0,1)$, the number of such blocks is $\chi(Y \cap (x + x^\perp)) = 2$. A combination of Proposition B.10 and (B.10), together with an explicit calculation gives the following corollary.

Corollary B.11. *Let $X \subseteq \mathbb{R}^3$ be a simply connected set with interior points that can be represented as the union of finitely many polytopes in $\mathcal{K}^3$. Then, equation* (B.5) *holds with $\beta(X) = V_2(X)$ and*

$$\alpha(X \cap L_{2[O]}^3) = 2 \sum_{i=1}^{m} V_2(B(y_i) \setminus B(y_{i+1})), \tag{B.45}$$

where $B(y) = \frac{y}{2} + \frac{\|y\|}{2}B_2$ *and* $y_1, \dots, y_m$, $y_{m+1} = y_1$ *are the consecutive vertices of* $X \cap L^3_{2[O]}$. *Equivalently,*

$$\begin{aligned}&\alpha(X \cap L^3_{2[O]})\\ &\quad = \frac{1}{2}\sum_{i=1}^{m}\big(\pi\|y_i\|^2 - \gamma\big(\|y_i\|, \tfrac{\|y_i\|^2 - \langle y_i, y_{i+1}\rangle}{\|y_i - y_{i+1}\|}\big) - \gamma\big(\|y_{i+1}\|, \tfrac{\|y_{i+1}\|^2 - \langle y_i, y_{i+1}\rangle}{\|y_i - y_{i+1}\|}\big)\big),\end{aligned} \tag{B.46}$$

where $\gamma(r, x) = r^2 \arccos\frac{x}{r} - x\sqrt{r^2 - x^2}$.

Proof. The measurement function (B.10) associated to the intrinsic volumes with $n = 3$ and $j = 1$ can be written as

$$\alpha(X \cap L^3_{2[O]}) = 2\int_{L^3_{2[O]}} \chi(X \cap L^3_{2[O]} \cap (z + z^\perp))\mathrm{d}z^2.$$

Therefore, using Proposition B.10, equation (B.45) is evident.

The latter representation (B.46) is obtained from the first one by direct calculation. We consider the triangle whose vertices are O and the midpoints of the circles $B(y_i)$ and $B(y_{i+1})$. Let ϕ be the angle between the line segments $[O, y_i/2]$ and $[y_{i+1}/2, y_i/2]$ and ϕ' the angle between $[O, y_{i+1}/2]$ and $[y_{i+1}/2, y_i/2]$. Furthermore, let $r = \|y_i\|/2$ and $r' = \|y_{i+1}\|/2$ be the radii of the circles and $m' = \frac{1}{2}\|y_i - y_{i+1}\|$ be the lenght of the line segment connecting the midpoints of the circles. Draw the line orthogonal to the line connecting $y_{i+1}/2$ and $y_i/2$ and passing through O and let

$$x = \frac{1}{2}\Big(m' + \frac{r^2 - (r')^2}{m'}\Big), \quad x' = \frac{1}{2}\Big(m' - \frac{r^2 - (r')^2}{m'}\Big).$$

Applying Pythagoras' theorem, we find

$$V_2(B(y_i) \setminus B(y_{i+1})) = \pi r^2 - (r^2\phi - x\sqrt{r^2 - x^2}) - ((r')^2\phi' - x'\sqrt{(r')^2 - (x')^2}).$$

Again using Pythagoras' theorem, we can write $\phi = \arccos\frac{x}{r}$, $\phi' = \arccos\frac{x'}{r'}$,

$$x = \frac{\|y_i\|^2 - \langle y_i, y_{i+1}\rangle}{2\|y_i - y_{i+1}\|} \quad \text{and} \quad x' = \frac{\|y_{i+1}\|^2 - \langle y_i, y_{i+1}\rangle}{2\|y_i - y_{i+1}\|}$$

and the result follows. □

When X in Corollary B.11 is a convex polytope in $\mathbb{R}^3$ with $O \in \mathrm{int}X$, alternatives to (B.46) can be found in [CO11, Proposition 3] and [CO12, Corollary 2].

B.5 Stereological applications

There are various applications in local stereology of the different representations of the measurement function given in Section B.4. We mention some of them here, with an emphasis on surface area estimation. We start by a review on existing

methods and then present applications of the new rotational Crofton formulae given in Section B.4.3.

Choosing $m = j - 1$ in (B.9) and mulitplying by two, a measurement function for the surface area of the boundary of $X \in \mathcal{R}^n$ is obtained. Similarly, with $m = j$ we obtain a measurement function for the volume of X. We assume $j = 1$ in the following, which gives the relations

$$S(\partial X) = 2V_{n-1}(X) = (n-1)c_1^n \int_{\mathcal{L}^n_{2[O]}} \int_{\mathcal{L}^2_1} V_0(X \cap L^n_{2[O]} \cap L^2_1) d(O, L^2_1)^{n-2} \mathrm{d}L^2_1 \mathrm{d}L^n_{2[O]},$$

$$V_n(X) = c_1^{n-1} \int_{\mathcal{L}^n_{2[O]}} \int_{\mathcal{L}^2_1} V_1(X \cap L^n_{2[O]} \cap L^2_1) d(O, L^2_1)^{n-2} \mathrm{d}L^2_1 \mathrm{d}L^n_{2[O]}.$$

Identical relations can be obtained for a smooth manifold by choosing $m = n - j$ and $j = 1$ or $j = 0$, respectively, in (B.13). As mentioned at the beginning of Section B.4.4, the above relations were first applied in stereology in [CO05] for bounded objects in $\mathbb{R}^3$ with piecewise smooth boundary of class C^1. As evident, an unbiased estimator for the surface area of ∂X is obtained by taking an IR two-dimensional subspace and then generating an IUR line (hitting a reference set) within this subspace, weighting that line by a power of its distance from O and counting how often the weighted line hits the section profile. In [CO05] for $n = 3$ a line obtained in this way is referred to as an r-weighted line, where r is its distance from O. Similarly, by measuring the length of the intersection of an r-weighted line and the section profile, an unbiased estimator for the volume of X is obtained. An r-weighted line in a two-dimensional plane in $\mathbb{R}^3$ can be generated by choosing a uniformly distributed point z in the section plane intersected with the reference set and taking a line through that point that is orthogonal to the line connecting z with O. Formally this follows by introducing polar coordinates in the section plane. An application of these estimators was illustrated in [CORHAP10], where they are denoted *invariator estimators*.

Already in [CO05] improved surface area estimators were suggested for three-dimensional convex objects containing O. A first approach is to measure the support function for a given angle in a given IR subspace instead of generating an r-weighted line. If the support function can be measured in *all* directions in the subspace the flower estimator is obtained

$$\hat{S}_{\mathrm{flo}} = 2 \int_{S^2 \cap L^3_{2[O]}} h^2_{X \cap L^3_{2[O]}}(u) \mathrm{d}u^1, \tag{B.47}$$

which is (B.12) with $n = 3, j = 1$, up to a factor 2. This is the area of the 1-flower set $H^1_{X \cap L^3_{2[O]}}$, called flower area in [CO11], up to a factor four. In [CO11], both the flower estimator for convex bodies and the wedge estimator for volume based on the invariator principle, were studied. In particular, simple formulae for calculating the flower area when the object of interest is either an ellipsoid or a convex polygon, were given. We already referred to the latter case in Section B.4.4. As anticipated in [CO05] a good compromise between accuracy and effort might be not to measure the whole flower area but apply angular systematic random sampling in the plane,

measuring the support function for N angles for a discrete approximation of the flower area. In [DJ13] it was shown that the flower estimator for three-dimensional ellipsoids with O in the interior is identical to its discretization when the support function is measured at four perpendicular directions. There, a semi-automatic estimation of the flower estimator was proposed and studied, in analogy to the approach in [HNAJ11] for the nucleator volume estimator.

Using the new rotational Crofton-type formulae derived in Section B.4.3, we obtain analogues of these improved estimators in general dimension and without assuming convexity of the object of interest. We state these in the following. We assume that $X \in \mathcal{R}^n$ or that X is a compact, topologically regular set with ∂X an $(n-1)$-dimensional smooth manifold satisfying $\partial X \pitchfork L^n_{2[O]}$ in $\mathbb{R}^n$ for almost all $L^n_{2[O]} \in \mathcal{L}^n_{2[O]}$. According to Theorem B.7 and Proposition B.8 we can use Hadwiger's index to write the surface area of ∂X as

$$S(\partial X) = c^n_{2,1} \int_{\mathcal{L}^n_{2[O]}} \int_{S^{n-1} \cap L^n_{2[O]}} M(X \cap L^n_{2[O]}, u) \mathrm{d}u^1 \mathrm{d}L^n_{2[O]}, \tag{B.48}$$

where M is given by (B.38) with $j = 1$. Then an unbiased estimator for the surface area of ∂X is given by

$$\hat{S}_1 = c^n_1 M(X \cap L^n_{2[O]}, U), \tag{B.49}$$

where U is uniformly distributed in $S^{n-1} \cap L^n_{2[O]}$ and $L^n_{2[O]} \in \mathcal{L}^n_{2[O]}$ is IR. When $X \in \mathcal{K}^n$ the determination of $M(X \cap L^n_{2[O]}, U)$ is equivalent to measuring the support function in the two opposite directions U and $-U$. The estimator can be improved further by finding the critical points in all directions in the two-dimensional IR subspace. The estimator

$$\hat{S}_{\mathrm{flo}} = c^n_{2,1} \int_{S^{n-1} \cap L^n_{2[O]}} M(X \cap L^n_{2[O]}, u) \mathrm{d}u^1, \tag{B.50}$$

where $L^n_{2[O]} \in \mathcal{L}^n_{2[O]}$ is IR, is an unbiased estimator for the surface area of X. For $X \in \mathcal{K}^3$ containing O, this is equivalent to the flower estimator (B.47) for surface area. A discretization of the generalized flower estimator gives the following unbiased estimator

$$\hat{S}_N = \frac{c^n_1}{N} \sum_{l=0}^{N-1} M(X \cap L^n_{2[O]}, u_{\alpha_0 + l\frac{\pi}{N}}), \tag{B.51}$$

where u_α is the unit vector making an angle α with a fixed axis in the IR section plane $L^n_{2[O]} \in \mathcal{L}^n_{2[O]}$, α_0 is uniformly distributed in the interval $[0, \pi/N)$ and N is the number of sampled angles. Choosing $N = 1$ in (B.51) gives (B.49). We refer to these estimators as the *Morse type surface area estimators*. As $M(\cdot, U) = M(\cdot, U + \pi)$, the Cauchy-Schwarz inequality implies

$$\mathbb{V}\mathrm{ar}(\hat{S}_{2N}) \leq \mathbb{V}\mathrm{ar}(\hat{S}_N) \leq \mathbb{V}\mathrm{ar}(\hat{S}_1)$$

for all $N \in \mathbb{N}$. This was shown for $X \in \mathcal{K}^3$ in [DJ13, p. 145]. Furthermore from the law of total variance $\mathbb{V}\mathrm{ar}(\hat{S}_{\mathrm{flo}}) \leq \mathbb{V}\mathrm{ar}(\hat{S}_N)$ for all $N \in \mathbb{N}$. The drawback of $\hat{S}_{\mathrm{flo}}$ is

that it requires finding critical points in *all* directions in the section plane, which is usually not feasible in practice (unless the object of interest is a simply connected polytope as then Corollary B.11 can be used).

In a separate work [TRK13] we present an interactive software based on these Morse type formulae and use it to estimate the average surface area of the nuclei of giant-cell glioblastoma from microscopy images. Also the precision gain in terms of variance reduction compared to earlier approaches is discussed in [TRK13].

The different representations of the measurement functions in Section B.4 all stem from the invariator expressions in Section B.3 and are therefore equivalent, for a given n, j, m and $\beta(\cdot)$. This shows in particular that estimators based on these expressions, some of which were originally derived independently of each other, coincide. We make this more precise for the intrinsic volumes in the following.

In [GACONnB10, Conjecture 4.1] it was asked if (B.5) with $\beta(X) = V_{n-j+m}(X)$ holds only if the measurement function is of the invariator form (B.9). Some light was shed on this uniqueness conjecture in [CO12] by showing that the integrated versions of the classical estimators of volume and surface area, the nucleator and the surfactor, respectively, coincide with the invariator estimators. More specifically, it was shown that the integrated nucleator [HNAJ11, Section 2.1.2] coincides with the mean wedge volume estimator [CO12, Eq. (10)] and that for a strictly convex object with O in its interior and C^2 boundary, or a convex polygonal object containing O, the flower estimator coincides with the integrated surfactor [CO12, Eq. (24)]; see [Jen98, Section 5.6] for a derivation of the classical surfactor. The proofs rely on the use of figures and differentials and are restricted to three-dimensional objects. Section B.4 presents alternative proofs of these results in arbitrary dimension, as (B.17) with $A = \mathbb{R}^n$ is the integrated nucleator and (B.21) essentially the integrated surfactor. In particular, as (B.21) and (B.12) with $j = 1$ are both derived from (B.9) with $m = 0$, $j = 1$, we have for $X \in \mathcal{K}^n$ with $O \in \operatorname{int} X$

$$\int_{S^{n-1}\cap L^n_{2[O]}} h^{n-1}_{X\cap L^n_{2[O]}}(u)\mathrm{d}u^1 = \int_{S^{n-1}\cap L^n_{2[O]}} \rho^{n-1}_{X\cap L^n_{2[O]}}(u)\frac{1}{\cos\alpha}F\Big(-\frac{1}{2},-\frac{n-2}{2};\frac{1}{2};\sin^2\alpha\Big)\mathrm{d}u^1,$$

which is a generalization of [CO12, Propositions 2 and 3] to arbitrary dimension and without assuming strict convexity of X. This relation even holds with arbitrary power of the support and radial functions. We formulate the result for two-dimensional convex bodies.

Proposition B.12. *Let $Y \in \mathcal{K}^2$ with $O \in \operatorname{int} Y$. Then for $i \in \{1, 2, \dots\}$*

$$\int_{S^1} h^i_Y(u)\mathrm{d}u^1 = \int_{S^1} \rho^i_Y(u)\frac{1}{\cos\alpha}F(-\tfrac{1}{2},-\tfrac{i-1}{2};\tfrac{1}{2};\sin^2\alpha)\mathrm{d}u^1, \tag{B.52}$$

where α is the angle between the (almost surely unique) outer unit normal of Y at $\rho(u)u$ and the line connecting this boundary point with O.

Proof. The derivation of (B.12) from (B.9) with $m = 0$ can be repeated with an arbitrary power of the distance, leading to

$$\int_{S^1} h^i_Y(u)\mathrm{d}u^1 = i\int_{S^1}\int_0^\infty \chi(Y\cap(ru+u^\perp))r^{i-1}\mathrm{d}r\mathrm{d}u^1.$$

The rest of the proof follows the one of Proposition B.5 word by word, where only the power $n-j-1$ has to be replaced with $i-1$. □

As for Proposition B.5, we obtain an expression analogous to (B.52) without assuming $O \in \operatorname{int} Y$ if Y is strictly convex and ∂Y is a C^1-curve

$$\int_{S^1} \operatorname{sgn}(h_Y(u))|h_Y(u)|^i \mathrm{d}u^1 = \int_{\{u\in S^1 \mid \exists \beta\in\mathbb{R}:\beta u\in Y\}} \rho_Y^i(u)\frac{1}{\cos\alpha} F(-\tfrac{1}{2}, -\tfrac{i-1}{2}; \tfrac{1}{2}; \sin^2\alpha)\mathrm{d}u^1.$$

When $i=1$ in Proposition B.12 we find a formula for the boundary length of $Y \in \mathcal{K}^2$

$$2V_1(Y) = \int_{S^1} \rho_Y(u)\frac{1}{\cos\alpha}\mathrm{d}u^1,$$

which is essentially the Horvitz-Thompson estimator for length [Jen98, p. 122].

Stereological estimators of Minkowski tensors follow directly from the Minkowski tensor relations (B.14) and (B.15) as shown in [JZ13, Proposition 1]. In [JZ13, Section 5] a detailed account of all the estimators obtained for $n=3$ and $r+s\leq 2$ is given. These include the classical estimators of volume and surface area but also new local stereological estimators of centres of gravity and tensors of rank two. As an example, choosing $n=3$ and $r=j=0$ in (B.15) gives the nucleator estimator for volume while for $j=1$ it is the integrated nucleator. Similarly, letting $n=3$, $r=s=0$ and $j=m=1$ in (B.14) we obtain the flower estimator for surface area.

Acknowledgement

Both authors have been supported by the Centre for Stochastic Geometry and Advanced Bioimaging, funded by the Villum Foundation.

Bibliography

[AC10] J. Auneau-Cognacq. A rotational Crofton formula for flagged intrinsic volumes of sets of positive reach. Technical report, CSGB, Aarhus University, 2010.

[ACZJ12] J. Auneau-Cognacq, J. Ziegel, and E.B.V. Jensen. Rotational integral geometry of tensor valuations. *Adv. Appl. Math.*, 50(3):429–444, 2012.

[AJ10] J. Auneau and E.B.V. Jensen. Expressing intrinsic volumes as rotational integrals. *Adv. Appl. Math.*, 45(1):1–11, 2010.

[Bre93] G.E. Bredon. *Topology and Geometry*, volume 139. Springer, New York, 1993.

[CO05] L.M. Cruz-Orive. A new stereological principle for test lines in three-dimensional space. *J. Microsc.*, 219(1):18–28, 2005.

[CO11] L.M. Cruz-Orive. Flowers and wedges for the stereology of particles. *J. Microsc.*, 243(1):86–102, 2011.

[CO12] L.M. Cruz-Orive. Uniqueness properties of the invariator, leading to simple computations. *Image Anal. Stereol.*, 31(2):89–98, 2012.

[CORHAP10] L.M. Cruz-Orive, M.L. Ramos-Herrera, and E. Artacho-Pérula. Stereology of isolated objects with the invariator. *J. Microsc.*, 240(2):94–110, 2010.

[DJ13] J. Dvořák and E.B.V. Jensen. On semiautomatic estimation of surface area. *J. Microsc.*, 250(2):142–157, 2013.

[Fu89] J.H.G. Fu. Curvature measures and generalized Morse theory. *J. Differ. Geom.*, 30:619–642, 1989.

[GACO09] X. Gual-Arnau and L.M. Cruz-Orive. A new expression for the density of totally geodesic submanifolds in space forms, with stereological applications. *Differ. Geom. Appl.*, 27:124–128, 2009.

[GACONnB10] X. Gual-Arnau, L.M. Cruz-Orive, and J.J. Nuño Ballesteros. A new rotational integral formula for intrinsic volumes in space forms. *Adv. Appl. Math.*, 44(3):298–308, 2010.

[Gla97] S. Glasauer. A generalization of intersection formulae of integral geometry. *Geom. Dedicata*, 68(1):101–121, 1997.

[Had55] H. Hadwiger. Eulers Charakteristik und kombinatorische Geometrie. *J. Reine Angew. Math.*, 194:101–110, 1955.

[HNAJ11] L.V. Hansen, J.R. Nyengaard, J.B. Andersen, and E.B.V. Jensen. The semi-automatic nucleator. *J. Microsc.*, 242(2):206–215, 2011.

[HSS08] D. Hug, R. Schneider, and R. Schuster. Integral geometry of tensor valuations. *Adv. Appl. Math.*, 41(4):482–509, 2008.

[Jen98] E.B.V. Jensen. *Local Stereology*. World Scientific, Singapore, 1998.

[JR08] E.B.V. Jensen and J. Rataj. A rotational integral formula for intrinsic volumes. *Adv. Appl. Math.*, 41:530–560, 2008.

[JZ13] E.B.V. Jensen and J.F. Ziegel. Local stereology of tensors of convex bodies. *Methodol. Comput. Appl. Probab.*, 2013.

[Lee00] J.M. Lee. *Introduction to Smooth Manifolds, Second Edition*. Springer, New York, 2000.

[LW69] A.T. Lundell and S. Weingram. *The Topology of CW Complexes, The University Series in Higher Mathematics*. Van Nostrand Reinhold Company, New York, 1969.

[Mil63] J.W. Milnor. *Morse Theory*. Princeton University Press, Princeton, 1963.

[Pet35] B. Petkantschin. Integralgeometrie 6. Zusammenhänge zwischen den Dichten der linearen Unterräume im n-dimensionalen Raum. In *Abh. Math. Sem. Univ. Hamburg*, volume 11, pages 249–310. Springer, Heidelberg, 1935.

[Sch88] R. Schneider. Curvature measures and integral geometry of convex bodies, III. *Rend. Sem. Mat. Univ. Politec. Torino*, 46:111–123, 1988.

[Sch93] R. Schneider. *Convex bodies: the Brunn-Minkowski theory*, volume 44. Cambridge University Press, Cambridge, 1993.

[SS02] R. Schneider and R. Schuster. Tensor valuations on convex bodies and integral geometry, II. *Rend. Circ. Mat. Palermo*, Ser. II, Suppl. 70:295–314, 2002.

[SW08] R. Schneider and W. Weil. *Stochastic and Integral Geometry*. Springer, Heidelberg, 2008.

[TRK13] Ó. Thórisdóttir, A.H. Rafati, and M. Kiderlen. Estimating the surface area of non-convex particles from central planar sections. In preparation, 2013.

[Whi49] J.H.C. Whitehead. Combinatorial homotopy I. *Bull. Am. Math. Soc.*, 55(3):213–245, 1949.

Paper C

Estimating the surface area of non-convex particles from central planar sections

Ó. Thórisdóttir[1], A.H. Rafati[2] and M. Kiderlen[1]

[1] *Department of Mathematics, Aarhus University*
[2] *Stereology and EM Research Laboratory, Aarhus University*

Abstract: In this paper, we present a new surface area estimator in local stereology. This new estimator is called the 'Morse type surface area estimator' and is obtained using a two-stage sampling procedure. First a plane section through a fixed reference point of a three-dimensional structure is taken. In this section plane a modification of the area tangent count method is used. The Morse type estimator generalizes Cruz-Orive's pivotal estimator for convex objects to non-convex objects. The advantages of the Morse type estimator over existing local surface area estimators are illustrated in a simulation study. The Morse type estimator is well suited for computer assisted confocal microscopy and we demonstrate its practicability in a biological application: the surface area estimation of the nuclei of giant-cell glioblastoma from microscopy images. We also present an interactive software that allows the user to efficiently obtain the estimator.

Keywords: surface area; local stereology; area tangent count; invariator principle; Morse type surface area estimator.

C.1 Introduction

In local stereology, statistical inference about geometric characteristics like volume and surface area is made by taking random sections through a fixed reference point of a spatial structure of interest. This branch of stereology is tailor-made for applications e.g. in biology, where a typical example is optical sectioning of a cell through its nucleus; see the monograph [Jen98] on local stereology. The nucleator [Gun88] is a well-established local stereological estimator for volume. Until recently, the

surfactor was the only local stereological estimator available for estimating surface area; see [JG87] and [Jen98, Section 5.6]. Unlike the nucleator, the surfactor has not become a standard estimation tool. This might be due to the fact that the surfactor requires measuring angles in a section of the object and angle measurements can be rather cumbersome in practice.

In [CO05] a new surface area estimator, the invariator estimator, was derived. It is an unbiased estimator for the surface area of the boundary of a spatial structure that only requires counting in a two-dimensional isotropic random plane. The estimator is obtained by combining the classical Crofton formula with the invariator principle. The invariator principle states how a line in an isotropic random plane must be chosen such that it is IUR in three-dimensions. The principle has been applied widely and we refer to [TK13] for an overview of invariator related results. An unbiased estimator for volume is also obtained by combining the invariator principle with Crofton's formula but the invariator estimator for volume does not seem to enjoy any advantages over the nucleator. We therefore restrict attention to surface area estimation.

When the spatial structure is convex, improved versions of the invariator estimator have been suggested: the flower estimator and a discretization of it called the pivotal estimator; see [CO05] and [CO11]. These estimators require more workload than the invariator estimator but adding this extra effort results in considerable variance reduction. Some clinical experts convey concern about the convexity assumption and claim that not many objects in practice can be assumed to be convex in shape. The new rotational Crofton formulae [TK13, Theorems 6 and 7] tackle this problem. They present an unbiased estimator for surface area, which is better (with respect to variance) than the invariator estimator but still works for non-convex objects. The aforementioned convex estimators, the flower estimator and discretizations of it, are special cases of this new estimator. The new estimator can be obtained using a modification of the *area tangent count* [DeH67] method on a section of the structure. For a given section profile and a given direction in the section plane, a sweeping line is used and all tangents to the section profile are recorded, together with their type (if they represent a positive or a negative tangent) and their distance from the origin. We call the distance of a tangent from the origin a *critical value* and the type an *index*. The new estimator can be written entirely in terms of these indices and critical values. The estimator was originally derived using classical Morse theory and is therefore called the *Morse type surface area estimator*. It is well suited for computer assisted confocal microscopy and the main goal of this paper is to illustrate its feasibility using an expert-assisted procedure.

After introducing some notation in Section C.2 we give a detailed overview of the sampling designs for the different surface area estimators discussed in this paper. The motivation for deriving the new rotational Crofton formulae came from studying the variance of the invariator estimator. The estimator is obtained by choosing three random variables: an IR section plane and both of the polar coordinates (a direction and a distance) of a uniformly distributed point in the section

plane. In Section C.3.1 we show how the variance of the invariator estimator can be decomposed according to these three different variables. These different variance contributions are calculated numerically when the object of interest is an ellipsoid as discussed in Section C.3.2. It turns out that the variance from choosing the distance of the uniformly distributed point from the origin is by far the biggest variance contributor. This variance contribution is not present in the new Morse type surface area estimator which is what makes it much more efficient than the invariator estimator. Instead of choosing a uniformly distributed point, only a uniform direction in the plane is chosen and all tangents are found at this direction. A further variance reduction is achieved by applying angular systematic sampling in the section plane, that is, by not only finding tangents for one direction but for several, as discussed in Section C.3.3.

In Section C.3.4 we give recommendations concerning the implementation of the Morse type estimator and compare it with the so-called invariator grid estimator [CO05, Section 3.1] in a simulation study. Finding tangents for four directions in the section plane gives a very precise estimator but using only two directions also results in a good estimator. The Morse type estimator should always be preferred to the invariator grid estimator, at least when the expert-assisted approach, derived in this paper, is used. The application of the Morse type surface area estimator is illustrated in a study of giant-cell glioblastoma in Section C.4. We present an expert-assisted procedure to obtain the estimator and use the procedure to estimate the surface area of the nuclei of giant-cell glioblastoma from microscopy images. The results are presented in Section C.4.4. We conclude the paper with a brief discussion.

C.2 Theoretical background

Before giving an overview of the different surface area estimators, we introduce the notation and recall some important concepts. Throughout, $\mathbb{R}^n$ denotes the n-dimensional Euclidean space, O its origin, $\|\cdot\|$ the Euclidean norm and $\langle\cdot,\cdot\rangle$ the Euclidean scalar product. We restrict consideration to three-dimensional space although many of the results can be generalized to arbitrary dimension. We let $RB_3 = \{x \in \mathbb{R}^3 \mid \|x\| \leq R\}$ be the 3-dimensional ball of radius R, centered at O, and $S^2 = \{x \in \mathbb{R}^3 \mid \|x\| = 1\}$ be the unit sphere. For $z \in \mathbb{R}^2$ we write $z^\perp$ for the line through O that is orthogonal to the axis joining z with O and $F_z = z + z^\perp$ for the line that is parallel to $z^\perp$ and passes through the point z.

We use $\mathcal{K}$ for the family of all *convex bodies* (compact, convex sets with nonempty interior) of $\mathbb{R}^3$. A non-degenerate ellipsoid is an example of a convex body. If the axes of an ellipsoid $E_3 \subseteq \mathbb{R}^3$ are parallel to the usual coordinate axes it is of the form

$$E_3 = \Big\{ x \in \mathbb{R}^3 \;\Big|\; \sum_{i=1}^{3} \Big(\frac{x_i - z_i}{a_i}\Big)^2 \leq 1 \Big\}, \tag{C.1}$$

where $a_1, a_2, a_3 > 0$ are the lengths of the semiaxes and $z = (z_1, z_2, z_3) \in \mathbb{R}^3$ is its

center. For $X \in \mathcal{K}$ its *support function*, h_X, is given by

$$h_X(u) = \max_{x \in X} \langle u, x \rangle, \qquad u \in S^2.$$

The value $h_X(u)$ is the signed distance from O to the supporting hyperplane to X with outer unit normal vector u.

We let $\mathcal{L}_2$ be the family of all two-dimensional linear (passing through O) planes. A random plane $L_2 \in \mathcal{L}_2$ is called *isotropic random* (IR) if its distribution is rotation invariant on $\mathcal{L}_2$. We introduce the surface area estimators for a fixed spatial structure $X \subseteq \mathbb{R}^3$. The spatial structure can either be a polyconvex set (composed of a finite union of convex bodies) or a compact set with smooth boundary. If X is a compact set with smooth boundary we have to add the technical requirement that $X \cap L_2$ has again a smooth boundary, for almost all $L_2 \in \mathcal{L}_2$. This assumption is discussed in [TK13] and typically imposes no restrictions in practice. In Section C.4 we extend the setting to a random particle X. We write ∂X for the boundary of X, $S(\partial X)$ for the surface area of its boundary, $V(X)$ for its volume and $\chi(X)$ for its Euler characteristic. If $X \subseteq \mathbb{R}^1$ is compact, $\chi(X)$ is the number of connected components of X. An overview of the notation of the different surface area estimators that will be discussed, their name and where they originate from can be found in Table C.1. All these estimators are unbiased and are based on measurements of X in central

Notation	Name	Reference
$\hat{S}_{\text{inv}}$	invariator estimator	[CO05]
$\hat{S}_{\text{grid}}$	invariator grid estimator	[CO05]
$\hat{S}_N^+$	pivotal estimator	[CO05]
$\hat{S}_{\text{flo}}$	generalized flower estimator	[TK13]
$\hat{S}_N$	Morse type estimator	[TK13]

Table C.1: An overview of the surface area estimators relevant for the present paper.

two-dimensional sections. In a typical application X could be a biological cell with a reference point (for instance a nucleus or nucleolus) which we identify with the origin. The data necessary for the estimators is obtained from an isotropic two-dimensional section through X.

C.2.1 The invariator estimator for surface area

Combining the classical Crofton formula and the invariator principle, the surface area of ∂X can be written as

$$S(\partial X) = \mathbb{E}\Big[4 \int_{L_2} \chi(X \cap L_2 \cap F_z) \mathrm{d}z^2\Big] \tag{C.2}$$

where the expectation is with respect to the IR distribution of the section plane $L_2 \in \mathcal{L}_2$; see [CO05, first eq. (2.10)]. Recall that F_z is the line in the section plane passing through z and orthogonal to the axis connecting z with O. Introducing polar

coordinates in the section plane, we have

$$S(\partial X) = \mathbb{E}\Big[4 \int_{S^2 \cap L_2} \int_0^\infty \chi(X \cap L_2 \cap F_{ru}) r \mathrm{d}r \mathrm{d}u\Big]. \tag{C.3}$$

The line F_{ru}, where r is its distance from O, is referred to as an r-weighted line in [CO05].

We assume now that X is contained in a known reference set, which we take to be a ball RB_3 of radius $R > 0$. The invariator estimator for surface area [CO05, first eq. (2.12)] can be expressed as

$$\hat{S}_{\mathrm{inv}} = 4\pi R^2 \chi(X \cap L_2 \cap F_Z), \tag{C.4}$$

where $L_2 \in \mathcal{L}_2$ is an IR plane and $Z \sim \mathrm{unf}(RB_3 \cap L_2)$ is a uniformly distributed point on the disk $RB_3 \cap L_2$. From (C.2) it follows that $\hat{S}_{\mathrm{inv}}$ is an unbiased estimator for $S(\partial X)$. It can be obtained using the following sampling procedure:

1. Choose $R > 0$ such that $X \subseteq RB_3$.

2. Choose an IR L_2 (for instance by parametrizing S^2 and choosing an isotropic unit vector $V \in S^2$, being a unit normal of L_2).

3. Choose a uniformly distributed point Z on the disk $RB_3 \cap L_2$.

4. Determine the estimator by counting the number of connected components of $X \cap L_2 \cap F_Z$.

It is important to notice that the estimator is unbiased for any given reference set containing the object.

C.2.1.1 Invariator grid estimator

To reduce the variance of the invariator estimator, it was suggested in [CO05, Section 3.1] to use systematic random sampling in the IR section plane as described in the following. Apply the first two steps in the sampling procedure described in Section C.2.1. For a given IR section plane L_2 a twice periodic point grid of grid distance $d > 0$, with O chosen uniformly at random in a square of area d^2, is thrown onto the section plane, see [CORHAP10, Fig.1] for illustration. For any grid point z in the reference space RB_3 consider the test line F_z. Then

$$\hat{S}_{\mathrm{grid}} = 4d^2 \sum_z \chi(X \cap L_2 \cap F_z), \tag{C.5}$$

where the sum is over all grid points z in the reference space, is an unbiased estimator for $S(\partial X)$. The application of this estimator was illustrated in [CORHAP10] on a group of rat brains.

C.2.2 Morse type surface area estimator

In this paper we promote another improvement of the invariator estimator, which also reduces variance. It uses the fact that the Euler characteristic in (C.3) only changes value (for $u \in S^2 \cap L_2$ fixed and $r \in [0, \infty)$ varying), if the line F_{ru} is tangent to the section profile $X \cap L_2$. We call the distance r of a tangent line from O a critical value. The innermost integral in (C.3) can be calculated explicitly in terms of the critical values of the section profile. This presents surface area estimators that can be written entirely in terms of critical values in a section plane. These estimators were derived in [TK13] in arbitary dimension using Morse theory. Morse theory studies the topology of manifolds in terms of functions defined on the manifolds; see the famous monograph [Mil63]. In our setting, the manifold is the boundary of the object of interest. Here we will not discuss Morse theory but rather give an intuitive explanation of critical values based on a procedure that is known in stereology under the name of *area tangent count* [DeH67]. We refer to [TK13] for a more mathematically rigorous derivation of the estimators.

C.2.2.1 A modification of the area tangent count method

For an IR section plane $L_2 \in \mathcal{L}_2$ let $Y = X \cap L_2$ be the section profile and $u \in S^2 \cap L_2$ a given direction in the section plane. The idea of the area tangent count method is to sweep the line $u^\perp$ through the section profile and find all translates of the line that are tangent to Y. We distinguish between *positive tangents* (+) and *negative tangents* (-). When the sweeping line passes a tangent there is either an increase or a decrease in the number of connected components (of the sweeping line section with the profile). If the tangent represents an increase in the number of connected components we say that it is a positive tangent and a negative tangent if it represents a decrease in the number of connected components.

In the classical use of the area tangent count method, e.g. when estimating the integral mean curvature in a structure [DeH67], only the number of tangents and their type are registered. As we are interested in calculating the weighted integral in (C.3), we also record the distance of each tangent from O. If the line $ru + u^\perp$ is tangent to Y we call the distance $r = r(u)$ a *critical value* of Y. Moreover we let $\iota_u(r) \in \{-1, 1\}$ be the type of the tangent, which we also call its *index*. A positive tangent (a tangent with index 1) can occur in two ways: either the sweeping line enters a new connected component of Y, like for the lowest critical value r_1 of Figure C.1, or a connected component splits up, like for the critical value r_2 in Figure C.1. A negative tangent (a tangent with index -1) indicates that the sweeping line leaves a part of Y, like for the remaining two critical levels in Figure C.1, or that two components of Y intersected with the line melt together (not represented in Figure C.1).

The above interpretation of critical values also leads to an intuitive protocol for finding them. Given a direction u in the section plane, find all tangents to the section profile Y that are parallel to $u^\perp$. For each of these tangents with critical value r_0, say,

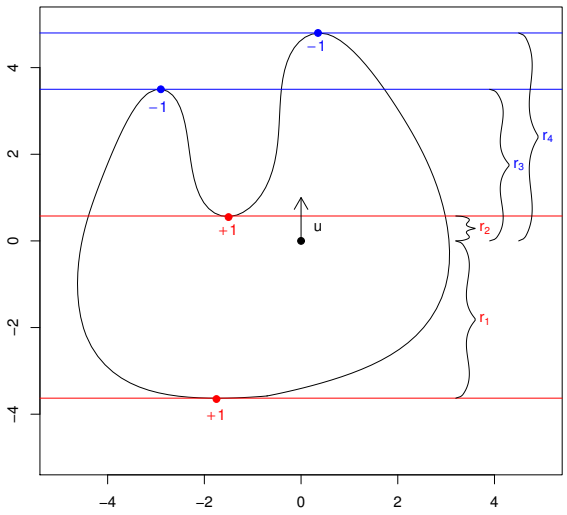

Figure C.1: Critical levels and indices for a given direction u in a section profile. Positive tangents are colored red while negative tangents are colored blue.

determine its index by checking if the number of connected components $\chi(Y \cap F_{ru})$ is increasing or decreasing when sweeping over value r_0.

A positive tangent is sometimes referred to as a 'convex' tangent and a negative one as a 'concave' tangent, see e.g. [Bad84]. In [Bad84] it is remarked that tangent counting is derived for ideal smooth objects and that it can therefore be unstable when it is applied to blurred images. This is not a severe practical limitation in our setting as we do not only use the number of tangents for a given section profile in a given direction, but rather their distances from O, the critical values.

C.2.2.2 Surface area in terms of critical values

If $m = m(u)$ is the number of critical values of a section profile Y in direction u, enumerated such that $r_1 < r_2 < \cdots < r_m$, the Euler characteristic in (C.3) can be written as

$$\chi(Y \cap F_{ru}) = \sum_{i:r_i \leq r} \iota_u(r_i) \tag{C.6}$$

for almost all r; see [TK13, Section 4.3]. This says that the number of connected components can be given entirely in terms of the tangents. For instance, for the example in Figure C.1, we have

$$\chi(Y \cap F_{2u}) = 1 + 1 = 2, \qquad \chi(Y \cap F_{4u}) = 1 + 1 - 1 = 1.$$

Inserting the expression for the Euler characteristic into (C.3), the innermost integral can be calculated explicitly, and we obtain

$$S(\partial X) = \mathbb{E}\Big[\int_{S^2 \cap L_2} M(X \cap L_2, u) \mathrm{d}u \Big] \tag{C.7}$$

where

$$M(Y,u) = \sum_{k=2}^{m} (r_k|r_k| - r_{k-1}|r_{k-1}|) \sum_{i=1}^{k-1} \iota_u(r_i) \tag{C.8}$$

depends on all the critical values $r_1 < r_2 < \cdots < r_m$ of $Y = X \cap L_2$ in direction $u \in S^2 \cap L_2$. The function M may look complicated but it is only a linear combination of the squared critical values. For the example in Figure C.1,

$$M(Y,u) = (r_2^2 + r_1^2) + (r_3^2 - r_2^2)2 + (r_4^2 - r_3^2) = r_1^2 - r_2^2 + r_3^2 + r_4^2.$$

It follows from (C.7) that the estimator

$$\hat{S}_1 = 2\pi M(X \cap L_2, U), \tag{C.9}$$

where $L_2 \in \mathcal{L}_2$ is IR and $U \sim \text{unf}(S^2 \cap L_2)$, is an unbiased estimator for the surface area of ∂X. The estimator can be obtained using the following sampling procedure:

1. Choose an IR L_2.
2. Choose a uniformly distributed direction $U \sim \text{unf}(S^2 \cap L_2)$ in the section plane.
3. For a given direction $U = u$ find all tangents of the section profile and record their critical values and indices.
4. Calculate the linear combination given by (C.8).

When $X \in \mathcal{K}$, there are only two critical values for every given direction and using the definition of the support function, the function M simplifies

$$M(Y,u) = h_Y(u)|h_Y(u)| + h_Y(-u)|h_Y(-u)|. \tag{C.10}$$

If furthermore $O \in X$, the support function is non-negative and

$$M(Y,u) = h_Y^2(u) + h_Y^2(-u), \tag{C.11}$$

so then the estimator given by (C.9) becomes

$$\hat{S}_1 = 2\pi(h^2_{X\cap L_2}(U) + h^2_{X\cap L_2}(-U)).$$

C.2.2.3 Generalized flower estimator

If it is possible to find tangents for *all* directions in the section plane, the unbiased estimator for surface area

$$\hat{S}_{\text{flo}} = \int_{S^2\cap L_2} M(X \cap L_2, u)\mathrm{d}u, \tag{C.12}$$

where $L_2 \in \mathcal{L}_2$ is IR, can be obtained. In other words

$$\hat{S}_{\text{flo}} = \mathbb{E}[\hat{S}_{\text{inv}}|L_2]. \tag{C.13}$$

When $X \in \mathcal{K}$ and $O \in X$, equation (C.12) can be written as

$$\hat{S}_{\text{flo}} = 2 \int_{S^2 \cap L_2} h^2_{X \cap L_2}(u) \mathrm{d}u, \tag{C.14}$$

where the reflection invariance of the Hausdorff measure has been used. This is the flower estimator given in [CO05].

The flower estimator can also be written as four times the area of a so-called flower set [CO05, (2.19)], which is the set whose radial function is the support function of $Y = X \cap L_2$ [TK13, p. 3]. When Y is a planar polygon, the flower set is a union of finitely many disks and resembles slightly a flower [CO11, Fig.5], which explains the terminology. The estimator $\hat{S}_{\text{flo}}$ in (C.12) can be referred to as the generalized flower estimator. There exists a simple computational formula for the generalized flower estimator when X is a simply connected polytope with interior points. The formula can be found in [TK13, Corollary 10] and only requires a list of the vertices of the polygon $Y = X \cap L_2$, where $L_2 \in \mathcal{L}_2$ is IR. When X is a convex polytope containing O, alternative formulae can be found in [CO11, Proposition 3] and [CO12, Corollary 2].

C.2.2.4 Morse type surface area estimator

When X is not a polytope, a good compromise between accuracy and effort might be cyclic systematic sampling of finitely many unit vectors in $S^2 \cap L_2$ for a discrete approximation of the integral in (C.12). Let $N \in \mathbb{N}$ be the number of directions to be sampled. Then the following unbiased estimator is obtained

$$\hat{S}_N = \frac{2\pi}{N} \sum_{l=0}^{N-1} M(X \cap L_2, u_{\alpha_0 + l\frac{\pi}{N}}), \tag{C.15}$$

where $L_2 \in \mathcal{L}_2$ is IR, $\alpha_0 \sim \text{unf}[0, \pi/N)$ and u_α is the unit vector in L_2 making an angle α with a fixed axis in the section plane. This estimator is referred to as the *Morse type surface area estimator* as, like already mentioned, it was originally derived using the theory of Morse. When $N = 1$, the estimator (C.9) is obtained. For convex X

$$\hat{S}_N = \frac{2\pi}{N} \sum_{l=0}^{N-1} (h^2_{X \cap L_2}(u_{\alpha_0 + l\frac{\pi}{N}}) + h^2_{X \cap L_2}(-u_{\alpha_0 + l\frac{\pi}{N}})). \tag{C.16}$$

For $N = 2$, equation (C.16) can be found in [CO05, Eq. (3.2)]. In [DJ13] it was shown that $\hat{S}_{\text{flo}}$ and $\hat{S}_2$ are identical when X is a three-dimensional ellipsoid with O in its interior. To avoid confusion we remark that the number of sampled directions N in (C.16) equals half the number of sampled rays in [DJ13, Eq. (8)]. More specifically, if rays are used and O is contained in the interior of X, the estimator

$$\hat{S}^+_N = \frac{4\pi}{N} \sum_{l=0}^{N-1} h^2_{X \cap L_2}(u_{\alpha_0 + l\frac{2\pi}{N}}), \tag{C.17}$$

where now $\alpha_0 \sim \text{unf}[0, 2\pi/N)$, is an unbiased estimator for the surface area of the boundary of X. This estimator is referred to as the pivotal estimator in [CO08] and

[DJ13, Eq. (8)]. We note that $\hat{S}_N = \hat{S}^+_{2N}$. In practice it is more natural to sweep a line at a given direction through the whole section profile and not stop when the line hits O. Therefore we introduced the Morse type estimator (C.15) using the M function given by (C.8) instead of using $2M^+$ given by

$$M^+(Y,u) = \sum_{k:r_k>0} (r_k^2 - \max(0, r_{k-1})^2) \sum_{i=1}^{k-1} \iota_u(r_i), \tag{C.18}$$

where $M^+(Y,u) = 0$ if $r_k < 0$ for all k.

C.3 Variance

The variance of the surface area estimators in Table C.1 has only been studied to a very limited extent and the purpose of this section is to analyse the variance in greater detail. The main result is a decomposition of the variance of the invariator estimator $\hat{S}_{\text{inv}}$. As these different variance contributions cannot be evaluated easily for general sets, we discuss the different variance contributions for ellipsoids. The decomposition can be used to express the variances of the Morse type- and the generalized flower estimator. A recommendation concerning the choice of N when applying $\hat{S}_N$ is given and it is compared to the invariator grid estimator $\hat{S}_{\text{grid}}$ in a simulation study.

C.3.1 Variance decomposition

To evaluate the quality of the invariator estimator $\hat{S}_{\text{inv}}$, we studied the different sources of variation separately. The variance of the estimator can be decomposed into three different contributions according to the integration variables in (C.3):

$$V_{\text{dist}} = \mathbb{E}\,\mathbb{V}\text{ar}(\hat{S}_{\text{inv}}|L_2, u), \tag{C.19}$$

which is the variance contribution from choosing the distance of the line F_z from O,

$$V_{\text{orient}} = \mathbb{E}\,\mathbb{V}\text{ar}(\mathbb{E}[\hat{S}_{\text{inv}}|L_2, u]|L_2), \tag{C.20}$$

which is the variance contribution from choosing the orientation of the line F_z and

$$V_{\text{plane}} = \mathbb{V}\text{ar}\,\mathbb{E}[\hat{S}_{\text{inv}}|L_2], \tag{C.21}$$

which is the variance contribution from choosing the IR section plane L_2. This is made more explicit in the following proposition.

Proposition C.1. *The variance of* $\hat{S}_{\text{inv}}$ *in* (C.4) *can be decomposed into three parts*

$$\mathbb{V}\text{ar}(\hat{S}_{\text{inv}}) = V_{\text{dist}} + V_{\text{orient}} + V_{\text{plane}}, \tag{C.22}$$

where

$$V_{\text{dist}} = 16\pi^2 \mathbb{E}\Big[M^+(X \cap L_2, u)(R^2 \sum_{k:r_k>0} \sum_{i=1}^{k-1} \iota_u(r_i) - M^+(X \cap L_2, u))\Big], \tag{C.23}$$

$$V_{\text{orient}} = 16\pi^2 \mathbb{E}\, \mathbb{V}\text{ar}(M^+(X \cap L_2, u)|L_2), \tag{C.24}$$

$$V_{\text{plane}} = 4\pi^2\, \mathbb{V}\text{ar}\, \mathbb{E}[M(X \cap L_2, u)|L_2]. \tag{C.25}$$

Here the function M is given by (C.8) *and M^+ by* (C.18)*.*

Proof. The variance of $\hat{S}_{\text{inv}}$ is finite and hence, by the law of total variance

$$\mathbb{V}\text{ar}(\hat{S}_{\text{inv}}) = \mathbb{E}\, \mathbb{V}\text{ar}(\hat{S}_{\text{inv}}|L_2) + \mathbb{V}\text{ar}\, \mathbb{E}[\hat{S}_{\text{inv}}|L_2].$$

Let $L_2 \in \mathcal{L}_2$ be a given IR section plane and (r, u) be the polar coordinates of a uniformly distributed point in $RB_3 \cap L_2$, with $r \in [0, \infty)$ and $u \in S^2 \cap L_2$. Using the conditional version of the law of total variance [BS12], we get

$$\mathbb{V}\text{ar}(\hat{S}_{\text{inv}}|L_2) = \mathbb{E}[\mathbb{V}\text{ar}(\hat{S}_{\text{inv}}|L_2, u)|L_2] + \mathbb{V}\text{ar}(\mathbb{E}[\hat{S}_{\text{inv}}|L_2, u]|L_2).$$

The variance of $\hat{S}_{\text{inv}}$ can therefore be decomposed into the three contributions given in (C.19)–(C.21). In the following we calculate these different contributions. Inserting the estimator $\hat{S}_{\text{inv}}$ into (C.21), introducing polar coordinates in the section plane and then using the expression (C.6) for the Euler characteristic we find

$$\begin{aligned}
V_{\text{plane}} &= \mathbb{V}\text{ar}\left(4\pi R^2 \frac{1}{\pi R^2} \int_{L_2 \cap RB_3} \chi(X \cap L_2 \cap F_z) \mathrm{d}z^2\right) \\
&= 16\pi^2\, \mathbb{V}\text{ar}\left(R^2 \frac{1}{2\pi} \int_{S^2 \cap L_2} \frac{1}{R^2} \int_{-\infty}^{\infty} \chi(X \cap L_2 \cap F_{ru}) |r| \mathrm{d}r \mathrm{d}u\right) \\
&= 16\pi^2\, \mathbb{V}\text{ar}\left(\frac{1}{2\pi} \int_{S^2 \cap L_2} \sum_{k=2}^{m} \sum_{i=1}^{k-1} \iota_u(r_i) \int_{r_{k-1}}^{r_k} |r| \mathrm{d}r \mathrm{d}u\right).
\end{aligned}$$

Integrating the inner integral explicitly and using the notation (C.8), we find

$$V_{\text{plane}} = 4\pi^2\, \mathbb{V}\text{ar}\, \mathbb{E}[M(X \cap L_2, u)|L_2].$$

By applying similar arguments and the notation (C.18), we obtain

$$\begin{aligned}
V_{\text{orient}} &= 16\pi^2 \mathbb{E}\, \mathbb{V}\text{ar}\left(2 \int_0^{\infty} \chi(X \cap L_2 \cap F_{ru}) r \mathrm{d}r \mid L_2\right) \\
&= 16\pi^2 \mathbb{E}\, \mathbb{V}\text{ar}(M^+(X \cap L_2, u)|L_2).
\end{aligned}$$

Furthermore, using that

$$V_{\text{dist}} = \mathbb{E}[\hat{S}_{\text{inv}}^2] - \mathbb{E}[\mathbb{E}[\hat{S}_{\text{inv}}|L_2, u]^2]$$

we get from (C.6) and (C.18) that

$$V_{\text{dist}} = 16\pi^2 \mathbb{E}\Big[R^2 M^+(X \cap L_2, u) \sum_{k:r_k>0} \sum_{i=1}^{k-1} \iota_u(r_i)\Big] - 16\pi^2 \mathbb{E}[(M^+(X \cap L_2, u))^2],$$

which simplifies to (C.23). □

Proposition C.1 implies in particular, that only the variance contribution (C.23) depends on the size R of the reference set, and it is increasing with R. More importantly, (C.13) and (C.21) show that

$$V_{\text{plane}} = \mathbb{V}\text{ar}(\hat{S}_{\text{flo}})$$

is the variance of the generalized flower estimator. Moreover, as all the surface area estimators $\hat{S}$ in Table C.1 satisfy $\mathbb{E}[\hat{S}|L_2] = \hat{S}_{\text{flo}}$ a variance decomposition similar to (C.22) for $\mathbb{V}\text{ar}(\hat{S})$ implies that $\hat{S}_{\text{flo}}$ has the lowest possible variance among them all. This is discussed further in Section C.3.3.

C.3.1.1 Variance decomposition for convex bodies

In view of (C.10) the different variance contributions in Proposition C.1 simplify when the particle X is convex. Using (C.11) and the rotation invariance of the Hausdorff measure, the expressions are particularly simple when the reference point is contained in X.

Remark C.2. *When $X \in \mathcal{K}$ and $O \in X$ the variance contributions* (C.23)–(C.25) *simplify to*

$$\begin{aligned} V_{\text{dist}} &= 16\pi^2 \mathbb{E}[h^2_{X\cap L_2}(u)(R^2 - h^2_{X\cap L_2}(u))], \\ V_{\text{orient}} &= 16\pi^2 \mathbb{E}\,\mathbb{V}\text{ar}(h^2_{X\cap L_2}(u)|L_2), \\ V_{\text{plane}} &= 16\pi^2\, \mathbb{V}\text{ar}\,\mathbb{E}[h^2_{X\cap L_2}(u)|L_2]. \end{aligned}$$

When X is a three-dimensional ellipsoid, the section profile $Y = X \cap L_2$ is an ellipse that can be expressed with respect to an orthonormal basis of the section plane L_2 [Thó10, Proposition 10]. Hence, the support function of Y can be obtained and using elementary but tedious calculations the different variance contributions in Proposition C.1 can be made more explicit. As the expressions are quite involved they are deferred to Proposition C.4 in the appendix. For illustration we give explicit analytic expressions for the different variance contributions when X in Proposition C.1 is a three-dimensional ball of radius r. We assume without loss of generality that the ball is centered at $O' = (0, 0, z)$, $z \geq 0$, and assume that the ball contains O.

Proposition C.3. *Let $X = O' + rB_3$, with $r > 0$, $O' = (0, 0, z)$, $z \in [0, r]$, and assume that $X \subseteq RB_3$. Then the different variance contributions* (C.23)–(C.25) *in Proposition C.1 can be expressed as*

$$\begin{aligned} V_{\text{dist}} &= 16\pi^2 r^2 \Big(R^2 - r^2 - \frac{4}{3}z^2\Big), \\ V_{\text{orient}} &= 16\pi^2 z^2 \Big(\frac{4}{3}r^2 - \frac{1}{5}z^2\Big), \\ V_{\text{plane}} &= \frac{16\pi^2 z^4}{5}. \end{aligned}$$

The proof uses Pythagoras' theorem and elementary but tedious calculations and can be found in [Thó10, p. 36–38]. Adding up the different variance contributions

in Proposition C.3, we obtain the total variance of the estimator when X is a ball of radius r

$$\mathbb{V}\mathrm{ar}(\hat{S}_{\mathrm{inv}}) = 16\pi^2 r^2 (R^2 - r^2); \tag{C.26}$$

see also [CO08].

C.3.2 Numerical results for ellipsoids

As mentioned earlier, Proposition C.4 in the appendix gives more explicit expressions for the different variance contributions of the estimator $\hat{S}_{\mathrm{inv}}$ when X is a three-dimensional ellipsoid. It is quite involved, if at all possible, to derive explicit analytic formulas for these expressions. We therefore turned to numerical methods in the language and interactive environment `Matlab` for calculating the different contributions (C.31)–(C.33). At the home page `home.imf.au.dk/olofth` programs for calculating the variance contributions in `Matlab` can be found. In the following we briefly describe the most important modules of this implementation.

We assume without loss of generality that the ellipsoid is of the form (C.1). In `calculations.m` the user reports the center (z_1, z_2, z_3) of the ellipsoid under study, the lengths, a_1, a_2 and a_3, of the ellipsoidal axes, and the radius R of the reference ball. The output are numerical estimates of the respective variance contributions V_{dist} (the variance from choosing the distance of the line F_z from O), V_{orient} (the variance due to the choice of the orientation of the line), V_{plane} (the variance due to choosing the IR section plane L_2), the total variance obtained by adding up the different contributions `Total variance` $= V_{\mathrm{dist}} + V_{\mathrm{orient}} + V_{\mathrm{plane}}$, and the total variance obtained from implementing the theoretical expression (C.35). We used the theoretical expression for the total variance (C.35) involving elliptic integrals to compare with the total variance obtained by adding up the different variance contributions. The comparison study included numerous different values of the parameters and implied that the algorithm is very stable and precise.

The function `dblquad` in `Matlab` was used to calculate numerically the double integrals in (C.31)–(C.33) and the program `elliptic12.m`, written by Moiseev Igor[1], was used to calculate the incomplete elliptic integrals of first and second kind to obtain (C.35). In Figure C.2 the contribution V_{dist} (dashed curve), V_{orient} (dashed-dotted curve), V_{plane} (dotted curve) and the total variance $T = V_{\mathrm{dist}} + V_{\mathrm{orient}} + V_{\mathrm{plane}}$ (solid curve) can be seen for ellipsoids embedded in a ball of radius 10.5 and given by

$$\left\{ x \in \mathbb{R}^3 \;\middle|\; \frac{(x_1 - 0.4)^2}{5^2} + \frac{(x_2 - 0.2)^2}{4^2} + \frac{(x_3 - 0.2)^2}{a_3^2} \leq 1 \right\}, \tag{C.27}$$

where a_3 varies from 0.2 to 10.

Further discussion on the different variance contributions for ellipsoids can be found in [Thó10, Section 3.5], where the shapes of the different curves, comparison between them and the role of the size of the reference space are discussed. The

[1] It was downloaded from: `http://www.mathworks.com/matlabcentral/fileexchange/8805-elliptic-integrals-and-functions`.

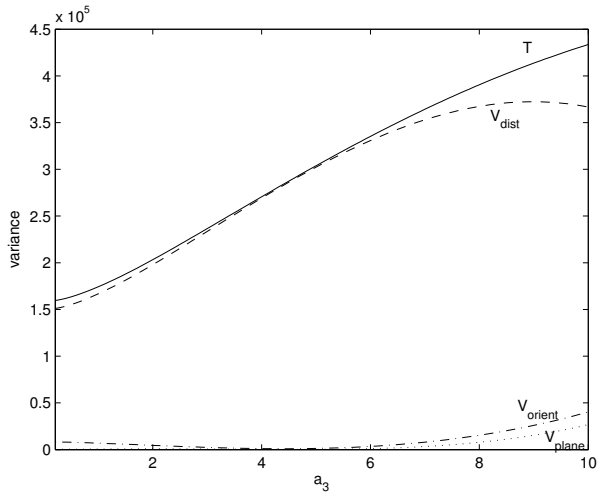

Figure C.2: The different variance contributions for ellipsoids centered at $(0.4, 0.2, 0.2)$, with axes of lengths $a_1 = 5$, $a_2 = 4$ and a_3 varying from 0.2 to 10.

general conclusion is that the variance contribution V_{dist} (the variance contribution from choosing the distance of the closest point on the line F_z from O), is very large relative to both V_{orient} and V_{plane}. Hence, to improve the estimator it is most efficient to concentrate on reducing V_{dist}.

C.3.3 Variance of the Morse type surface area estimator

The study of three-dimensional ellipsoids suggests strongly that the variance of $\hat{S}_{\text{inv}}$ primarily comes from choosing the distance of the line F_z in (C.4) from O. We believe this to hold for more general sets, too. As this variance contribution is not present in the Morse type estimator $\hat{S}_N$, it is highly recommended to add the extra effort needed to find tangents, as a dramatic variance reduction is obtained.

As an example of the variance reduction obtained, the standard error is reduced by a factor of 2.9 for the ellipsoid given by (C.27), with $a_3 = 10$ and $R = 10.5$, when the pivotal estimator $\hat{S}_1^+$ is used instead of the invariator estimator $\hat{S}_{\text{inv}}$. When X is a ball of radius $r > 0$, centered at $(0, 0, z)$, we obtain from Proposition C.3 that the coefficient of variation of $\hat{S}_1^+$ is

$$CV(\hat{S}_1^+) = \frac{\sqrt{\mathbb{V}\text{ar}(\hat{S}_1)}}{\mathbb{E}\hat{S}_1} = \frac{2z}{\sqrt{3}r}. \tag{C.28}$$

This has been reported earlier when X is a unit ball [CO08, Eq. (6)]. In [CO08] this coefficient of variation was compared to the one obtained for the surfactor estimator [JG87]. For the unit ball, $\hat{S}_1^+$ had smaller coefficient of variation than the surfactor.

As already mentioned after Proposition C.1, the law of total variance immediately gives $\mathbb{V}\text{ar}(\hat{S}_{\text{flo}}) \leq \mathbb{V}\text{ar}(\hat{S}_N)$ for all $N \in \mathbb{N}$ but as $\hat{S}_{\text{flo}}$ requires finding tangents in all directions in the section plane it is usually not feasible in practice (unless the section profile is a polygon or if its boundary can be approximated by a polygon

using automated segmentation as briefly discussed in Section C.5.2). We therefore restrict attention to $\hat{S}_N$ in what follows.

Let $Y = X \cap L_2$, $L_2 \in \mathcal{L}_2$, be the section profile. Applying systematic sampling in the section plane typically reduces the variance. More specifically, using that $M(Y, U) = M(Y, U + \pi)$, $U \sim \text{unf}(S^2 \cap L_2)$, and Cauchy-Schwarz inequality, we obtain

$$\mathbb{V}\text{ar}(\hat{S}_{2N}) \leq \mathbb{V}\text{ar}(\hat{S}_N) \leq \mathbb{V}\text{ar}(\hat{S}_1) \tag{C.29}$$

for all $N \in \mathbb{N}$. This was shown for $X \in \mathcal{K}$ in [DJ13, Section 2.2]. We only mention here that using [GACO00, Eq. (2.4)], the variance of the Morse type estimator $\hat{S}_N$ can be expressed as

$$\mathbb{V}\text{ar}(\hat{S}_N) = V_{\text{plane}} + \mathbb{E}\Big[\frac{2\pi}{N}\sum_{l=0}^{N-1} g(u_{l\frac{\pi}{N}}) - \int_{S^2\cap L_2} g(\omega)\mathrm{d}\omega \mid L_2\Big],$$

where the function g is the circular covariogram of M on the section profile

$$g(\omega) = \int_{S^2\cap L_2} M(Y, u)M(Y, u + \omega)\mathrm{d}u, \quad \omega \in S^2 \cap L_2.$$

C.3.4 Efficiency of the Morse type surface area estimator

We now discuss how the number N of directions in L_2 should be chosen so that the variance of $\hat{S}_N$ becomes small while still keeping a reasonable workload of the sampling procedure in L_2. As the variance contribution V_{plane} is common for all surface area estimators considered here, we ignore this contribution in the following discussion and consider the variance of $\hat{S}_N$ given L_2. Clearly, the function $f(N) = \mathbb{V}\text{ar}(\hat{S}_N|L_2)$ depends crucially on the shape of the underlying object. We therefore carried out a simulation study with a variety of different shapes shown in Figure C.3. The simulations were done using `R`.

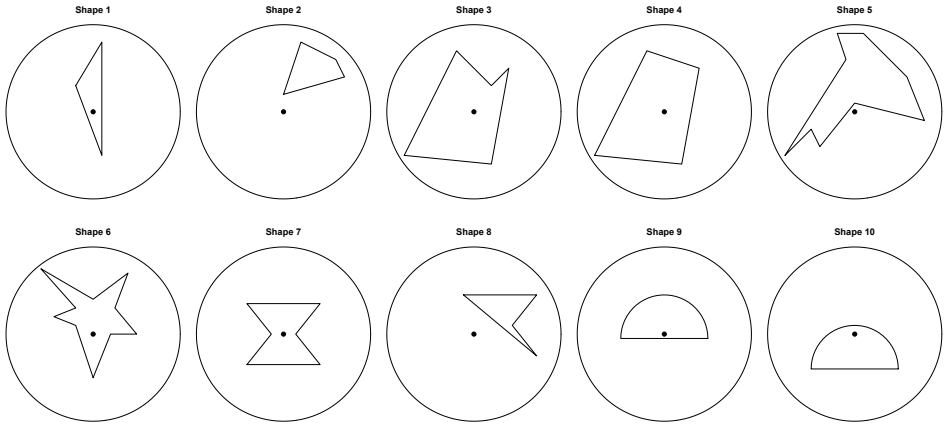

Figure C.3: Polygons and half-circles.

In the next section, we determine the empirical CV's of $\hat{S}_N$, $N \in \{1,2,3,4,5\}$, from independent Monte Carlo replications and derive an empirical recommendation for the choice of N. In Section C.3.4.2 we compare empirically the precision and workload required for the new estimator $\hat{S}_N$ and the well-known estimator $\hat{S}_{\text{grid}}$.

C.3.4.1 Choice of N

Although the variance of $\hat{S}_N$ for a given section profile does not increase when the number of orientations sampled is doubled, as shown in (C.29), it is not a non-increasing function of N. Table C.2 presents estimates of the CV's for the shapes in

CV	N = 1	N = 2	N = 3	N = 4	N = 5
Shape 1	0.6388	**0.0242**	0.0151	0.0085	0.0055
Shape 2	0.3410	0.0848	**0.0146**	0.0141	0.0123
Shape 3	0.2652	0.1048	**0.0249**	0.0087	0.0120
Shape 4	0.2587	0.1487	**0.0246**	0.0149	0.0090
Shape 5	0.1376	**0.0188**	0.0239	0.0084	0.0049
Shape 6	0.1970	**0.0228**	0.0065	0.0080	0.0029
Shape 7	0.2217	0.0747	0.0456	**0.0167**	0.0072
Shape 8	0.3025	0.0422	0.0331	**0.0204**	0.0082
Shape 9	0.2783	**0.0129**	0.0037	0.0023	0.0013
Shape 10	0.2542	0.0908	0.0255	**0.0162**	0.0091

Table C.2: CV for the shapes in Figure C.3.

Figure C.3, which are all contained in a reference disk of radius one, centered at O. To recommend a value of N, we suggest that a CV of not more than 2.5% is acceptable. Hence, the smallest N for a given shape where the empirical CV is 2.5% or less, is our recommendation for the choice of N. We only need to find tangents in two directions for shapes 1, 5, 6 and 9, in three directions for shapes 2, 3 and 4 and in four directions for shapes 7, 8 and 10. For all simulated ellipses, two orientations give a CV of less than 2.5%. This is even true for ellipses not containing the reference point O. This is not surprising as it follows from [DJ13] that $\hat{S}_2$ and $\hat{S}_{\text{flo}}$ are identical when Y is an ellipse with O in its interior, as already mentioned at the end of Section C.2.2 for three-dimensional ellipsoids. When the reference point is moved away from the center of an ellipse, the CV increases. This is evident for a disk from (C.28). The elongation of the ellipse does not seem to influence the CV when $N > 1$. For $N = 1$, the CV increases slightly for increased elongation of the ellipse.

A number of simulations were carried out and they suggest strongly that taking $N = 4$ is sufficient for obtaining a CV of less than 2.5% for a large class of shapes. Although the CV can increase as N increases, as is the case for Shape 5 with $N = 2$ and $N = 3$, it is our experience that this increase is rare, and, when it occurs, it is not substantial. Therefore taking $N = 4$ instead of $N = 3$ should typically not decrease the precision of the estimator. When the object of interest resembles an ellipse, we recommend using $N = 2$. We note that these recommendations are only based on

the variance of the sampling procedure. When there are other sources of variation that are much larger than the variance due to the sampling procedure, $N = 2$ is typically adequate, see Section C.4.4.

C.3.4.2 Comparison of $\hat{S}_N$ and $\hat{S}_{\text{grid}}$

We still consider a given section profile $Y = X \cap L_2$ and fix $L_2 \in \mathcal{L}_2$. An alternative to the Morse type estimator $\hat{S}_N$ is the invariator grid estimator $\hat{S}_{\text{grid}}$ given by (C.5). We compare the efficiency of these two estimators by finding the amount of workload needed to estimate $\mathbb{E}[\hat{S}_{\text{flo}}|L_2]$ at a given precision. Define the complexity numbers

$$\begin{aligned} C_{\hat{S}_N} &= \text{ total number of tangents for the } N \text{ directions,} \\ C_{\hat{S}_{\text{grid}}} &= 2\sum_z \chi(Y \cap F_z) + \sum_z \mathbf{1}_{\{(Y\cap F_z)=\emptyset\}}\,. \end{aligned}$$

Hence, $C_{\hat{S}_{\text{grid}}}$ is the total number of points in the intersection of the boundary of the section profile with the test lines plus the number of test lines that do not hit the section profile. Both complexity numbers are motivated by the number of mouse clicks in an interactive microscopy software to determine the estimator; see also Section C.4.3. The workload in obtaining these numbers is typically not equivalent, as determining a critical point is most likely more difficult than to determine if a line hits the boundary of the object or not. But given the ratio $Q = C_{\hat{S}_{\text{grid}}}/C_{\hat{S}_N}$, a clinical expert can decide if it is more feasible to use $\hat{S}_N$ or $\hat{S}_{\text{grid}}$. The simulation study shows strong evidence for that $\hat{S}_N$ should be preferred to $\hat{S}_{\text{grid}}$, at least when $N > 1$.

For a given polygon we generated 1000 independent replications of $\hat{S}_N$ for a given N and of $\hat{S}_{\text{grid}}$ for a given grid distance d. From these observations we calculated an empirical estimate for the variance of $\hat{S}_N$, $\hat{S}_{\text{grid}}$, respectively, and recorded the complexity constants $C_{\hat{S}_N}$. We then used a normal kernel with smoothness parameter s to smooth $\widehat{\mathbb{V}\text{ar}}(\hat{S}_{\text{grid}})$ as a function of the grid distance d. We denote the smoothed estimate of the variance by $\widehat{\mathbb{V}\text{ar}}_s(\hat{S}_{\text{grid}})$. For a given N we found d such that $\hat{S}_{\text{grid}}$ has essentially the same precision as $\hat{S}_N$, that is, such that

$$|\widehat{\mathbb{V}\text{ar}}_s(\hat{S}_{\text{grid}}) - \widehat{\mathbb{V}\text{ar}}(\hat{S}_N)| \leq 10^{-6}.$$

Given this d we then again generated 1000 independent replications of $\hat{S}_{\text{grid}}$ and calculated $C_{\hat{S}_{\text{grid}}}$. For a given N and the corresponding d we obtained an unbiased estimate of the ratio Q

$$\hat{Q} = \frac{1}{1000}\sum_{i=1}^{1000} \frac{C_{\hat{S}_{\text{grid}}}}{C_{\hat{S}_N}}.$$

In Table C.3 results for the shapes in Figure C.3 can be seen, where the smoothness parameter $s = 0.1$ has been used. When $N > 2$, d is close to zero and $\hat{Q}$ very large (much greater than 100) for all the shapes in Figure C.3. This means that $\hat{S}_{\text{grid}}$ only attains the efficiency of $\hat{S}_N$ when unrealistically many test lines are used, making the complexity number of $\hat{S}_{\text{grid}}$ large compared to the one of $\hat{S}_N$. For ellipses we find that $\hat{Q} > 2$ when $N = 1$ and that it is very large when $N = 2$. The ratio Q typically decreases with increased elongation of an ellipse.

		$\mathbb{V}\mathrm{ar}$	d	$\hat{Q}$
Shape 1	N = 1	3.52	0.81	2.9
	N = 2	$4.8 \cdot 10^{-3}$	$\simeq 0$	$\gg 100$
Shape 2	N = 1	$6.7 \cdot 10^{-2}$	0.64	4.9
	N = 2	$7.2 \cdot 10^{-3}$	0.21	22.6
Shape 3	N = 1	$2.56 \cdot 10^{-1}$	0.65	3.7
	N = 2	$3.84 \cdot 10^{-2}$	0.32	7.9
Shape 4	N = 1	$2.08 \cdot 10^{-1}$	0.68	4.9
	N = 2	$7.2 \cdot 10^{-2}$	0.46	5.3
Shape 5	N = 1	1.23	0.48	5.0
	N = 2	$2.08 \cdot 10^{-2}$	$\simeq 0$	$\gg 100$
Shape 6	N = 1	1.47	0.51	3.2
	N = 2	$1.6 \cdot 10^{-2}$	$\simeq 0$	$\gg 100$
Shape 7	N = 1	$5.92 \cdot 10^{-1}$	0.36	8.6
	N = 2	$6.72 \cdot 10^{-2}$	0.10	52.1
Shape 8	N = 1	1.33	0.58	4.4
	N = 2	$1.34 \cdot 10^{-2}$	0.04	$\gg 100$
Shape 9	N = 1	$4.06 \cdot 10^{-1}$	0.43	10.0
	N = 2	$8.30 \cdot 10^{-4}$	$\simeq 0$	$\gg 100$
Shape 10	N = 1	$4.19 \cdot 10^{-1}$	0.40	12.0
	N = 2	$5.41 \cdot 10^{-2}$	0.16	35.0

Table C.3: Comparison for the shapes in Figure C.3.

The simulations imply that Q is always greater than 2. Hence, $\hat{S}_N$ should at least be preferred to $\hat{S}_{\text{grid}}$ if the workload needed to identify a tangent, as well as its type and critical value, is not more than twice of that needed to determine if a line hits the boundary of an object or not. It should be noted that this factor 2 is a worst-case scenario. The ratio Q can be much larger than two even when $N = 1$, as can be seen in Table C.3. When the software, described in Section C.4.3, is used, the estimator $\hat{S}_N$ can be obtained very efficiently and should therefore always be preferred to $\hat{S}_{\text{grid}}$.

C.3.4.3 Convex hull

Rather surprisingly it is not necessarily better (with respect to variance) to find $\hat{S}_N$ for the convex hull of an object than for the true object. We show this by an example. The object in Figure C.4 to the left is a disk of radius r, where one fourth has been cut off, and the one to the right is its convex hull. In Table C.4 estimates for the CV's based on 1000 independent replications of $\hat{S}_N$ for $N \in \{1, 2, 3\}$ and each of the two objects can be seen.

We note that the CV's for the convex hull, the object to the right in Figure C.4, are considerably larger than those for the object to the left. This can be explained by

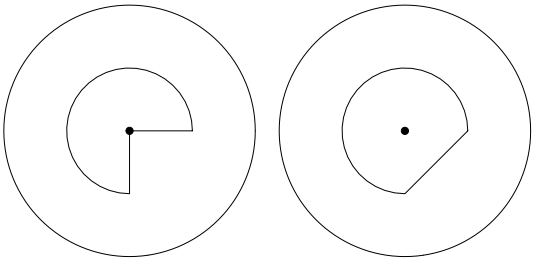

Figure C.4: A disk of radius r, where one fourth has been cut off, and its convex hull.

CV	$N = 1$	$N = 2$	$N = 3$
Fig. C.4 left	**0.001140**	0.000165	0.000357
Fig. C.4 right	0.075878	0.040691	**0.020190**

Table C.4: CV for the objects in Figure C.4

considering the integrand in the generalized flower estimator, the function M. The true value $\mathbb{E}[\hat{S}_{\text{flo}}|L_2]$ can be written as

$$\mathbb{E}[\hat{S}_{\text{flo}}|L_2] = 2\int_0^{2\pi} f(\alpha)\mathrm{d}\alpha.$$

where for the object to the left the function f is a constant, $f(\alpha) = r^2$ for all $\alpha \in [0, 2\pi)$, while for the convex hull

$$f(\alpha) = \begin{cases} r^2, & \alpha \in [0, 3\pi/2) \\ r^2 \sin^2 \alpha, & \alpha \in [\frac{3\pi}{2}, \frac{7\pi}{4}) \\ r^2 \cos^2 \alpha, & \alpha \in [\frac{7\pi}{4}, 2\pi). \end{cases}$$

This explains the greater variance of $\hat{S}_N$ for the convex hull.

C.4 Application of the Morse type surface area estimator to giant-cell glioblastoma

We illustrate the application of the Morse type estimator $\hat{S}_N$ in a study of giant-cell glioblastoma. The goal is to estimate the average surface area of the nucleus of giant-cell glioblastoma from microscopy images. Giant-cell glioblastoma is a rare brain neoplasm which accounts for 1% of glioblastomas. It is formerly known as monstro-cellular brain tumour. Histologically, the tumour is characterized by bizarre-looking, variable sized and shaped multinucleated giant-cells with abundant eosinophilic cytoplasm [OPN+00]. Giant-cell glioblastoma is a subtype of glioblastoma multiforme, however the rarity of giant-cell glioblastoma has prevented further characterization. Giant-cell glioblastoma is more prevalent in young-male patients and tends to occur more in parietal and temporal lobe of brain. We chose to illustrate the estimator for the nuclei of giant-cell glioblastoma as they are typically non-convex in shape, see Figure C.5.

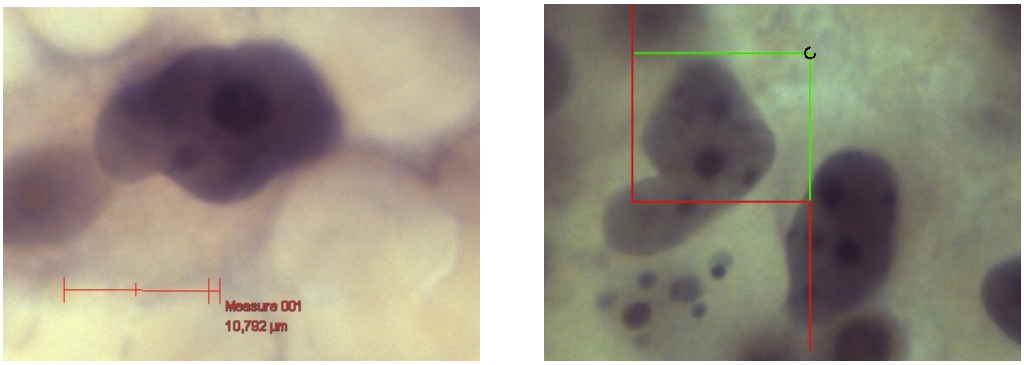

Figure C.5: Section profiles through a nucleoli of the nuclei of two giant-cell glioblastoma.

C.4.1 Model-based setting

In the preceding sections we have assumed that the structure of interest is deterministic and the section plane is random, that is we have worked in a design-based setting. We will now adopt the common model-based approach, where the particles, here nuclei of giant-cell glioblastoma, are random isotropic and the plane is deterministic. This isotropy assumption allows us to avoid a complicated, time consuming protocol, where each particle is sectioned physically or optically by a new isotropically generated plane. Hence we assume that the nuclei are realizations of an ergodic isotropic random process, meaning that nuclei far away from each other have independent orientations. We then can apply a model-based version of the estimator $\hat{S}_N$. The estimator is identical to the one given by (C.15), but now the particle X is assumed to be random and the section plane L_2 fixed. For all random nuclei X we assume that $\mathbb{E}S(X) = \bar{S}$, where the expectation is with respect to the random particle process and $\bar{S}$ is the average surface area of the typical particle. $\bar{S}$ is the target quantity. The unbiasedness of the model-based version of the estimator then follows from the unbiasedness of the design-based estimator and the strong law of large numbers.

C.4.2 Materials and preparation methods

From ten small pieces of tissue biopsies sized 1 mm^3 to 2 mm^3, one piece was randomly chosen, embedded in glycol methacrylate (GMA) for preparation of a plastic block. Two 40 µm-thick plastic sections were serially sectioned on a microtome (HM355, Microm, DMK & Michelsen, Denmark) and stained with hematoxylin and eosin stain for light microscopy. Data-acquisition was performed using a stereological microscopy system (BX-51 microscope, Olympus, Denmark) equipped with the NewCast Version 4.1 software package (Visiopharm, Hoersholm, Denmark) and mounted with a digital camera (Olympus DP72) on top of the microscope to project live views of tissue sections on a monitor. The z-axis of the microscope was monitored with a Heidenhain electronic microcator and the x-y position was monitored by motorized stage system (ProscanTM, Prior Scientific Instruments Ltd., Cambridge, U.K).

The image of the tumour region was captured and delineated by navigator tool of NewCast with 4× objective. An unbiased counting frame ($X \times Y, 15 \times 13 = 195\,\mu m^2$) was used to sample randomly a total of $n = 51$ nuclei. The red and green 'rectangle' on the images in Figure C.6 is a counting frame. The images of nuclei were captured by optical disector with an oil objective (100×, NA: 1.25).

As already mentioned in Section C.2, any point in the nucleus can serve as reference point as long as it is easily identifiable in any section direction. We chose the nucleoli in the selected nuclei as reference points. If a nucleus contained several nucleoli, we chose one out of all the admissible nucleoli (with respect to the counting frame) with uniform probability. In order to decrease the variance of the estimator systematic sampling was applied in the tissue by using a counting frame with a step-length of 400 µm in both x and y direction. This assures that the nuclei can be assumed to have independent orientations. In other words, we can assume that the n sampled nuclei are realizations of independent, isotropic random particles $X_1, X_2, \ldots, X_n$ satisfying $\mathbb{E}S(X_i) = \bar{S}$ for $i = 1, \ldots, n$.

C.4.3 Implementation of the Morse type surface area estimator

The estimator $\hat{S}_N$ was used to estimate the surface areas of the sampled nuclei. In Section C.3.4.1 we recommended to use $N = 4$, that is to find tangents for four directions in the section plane ($N = 2$ when the object of interest resembles an ellipsoid), to obtain a good precision of the surface area. In the present implementation we used one, two and four directions in the section plane in order to be able to compare the performance of the estimators. The estimation was done using an expert-assisted procedure which was implemented using `Matlab`. It is based on a program derived in [Kal12] for estimating the perimeter of planar geometric structures. The interactive software is available at the home page `home.imf.au.dk/olofth`. We give a brief description of it in the following.

The present implementation is an off-line expert-assisted procedure, where the sampled section profiles – microscopy images in JPEG format – are used as input. The user, preferably a clinical expert, can choose the number N of directions that are to be sampled. As previously stated we recommend using $N = 4$ ($N = 2$ for ellipsoids) but we describe the procedure for an arbitrary N. Microscopy images are often stored with a scale, see for instance Figure C.5 to the left. If this is the case, the user should indicate the scale before running the procedure. If a scale is reported, the calculated surface area estimate is given on this scale, otherwise it is given in pixel units. We assume in the following that a scale is given.

When the procedure is run, the image pops up with a short explanation of what the user should do next. The measurement procedure consists of three steps which are illustrated in Figure C.6.

Scale The user left clicks on the endpoints of the scale, see the image in the upper left corner in Figure C.6. This tells the program that the length of the red 'measure' line segment is 10.706 µm.

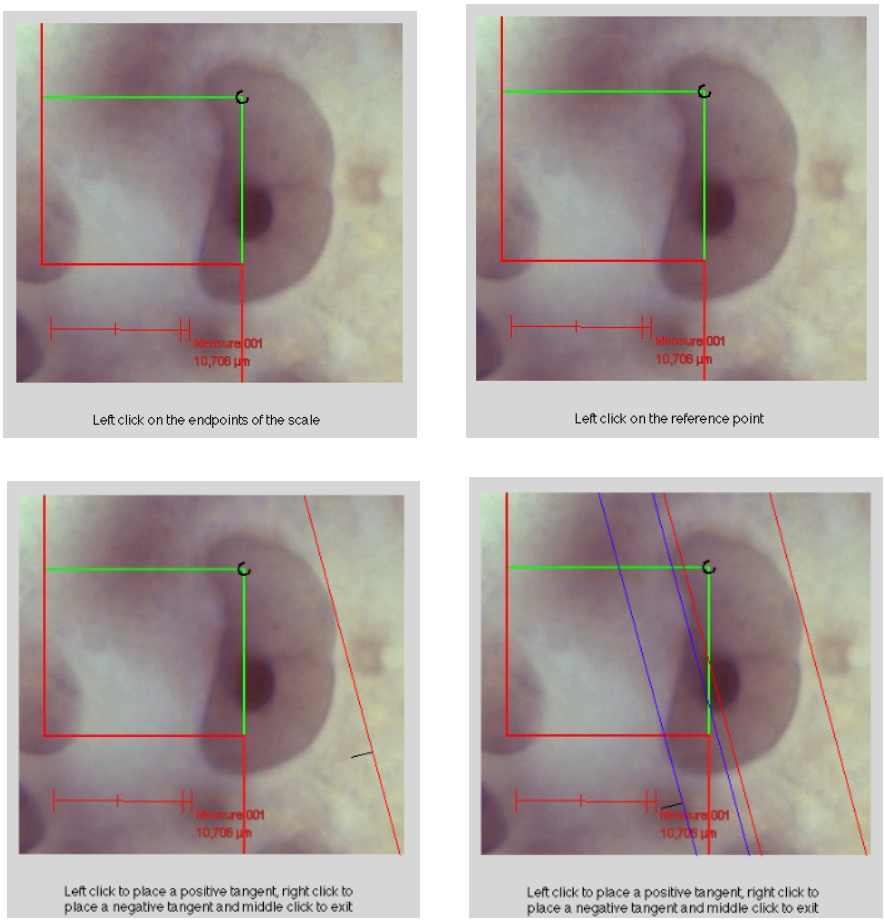

Figure C.6: An illustration of the expert-assisted procedure on one section profile through a nucleolus of the nucleus of a giant-cell glioblastoma. The short black line segment indicates the sampled direction. Positive tangents are colored red while negative tangents are colored blue.

Reference point The user left clicks on the reference point, see the image in the upper right corner in Figure C.6.

Tangents The computer generates a random unit vector U in the section plane including an angle α_0 with the x-axis that is uniform in $[0, \pi/N)$. In the image in the lower left corner in Figure C.6, this vector is indicated as a short black line segment attached to the red line orthogonal to U, passing through the position of the mouse cursor. The line can be translated using the mouse. The user now marks all tangent positions of this line to the section profile, clicking left whenever a positive tangent is located, and clicking right for every negative tangent. If $N > 1$ this step is repeated with all $N - 1$ lines with associated angles $\alpha_0 + l\pi/N$, $l \in \{1, 2, \ldots, N-1\}$.

When these three steps are completed and the user has found all tangents for the N sampled directions an estimate $\hat{S}_N$ of the surface area is calculated. The number of tangents that need to be placed gives the complexity number $C_{\hat{S}_N}$ defined in

Section C.3.4.2. It should be noted again that it certainly is more time consuming to place tangents at a given direction than just counting intersection points of the profile boundary with a given line, as is the case for the invariator estimator. But for an experienced user of the software, the Morse type estimator $\hat{S}_N$ can be obtained very efficiently and should be preferred to the alternative invariator grid estimator $\hat{S}_{\text{grid}}$.

As biological images are blurred, there might be tangents that appear to pass through a point of inflection of the boundary (although this event has probability zero with idealized mathematical particles). The easiest solution is to ignore these tangent lines, and neither left- nor right click at these positions. This is in correspondence with the theory, as a sweeping line passing through this tangent will neither increase nor decrease the associated Euler characteristic. It can also happen in practice, that the sweeping line appears to be tangent to the section profile at more than one point for certain critical values. As the images are blurred, it could for example appear that the sweeping line enters more than one new connected component at a critical value or that it enters a new connected component and leaves a part of the section profile at the same critical value. These events also have probability zero with idealized mathematical particles. To deal with these tangents, we simply suggest making a left- or a right mouse click for every change, without translating the line.

C.4.4 Results

We used the expert-assisted procedure to obtain estimates of the surface area of the $n = 51$ section profiles. We did this for $N = 1, 2$ and 4. An unbiased estimator for the average surface area of the nucleus X of a giant-cell glioblastoma is then given by

$$\hat{S}_N^{\text{ave}}(X) = \frac{1}{51} \sum_{i=1}^{51} \hat{S}_N(X_i \cap L_2),$$

where L_2 is a fixed plane and $\hat{S}_N$ is the Morse-type estimator given by (C.15). Empirical estimates for the average surface areas can be found in Table C.5.

	$N = 1$	$N = 2$	$N = 4$
$\hat{S}_N^{\text{ave}}(X)$	675.0 µm^2	597.8 µm^2	599.3 µm^2

Table C.5: Empirical estimates for the average surface area of the nucleus of a giant-cell glioblastoma, depending on the number N of systematic directions used in the section plane.

In Figure C.7 boxplots for the surface area estimates of the nuclei for $N = 1, 2$ and 4, respectively, can be found. The red lines in Figure C.7 are the medians, the bottom and the top of the boxes represent the lower quartiles (25th percentiles) and the upper quartiles (75th percentiles), respectively, and the red 'pluses' are outliers (more than 1.5 IQR from the upper quartiles). The boxplots in Figure C.7 do not suggest that sampling with a higher number N of directions gives a more precise

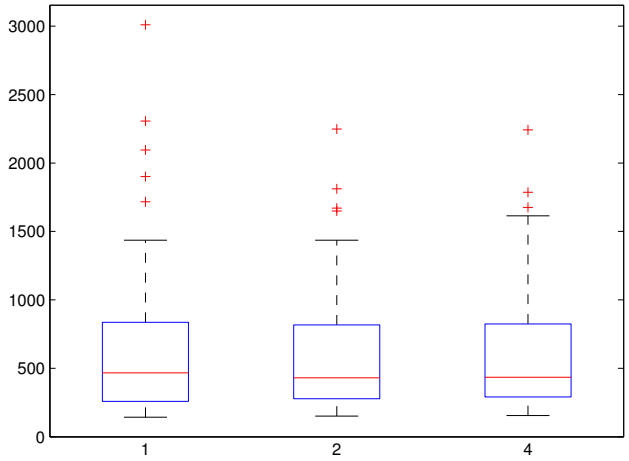

Figure C.7: Boxplots for the surface area estimates of the 51 nuclei for $N = 1$, 2 and 4, respectively.

estimator. This seemingly counter-intuitive result can be explained by looking at the different sources of variation of $\hat{S}_N^{\text{ave}}(X)$. The variance of $\hat{S}_N^{\text{ave}}(X)$ can be decomposed into the true population variance, that is the variation in surface area among the nuclei, and the mean variance due to the estimation procedure within each nucleus. The variance due to the estimation procedure within each nucleus can then again be decomposed into V_{plane} and V_{orient}, as shown in Proposition C.1. The true population variance is unknown and as the data only consist of one section profile for each sampled nuclei we can not assess V_{plane}. For a given nucleus, V_{orient} can be estimated from the section profile. This was done for each of the estimators in Table C.5 for a few of the section profiles. A large decrease in V_{orient} was observed for each of the studied nuclei when N was increased. This decrease in V_{orient} was much more pronounced when N was increased from one to two than when it was increased from two to four. However, this variance contribution is very small compared to the sum of the true population variance and the mean variance due to choosing the plane within each nucleus. This explains why there is no noticeable precision gain in Figure C.7 when N is increased. In the present application the choice $N = 1$ led to an extreme outlier and V_{orient} that is much larger than when $N = 2$. As a conclusion, this example suggests that the choice $N = 2$ is preferrable in situations where a relatively large population variance is present. The workload for the choice $N = 2$ is not very high.

C.5 Discussion

C.5.1 Account of main results

We have presented the Morse type surface area estimator and an expert-assisted protocol to apply it in practice. The Morse type estimator is a generalization of Cruz-Orive's surface area estimator for convex objects [CO05, Eq. (3.2)] ((C.16) with $N = 2$) to non-convex objects.

The surfactor is an alternative surface area estimator. The surfactor does not only require measuring distances in an IR section plane but also angles of the section profile with certain test rays. It was implied in [CO05] that this requirement to perform angle measurements might be difficult in practice and yield inaccurate estimates due to the singularity in its representation. In light of this belief and the simplicity of the estimator (C.16) it was claimed in [CO05] that (C.16) was the only reasonably efficient surface area estimator available at that time.

As mentioned in Section C.3.3, the surfactor was compared to the one-ray pivotal estimator, (C.17) with $N = 1$, in [CO08]. This variance comparison was extended to ellipsoidal particles in [DJ13]. The results obtained in [DJ13] show that the surfactor performs better than previously thought. In a simulation study involving ellipsoids, the surfactor was shown to be neither much affected by the singularity in its representation nor by inaccuracies in the necessary angle measurements. In [DJ13] it was also shown that the surfactor with two orthogonal directions sampled in the section plane [DJ13, Eq. (12) with $N = 4$] needs twice as much workload to obtain similar precision as (C.16) with $N = 2$. Hence, although the surfactor is a better competitor to (C.16) than previously expected, (C.16) is more efficient and should be preferred when the object of interest is convex. This recommendation can be transferred to the Morse type surface area estimator, which we showed to be the preferred surface area estimator available.

We have shown in Section C.3.1 that the variance of the pivotal estimator $\hat{S}_{\text{piv}}$ decomposes into three parts V_{plane}, V_{orient} and V_{dist} according to the randomization of the section plane, and the orientation and position of the test line, respectively. Among all estimators considered in the present paper, the generalized flower estimator has the lowest variance, as this variance coincides with V_{plane}. However, this estimator requires exact knowledge of the boundary of the section profile. We therefore also considered estimators derived from $\hat{S}_{\text{inv}}$ that still have a reasonable workload but a better variance than $\hat{S}_{\text{inv}}$. The detailed analysis of the three variance contributions in Section C.3.2 in the case of ellipsoidal particles showed that V_{dist} is by far the largest variance contribution. We therefore suggested the Morse type surface area estimator $\hat{S}_N$ for which this variance contribution vanishes. By choosing the number N of systematic random test directions, also the variance contribution due to the randomization of the direction can be decreased. However, we have seen that only small values of N have to be considered, and that values $N = 2$ or $N = 4$ are theoretically advisable depending on the regularity of the objects. This also is in agreement with Figure C.2 that shows that V_{orient} is a relatively small variance

contribution (in the case of ellipsoids).

The application example of giant-cell glioblastoma showed that other sources of variation, such as the population variance or the uncertainty of measurements due to blurred or ambiguous images can be of the same order or larger than the theoretical variance contribution of the estimator. This indicates that the choice $N = 2$ appears to be appropriate in real-world applications.

C.5.2 Automatic and semi-automatic estimation of surface area

Inspired by [CO12] it was shown in [TK13] that the generalized flower estimator $\hat{S}_{\text{flo}}$ given by (C.12) and the integrated surfactor [CO12, Eq. (24)] coincide. The generalized flower estimator is the optimal estimator with respect to variance (among all the estimators considered in this paper) but as mentioned in Section C.3.3 it can typically not be calculated in practice if the section profile is not a polygon. However, if it is possible to identify the boundary of a given section profile by automated segmentation, the boundary can be approximated by a polygon. Using this approximation the generalized flower estimator $\hat{S}_{\text{flo}}$, with the true section profile $Y = X \cap L_2$ replaced by its estimate, can be obtained using [TK13, Corollary 10] as mentioned in Section C.2.2.3. If the segmentation is flawless, this automatic estimator is unbiased. However, if it is of poor quality, the estimator can be heavily biased. To deal with this problem a semi-automatic procedure for estimating surface area was proposed in [DJ13], based on a similar approach for volume estimation in [HNAJ11]. In the semi-automatic procedure, a clinical expert supervises the process and determines if the automated segmentation of the boundary of a given section profile is satisfactory or not. If it is determined to be satisfactory the surface area is obtained using $\hat{S}_{\text{flo}}$ with Y being the estimate obtained by the automated segmentation. If it is unsatisfactory, the clinical expert intervenes and performs the necessary measurements in the section plane. In [DJ13] it was suggested to use (C.16) in the case where all particles are convex. We suggest to use the Morse-type estimator, which does not require any convexity assumption and reduces to (C.16) when the particles are convex. This semi-automatic procedure can reduce the workload substantially.

Acknowledgement

This research was supported by Centre for Stochastic Geometry and Advanced Bioimaging, funded by the Villum Foundation. The authors want to thank Benedicte Parm Ulhøi at the Institute of Pathology, Aarhus University Hospital NBG, for providing the tissue biopsies and expert knowledge on histological aspects of tumours. The authors also want to thank Thomas Kallemose for writing the program which the expert-assisted procedure is based on.

Appendix: Variance decomposition for ellipsoids

The following proposition gives the different variance contributions in Proposition C.1 more explicitly when X is a three-dimensional ellipsoid containing O. A proof can be found in [Thó10, Theorem 25]. As the reference set RB_3 is trivially invariant under all rotations at the origin, and as the sampling procedure is rotation invariant, we may assume without loss of generality that the ellipsoid's main axes are parallel to the standard coordinate axes.

Proposition C.4. *Let $E_3 \subseteq RB_3$ be a non-degenerate ellipsoid given by*

$$E_3 = \Big\{ x \in \mathbb{R}^3 \;\Big|\; \sum_{i=1}^{3} \Big(\frac{x_i - z_i}{a_i} \Big)^2 \leq 1 \Big\}, \tag{C.30}$$

where $a_1, a_2, a_3 > 0$ and $(z_1, z_2, z_3) \in \mathbb{R}^3$. If $O \in E_3$, the variance of $\hat{S}_{inv}$ given by (C.4)*, can be expressed as*

$$\mathbb{V}\mathrm{ar}(\hat{S}_{\mathrm{inv}}) = V_{\mathrm{dist}} + V_{\mathrm{orient}} + V_{\mathrm{plane}},$$

where

$$\begin{aligned} V_{\mathrm{dist}} = 4\pi \int_0^{2\pi} \int_0^{\pi/2} \Big(R^2 \Big(\frac{1}{\lambda_1} + \frac{1}{\lambda_2} + (z_1')^2 + (z_2')^2 \Big) - \Big(\frac{3}{4\lambda_1^2} + \frac{1}{2\lambda_1\lambda_2} + \frac{3}{4\lambda_2^2} \\ + \frac{3}{4}((z_1')^4 + 2(z_1')^2(z_2')^2 + (z_2')^4) + ((z_1')u_1' + (z_2')u_2')^2 \Big(\frac{9}{2}\frac{1}{\lambda_1} + \frac{3}{2}\frac{1}{\lambda_2} \Big) \\ + (z_1'u_1'' + z_2'u_2'')^2 \Big(\frac{3}{2\lambda_1} + \frac{9}{2\lambda_2} \Big) \Big) \Big) \sin\theta \mathrm{d}\theta \mathrm{d}\phi, \end{aligned} \tag{C.31}$$

$$\begin{aligned} V_{\mathrm{orient}} = 4\pi \int_0^{2\pi} \int_0^{\pi/2} \Big(\frac{3}{4\lambda_1^2} + \frac{1}{2\lambda_1\lambda_2} + \frac{3}{4\lambda_2^2} + \frac{3}{4}((z_1')^4 + 2(z_1')^2(z_2')^2 + (z_2')^4) \\ + (z_1'u_1' + z_2u_2')^2 \Big(\frac{9}{2\lambda_1} + \frac{3}{2\lambda_2} \Big) + (z_1'u_1'' + z_2'u_2'')^2 \Big(\frac{3}{2\lambda_1} + \frac{9}{2\lambda_2} \Big) \\ - \frac{1}{2} \Big(\frac{1}{\lambda_1} + \frac{1}{\lambda_2} + (z_1')^2 + (z_2')^2 \Big)^2 \Big) \sin\theta \mathrm{d}\theta \mathrm{d}\phi, \end{aligned} \tag{C.32}$$

$$\begin{aligned} V_{\mathrm{plane}} = 2\pi \int_0^{2\pi} \int_0^{\pi/2} \Big(\frac{1}{\lambda_1} + \frac{1}{\lambda_2} + (z_1')^2 + (z_2')^2 \Big)^2 \sin\theta \mathrm{d}\theta \mathrm{d}\phi \\ - \Big(\int_0^{2\pi} \int_0^{\pi/2} \Big(\frac{1}{\lambda_1} + \frac{1}{\lambda_2} + (z_1')^2 + (z_2')^2 \Big) \sin\theta \mathrm{d}\theta \mathrm{d}\phi \Big)^2. \end{aligned} \tag{C.33}$$

Here $\lambda_1^{-1/2}$ and $\lambda_2^{-1/2}$ are the lengths of the semiaxes of the ellipse $E_3 \cap L_2$, $u' = (u_1', u_2')^t$, $u'' = (u_1'', u_2'')^t$ its corresponding principal axes and $(z_1', z_2')^t$ its center, all written with respect to a suitably chosen orthonormal basis of the IR plane L_2.

Although the decomposition formulae for ellipsoids are quite complicated it is not difficult to derive a theoretical formula for the total variance of $\hat{S}_{\mathrm{inv}}$ when X is an

ellipsoid. When X is a convex body, $\chi(X \cap L_2 \cap F_z)$ is a Bernoulli random variable and hence using the unbiasedness of $\hat{S}_{\text{inv}}$

$$\mathbb{V}\text{ar}(\hat{S}_{\text{inv}}) = S(\partial X)(S(\partial(RB_3)) - S(\partial X)). \tag{C.34}$$

As a side note, this immediately gives the coefficient of variation of the estimator, which is

$$CV(\hat{S}_{\text{inv}}) = \Big(\frac{4\pi R^2}{S(\partial X)} - 1\Big)^{1/2},$$

in accordance to [CO08, Eq. (18)], as well as the total variance (C.26) of the estimator when X is a ball.

Let now E_3 be a non-degenerate ellipsoid given by (C.30). Assume without loss of generality that $a_1 \geq a_2 \geq a_3$. Then the surface area of E_3 is given by [Eag58, (12) on p. 281]

$$S(\partial E_3) = 2\pi\Big(a_3^2 + \frac{a_2 a_3^2}{\sqrt{a_1^2 - a_3^2}}F(\sigma, m) + a_2\sqrt{a_1^2 - a_3^2}E(\sigma, m)\Big),$$

where

$$\sigma = \arcsin\sqrt{\frac{a_1^2 - a_3^2}{a_1^2}}, \quad m = \frac{a_1^2(a_2^2 - a_3^2)}{a_2^2(a_1^2 - a_3^2)}$$

and $F(\cdot,\cdot)$ and $E(\cdot,\cdot)$ are the incomplete elliptic integrals of the first kind and of the second kind, respectively. Inserting this into (C.34), we find

$$\begin{aligned}\mathbb{V}\text{ar}(\hat{S}_{\text{inv}}) = 4\pi^2\Big(2R^2\Big(a_3^2 + \frac{a_2 a_3^2}{\sqrt{a_1^2 - a_3^2}}F(\sigma, m) + a_2\sqrt{a_1^2 - a_3^2}E(\sigma, m)\Big)\\ - \Big(\Big(a_3^2 + \frac{a_2 a_3^2}{\sqrt{a_1^2 - a_3^2}}F(\sigma, m) + a_2\sqrt{a_1^2 - a_3^2}E(\sigma, m)\Big)\Big)^2\Big).\end{aligned} \tag{C.35}$$

For an oblate ellipsoid (that is when $a_1 = a_2 > a_3$), the surface area has an explicit form and the total variance becomes

$$\begin{aligned}\mathbb{V}\text{ar}(\hat{S}_{\text{inv}}) = 4\pi^2\Big(2R^2\Big(a_1^2 + \tfrac{a_1 a_3^2}{\sqrt{a_1^2 - a_3^2}}\log\Big(\tfrac{\sqrt{a_1^2 - a_3^2} + a_1}{a_3}\Big)\Big)\\ - \Big(a_1^2 + \tfrac{a_1 a_3^2}{\sqrt{a_1^2 - a_3^2}}\log\Big(\tfrac{\sqrt{a_1^2 - a_3^2} + a_1}{a_3}\Big)\Big)^2\Big);\end{aligned}$$

see [Thó10, p. 34] for a derivation. When X is an oblate or a prolate ellipsoid, explicit analytic expressions for V_{plane} can be found in [DJ13, Eq. (2.5) and (2.6)].

Bibliography

[Bad84] A.J. Baddeley. Stochastic geometry and image analysis. In *Proceedings of the CWI symposium on mathematics and computer science*. CWI Monographs, 1984.

[BS12] C.G. Bowsher and P.S. Swain. Identifying sources of variation and the flow of information in biochemical networks. *Proceedings of the National Academy of Sciences*, 109(20):E1320–E1328, 2012.

[CO05] L.M. Cruz-Orive. A new stereological principle for test lines in three-dimensional space. *J. Microsc.*, 219(1):18–28, 2005.

[CO08] L.M. Cruz-Orive. Comparative precision of the pivotal estimators of particle size. *Image Anal. Stereol.*, 27(1):17–22, 2008.

[CO11] L.M. Cruz-Orive. Flowers and wedges for the stereology of particles. *J. Microsc.*, 243(1):86–102, 2011.

[CO12] L.M. Cruz-Orive. Uniqueness properties of the invariator, leading to simple computations. *Image Anal. Stereol.*, 31(2):89–98, 2012.

[CORHAP10] L.M. Cruz-Orive, M.L. Ramos-Herrera, and E. Artacho-Pérula. Stereology of isolated objects with the invariator. *J. Microsc.*, 240(2):94–110, 2010.

[DeH67] R.T. DeHoff. The quantitative estimation of mean surface curvature. *Trans. Metal. Soc. AIME*, 239:617–621, 1967.

[DJ13] J. Dvořák and E.B.V. Jensen. On semiautomatic estimation of surface area. *J. Microsc.*, 250(2):142–157, 2013.

[Eag58] A. Eagle. *The Elliptic Functions as they should be: An account, with applications, of the functions in a new canonical form*. Galloway and Porter, Cambridge, 1958.

[GACO00] X. Gual-Arnau and L.M. Cruz-Orive. Systematic sampling on the circle and on the sphere. *Adv. Appl. Prob.*, 32(3):628–647, 2000.

[Gun88] H.J.G. Gundersen. The nucleator. *J. Microsc.*, 151(1):3–21, 1988.

[HNAJ11] L.V. Hansen, J.R. Nyengaard, J.B. Andersen, and E.B.V. Jensen. The semi-automatic nucleator. *J. Microsc.*, 242(2):206–215, 2011.

[Jen98] E.B.V. Jensen. *Local Stereology*. World Scientific, Singapore, 1998.

[JG87] E.B.V. Jensen and H.J.G. Gundersen. Stereological estimation of surface area of arbitrary particles. *Acta Stereol.*, 6:25–30, 1987.

[Kal12] T. Kallemose. Application of stereological projection formulae for perimeter estimation. Master's thesis, Aarhus University, 2012.

[Mil63] J.W. Milnor. *Morse Theory*. Princeton University Press, Princeton, 1963.

[OPN+00] H. Ohgaki, A. Peraud, Y. Nakazato, K. Watanabe, and A. Von Deimling. Giant cell glioblastoma. In *World Health Organization classification of tumours. Pathology and genetics of tumours of the nervous system*, pages 40–41. IARC Press, Lyon, 2000.

[Thó10] Ó. Thórisdóttir. Variance for surface area estimation based on the invariator. Master's thesis, Aarhus University, 2010.

[TK13] Ó. Thórisdóttir and M. Kiderlen. The invariator principle in convex geometry. Submitted, 2013.